Design of a High Speed Clutch with Mechanical Pulse-Width Control

A Thesis

Submitted to the Faculty of the

WORCESTER POLYTECHNIC INSTITUTE

In partial requirement for the

Degree of Master of Science

In

Mechanical Engineering

By:

_____

Jessy Cusack
2/6/2013

Approved:

_____

Professor James D. Van de Ven, Advisor

_____

Professor Holly K. Ault, Thesis Committee Member

_____

Professor John M. Sullivan, Thesis Committee Member

_____

Professor Mark W. Richman, Graduate Committee Member

Abstract

Kinetic energy storage via flywheels is an emerging avenue for hybrid vehicle research, offering both high energy and power density compared to more established electric and hydraulic alternatives. However, connecting the high speed flywheel to the relatively low speed drivetrain of the vehicle is a persistent challenge, requiring a transmission with high variability and efficiency. A proposed solution drawing inspiration from the electrical domain is the Switch-Mode Continuously Variable Transmission (SM CVT), which uses a high speed clutch to transfer energy to a torsion spring in discrete pulses with a variable duty cycle. The greatest limitation to the performance of this system is the speed and efficiency of commercial clutch technology. It is the goal of this thesis to develop a novel clutch which meets the actuation speed, controllability, and efficiency requirements of the SM CVT, with potential for reapplication in other rotary mechanical systems with switching functionality.

The performance demands of the clutch were derived via a theoretical design case based on the performance requirements of a typical passenger vehicle, indicating the need for a sub-millisecond engagement and disengagement cycle. This is not met by any conventional clutch. Several concepts were considered across the fluid, electromagnetic and mechanical energy domains. A final concept was chosen which employs a friction disk style architecture, with normal force produced by compressing springs via an axial cam mounted to the flywheel. To control duty cycle, the cam was designed with a radially varying profile such that increasing radial position results in proportionally increasing ratio of high dwell to low dwell. Three synchronized followers are then translated radially on the cam by a control linkage. Analysis of the follower train dynamics and system stiffness were carried out to inform the design of a scaled benchtop prototype. Experimental testing was carried out to characterize the performance of the prototype. It was found that the intended functionality of the design was achieved, with discrete energy transfer accomplished via pulsing of the clutch. However, maximum efficiency was only 33% and torque capacity was only 65% of the intended 70Nm. Significant opportunity exists for improvement of the clutch performance in future research.

Acknowledgements

I would like to thank my advisor Jim Van de Ven for his guidance and his generosity of time and energy. His breadth and depth of knowledge as well as his ability to maintain perspective and a level head is something I aspire to.

I would like to thank my thesis committee, Professor Ault, Professor Sullivan, and Professor Richman, for their support and honest feedback. Thank you to Professor Norton for his invaluable input on the cam design. Thank you to the ladies in the Mechanical Engineering office for guiding me through the process with a smile, and to all of the knowledgeable staffers in the machine shop who helped me to learn. Thank you to L&M Machine for their friendliness and extra effort for a quick turnaround in a pinch.

Thank you to my fellow members of the MEPS lab for being critics and collaborators. Thank you to my friends for rooting me on. Thank you to Sara for being a motivator and keeping an eye on the prize when I didn't.

Lastly I'd like to thank my parents, whose unending support gave me the motivation to push through and succeed. I wouldn't have been able to do this without you.

Table of Contents

List of Figures

List of Tables

Nomenclature

a	Follower acceleration [$\frac{mm}{s^2}$]
A_{pin}	Stress in linkage pin [mm^2]
$A_{coupler}$	Stress in coupler link [mm^2]
A_{clevis}	Stress in clevis of center link and carriage [mm^2]
α_{out}	Angular acceleration of output shaft [$\frac{rad}{s^2}$]
β	Angular duration of cam profile segment [deg]
$\beta_{dwell,max}$	Maximum angular duration of dwell segment [mm]
E_f	Flywheel kinetic energy [kJ]
ΔE_f	Change in flywheel kinetic energy from one clutch pulse [J]
E_{slip}	Energy lost to clutch slip [J]
E_{trans}	Energy transmitted to the output [J]
F_n	Normal force applied to the friction surfaces of the clutch [N]
F_x	Lateral force on follower tip due to pressure angle of cam [N]
F_y	Radial force on follower tip due to pressure angle of cam [N]
F_z	Vertical force on follower tip due to pressure angle of cam [N]
h	Rise height of cam [mm]
h_{arm}	Height of center link arms [mm]
$h_{coupler}$	Height of coupler link [mm]
h_{clevis}	Height of clevis of center arm and carriage [mm]
I_{arm}	Center link arm area moment of inertia [m^4]
I_f	Flywheel mass moment of inertia [kgm^2]
$I_{f,h}$	Hollow flywheel mass moment of inertia [kgm^2]
$I_{f,s}$	Solid flywheel mass moment of inertia [kgm^2]
I_{out}	Output assembly mass moment of inertia [kgm^2]
$K_{BasePlate}$	Base plate stiffness [$\frac{N}{mm}$]
$K_{Flywheel}$	Flywheel stiffness [$\frac{N}{mm}$]
$K_{Follower}$	Follower stiffness [$\frac{N}{mm}$]

K_{Guide}	Follower guide stiffness $[\frac{N}{mm}]$
$K_{InputDisk}$	Input disk stiffness $[\frac{N}{mm}]$
$K_{InputShaft}$	Input shaft stiffness $[\frac{N}{mm}]$
$K_{OutputDisk}$	Output disk stiffness $[\frac{N}{mm}]$
$K_{OutputShaft}$	Output shaft stiffness $[\frac{N}{mm}]$
K_{Post}	Support post stiffness $[\frac{N}{mm}]$
K_{Spring}	Disk spring stiffness $[\frac{N}{mm}]$
K_{System}	Total system stiffness $[\frac{N}{mm}]$
$K_{TopPlate}$	Top plate stiffness $[\frac{N}{mm}]$
K_{ts}	Torsion spring stiffness $[\frac{Nm}{rad}]$
L_{arm}	Length of center link arms [mm]
L_f	Flywheel axial length [mm]
L_x	Lateral distance from follower tip to center of linear slide [mm]
L_y	Radial distance from follower tip to center of linear slide [mm]
L_z	Vertical distance from follower tip to center of linear slide [mm]
m_f	Flywheel mass [kg]
M_x	Moment on linear slide about the x axis [Nm]
M_y	Moment on linear slide about the y axis [Nm]
M_z	Moment on linear slide about the z axis [Nm]
μ	Dynamic coefficient of friction
ω	Angular velocity $[\frac{rad}{s}]$
ω_{in}	Input shaft angular velocity $[\frac{rad}{s}]$
ω_{out}	Output shaft angular velocity $[\frac{rad}{s}]$
ϕ	Pressure angle of cam profile [deg]
r	Radial position on cam [mm]
r_f	Mean radius of friction surfaces [mm]
r_{max}	Maximum cam radius [mm]

r_{min}	Minimum cam radius [mm]
R_T	Torque resolution
R_Θ	Angular resolution
ρ	Radius of curvature of cam profile [mm]
ρ_f	Flywheel density [$\frac{kg}{m^3}$]
s	Follower displacement [mm]
σ_{pin}	Stress in linkage pin [MPa]
$\sigma_{coupler}$	Stress in coupler link [Mpa]
σ_{clevis}	Stress in clevis of center link and carriage [Mpa]
σ_{arm}	Bending stress of center link arms [Mpa]
t_p	Duration of a clutch pulse [s]
T_b	Brake torque [Nm]
T_c	Torque transmitted by the clutch [Nm]
T_i	Inertial torque [Nm]
T_{ts}	Torque of torsion spring [Nm]
$T_{ts,max}$	Maximum torsion spring torque [Nm]
ΔT_{ts}	Change in torsion spring torque from one clutch pulse [Nm]
θ	Angular position within cam profile [deg]
θ_{out}	Output shaft angular position [rad]
θ_{ts}	Torsion spring deflection [rad]
$\theta_{ts,max}$	Maximum torsion spring deflection [rad]
$\Delta\theta_{ts}$	Change in torsion spring deflection from one clutch pulse [rad]
v	Follower velocity [$\frac{mm}{s}$]
w_{clevis}	Width of clevis of center link arm and carriage [mm]
$w_{coupler}$	Width of coupler link [mm]

Chapter 1 - Introduction

This chapter introduces the concept of switch mode control in rotary mechanical systems. A gap in available technology to meet the switching needs of such systems via a high speed clutch is discussed, with a review of the literature in this area. Lastly, the remaining content of the thesis is summarized.

1.1 Background

The demand for high efficiency in a world of increasing resource usage has led way to many new engineering challenges. Established systems are being reconsidered and renovated with the added constraint of minimizing energy waste. The automotive industry provides excellent examples. High efficiency vehicles challenge traditional powertrain design, using auxiliary power systems in addition to or in lieu of an internal combustion engine (ICE). These hybrid systems are employed in a variety of designs across hydraulic, electrical, and mechanical domains, as will be detailed in the following section. A commonly employed strategy is regenerative braking, in which energy otherwise lost to heat in friction brakes while decelerating the vehicle is stored in an auxiliary power system for later reuse in acceleration.

Use of flywheel energy storage is one of the least explored hybrid vehicle options in comparison to electrical or hydraulic hybrid systems. Flywheels have attractive advantages in their high energy and power per unit volume. However, in order to store large amounts of energy in a reasonable weight and package size, they must operate at extremely high angular velocities. Connecting this high speed

energy storage device to a relatively low and highly variable output speed presents significant challenge, especially when efficiency is considered as a chief constraint.

A proposed solution draws inspiration from the electrical domain. The switch mode continuously variable transmission (SM CVT) is a rotary mechanical system conceived and prototyped at Worcester Polytechnic Institute's Mechanical Energy and Power Systems Laboratory [1]. Intended for flywheel power transmission, it is a mechanical analog of the DC-DC boost converter circuit. Figure 1.1 illustrates the two systems.

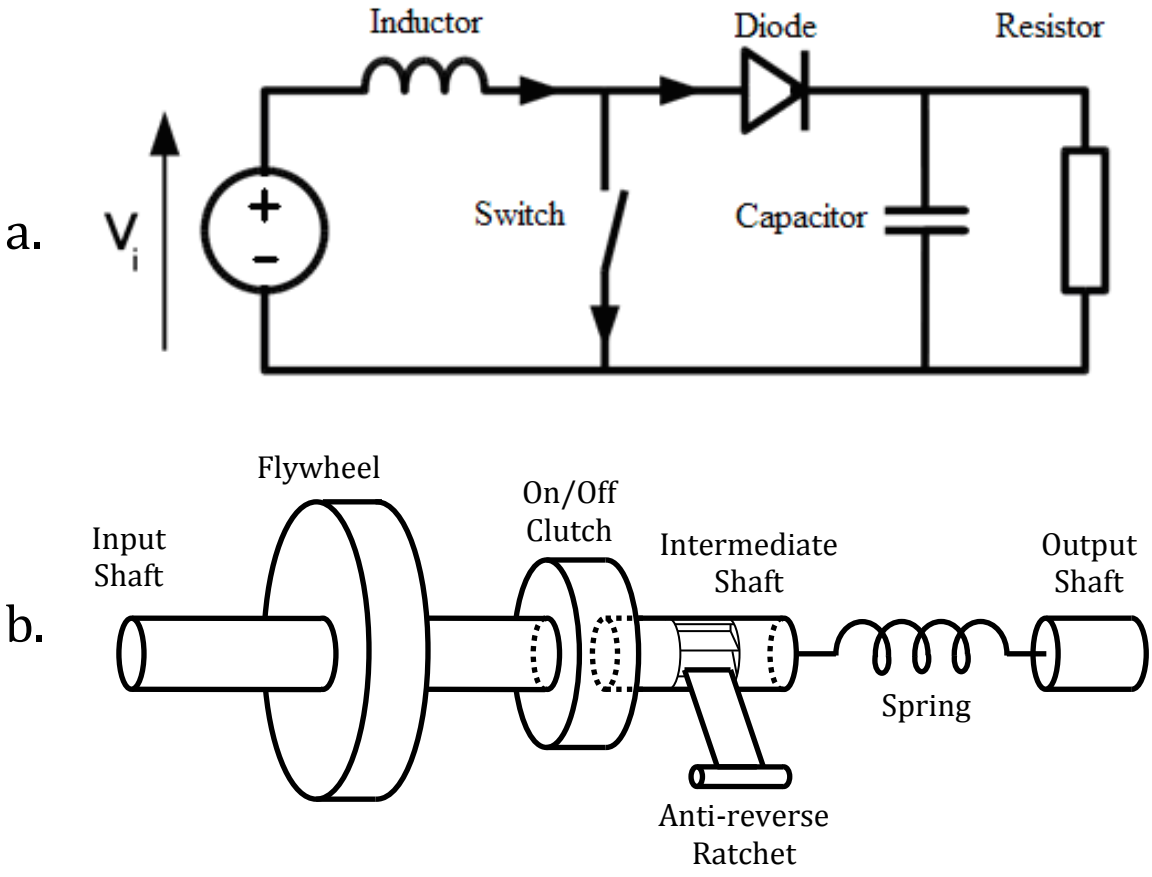

Figure 1.1 Switch-mode electrical (a.) and mechanical (b.) circuits [1]

Both circuits operate in either an “on” or “off” state. In the off state, the electrical switch is closed, and the inductor circulates current with ideally zero load or energy expenditure. Similarly, in the mechanical system, when the clutch is disengaged, or off, the flywheel spins freely. In the on state, the electrical switch is open, and the current from the inductor charges the capacitor. Mechanically, when the clutch is engaged, or on, the flywheel advances the spring, storing energy through angular deflection. When the electrical switch is turned off again, the diode prevents the backward flow of current from the capacitor, and so it releases its stored energy into the output load, the resistor. The inductor continues to circulate current with ideally zero loss, but has lost some energy to charging the capacitor. Mechanically, the ratchet prevents the wound spring from freely spinning at its input end, and so its deflection energy goes into driving the output shaft. The flywheel again spins freely, but at a decreased angular velocity due to energy transfer to the spring.

The key to the functionality of both systems is that by controlling the ratio of time on versus off via the switching component, the average loading of the compliant element – voltage of the capacitor and torque of the spring – can also be controlled. In the SM CVT, by pulsing the clutch for very short durations, small increases in deflection can be created in the spring, and thus small increases in output torque. Conversely, leaving the clutch off allows the spring to unwind, release energy, and decrease output torque. By controlling the duty cycle of the clutch, defined as the fraction of time spent in the on state to the total time, the

average output torque can be controlled. Figure 1.2 illustrates how the SM CVT increases torque in discrete jumps, approximating a continuously variable transmission.

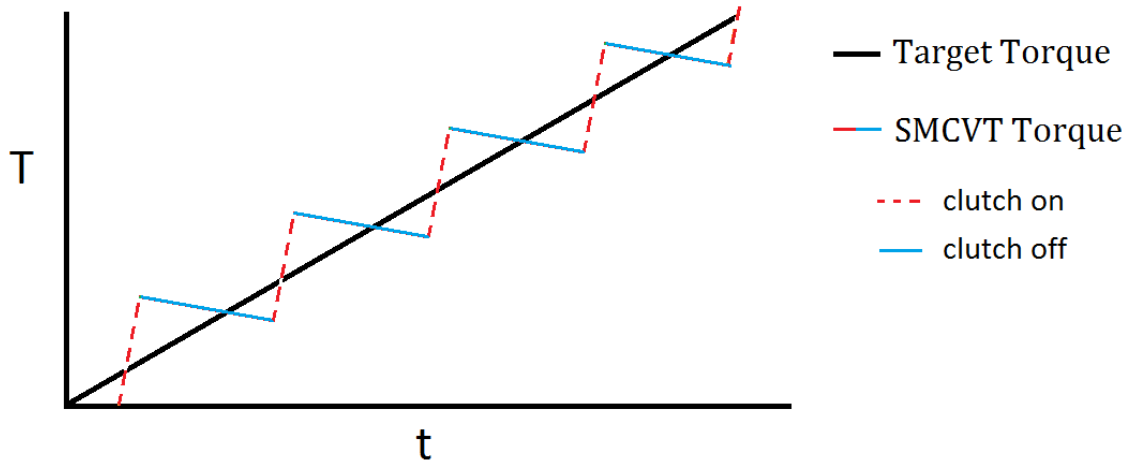

Figure 1.2: Target continuous torque vs. stepped SM CVT response. In the on state of the clutch, the spring advances with the flywheel and increases torque. In the off state, the spring unwinds, decreasing torque and transferring energy to the output load.

Regenerative braking is made possible by adding a brake and an over-running clutch between the flywheel and spring, as illustrated in Figure 1.3. When vehicle deceleration is desired, the brake is applied, and the spring now winds to oppose the forward motion of the vehicle, building energy. The brake is then pulsed similarly to the clutch, with the spring transmitting torque via the overrunning clutch back to the flywheel when the brake is disengaged, increasing the flywheel's kinetic energy [2].

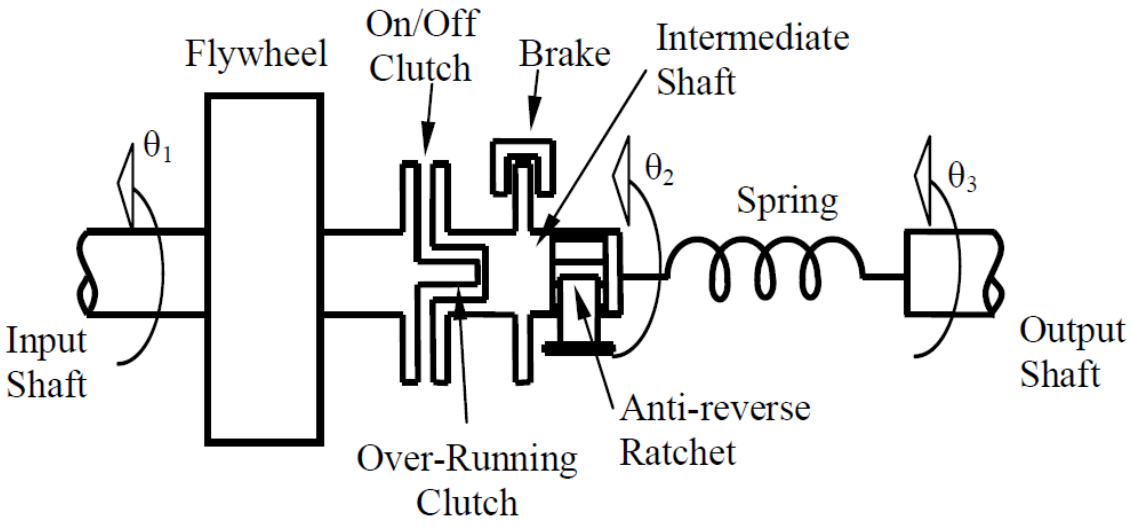

Figure 1.3: SM CVT with brake and over-running clutch for regeneration [2].

The SM CVT is an example of emerging technology wherein established digital control theory of the electrical world is brought to a different energy domain. Pulse modulation control of mechanical systems is an ill explored area of research, which offers distinct advantages to kinetic energy storage mechanisms where an "off" state is critical to energy conservation.

However, a significant challenge exists in the translation of electronic circuits to mechanical systems. Where electronic switching components can closely approximate their theoretical representations with near instant changes in state producing discontinuous current flows, physical systems must contend with greater dynamic forces. Clutches, the switching components of rotary mechanical systems, are constrained by inertia, stiffness, and damping and carry latency and energy loss that detract from the ideal operation of a digital mechanical system. As will be discussed later, current clutch technology does not meet the needs of the SM CVT,

and stands as the greatest barrier to the advancement of mechanical switch mode technology as a whole.

It is the goal of this research to address this performance gap in the context of the SM CVT. The following chapters detail the development of a clutch to meet the efficiency, controllability, and torque resolution requirements of the SM CVT, and, more broadly, rotary mechanical systems utilizing pulse modulation for control. It is shown that commercial clutch options are inadequate to facilitate the goal of a continuously variable transmission at passenger vehicle scale with sufficiently small discrete steps in torque.

1.2 Literature Review

The following section reviews the state of research surrounding the subject of this thesis, the design of a high speed switching clutch with pulse modulation. The increased global focus on high efficiency systems is discussed, specifically in the context of transportation and the rise of hybrid vehicles. Different hybrid vehicle types are explained, with flywheel energy storage determined as a research area with high potential. Challenges of flywheel power transmission are discussed, with a review of proposed methods. Switch-mode control is identified as an ill-explored area of research. Several switch-mode torque transfer concepts are reviewed, including the Switch-Mode Continuously Variable Transmission. Finally, a gap in current technology is discussed with respect to mechanical switching components in the form of clutches.

1.2.1 Hybrid Vehicles

In the United States, transportation accounts for 28% of total energy consumption, and 97% of transportation energy is currently from non-renewable sources [3]. With global energy demand rising, means of improving the fuel efficiency of vehicles is an area of increasing focus. A major area of research is hybrid vehicles. The goal of a hybrid vehicle is to increase operating efficiency via storage and retransmission of energy in a form other than liquid fuel.

Hybrid vehicles employ an auxiliary power source capable of recapturing energy in addition to a traditional power source, typically an ICE, which cannot recapture energy. There are 3 main methods for increasing efficiency with an auxiliary power source. 1) The auxiliary system handles the transient high-power needs of the vehicle such as rapid acceleration or ascending a steep grade, allowing the ICE to be sized to meet only the lower steady state power needs. 2) The ICE operates only in a narrow power band around its highest efficiency, with excess power not needed for driving the vehicle diverted to an auxiliary storage medium. Once the energy storage device is fully charged, the ICE is turned off, and the auxiliary power source is used to drive the vehicle. 3) Energy normally lost to friction during braking events such as coming to a stop or descending a grade is stored in an auxiliary storage medium. This energy is then used to accelerate the vehicle once again [4].

Hybrid vehicles have been designed with a variety of energy storage mediums, with the most common being electric batteries, hydraulic accumulators, and flywheels. Electric hybrids have the advantage of high energy density, at 400-700 kJ/kg for modern lithium ion batteries [5]. A major drawback however is relatively

low power density of both batteries and electric motors and generators, at 30-100 W/kg [6]. This low power capability means that traditional friction brakes must be used to handle high deceleration, and a portion of the braking energy is converted to heat. Batteries also lose storage capacity over repeated charging and discharging cycles. Hydraulic hybrids store energy via compression of fluid in an accumulator. Modern accumulators have very high power densities, at 500-1000 W/kg, but conversely low energy density, at only about 5 kJ/kg [6]. This low energy density leads to high weight needed to store suitable energy for regenerative braking.

Flywheel energy storage, the method considered in this paper, has both high energy density and high power density. Composite flywheels may have energy densities of 200 kJ/kg and power densities in excess of 5000 W/kg, as power is limited only by the torque capacity of the means of transmission [5]. A difficulty faced in flywheel energy storage is coupling the high speed flywheel, often spinning over 50,000 RPM, to the relatively low speed vehicle wheels. A transmission capable of converting flywheel energy to useful driving energy for a vehicle must have a very high range of reduction to account for the extreme difference between input and output speed. Since the angular velocity of a flywheel is a dependent on its energy content, a traditional geared transmission with a discrete set of drive ratios as is not an option. A flywheel must be coupled to its output through a CVT, allowing a full range of power transfer from high to low relative RPM. Additionally the transmission must operate at a high efficiency to conserve energy. As such, the conversion of kinetic energy from a flywheel to a vehicle is a non-trivial challenge.

1.2.2 Flywheel Energy Transmission

In the 2009 season, Formula 1 racing permitted the use of kinetic energy recovery systems (KERS). It was specified that braking energy may be stored either electrically via batteries or capacitors or mechanically via a flywheel. As a result, flywheel hybrid technology saw significant development. Figure 1.4 shows a KERS system by Flybrid LLP coupling a vacuum-sealed flywheel spinning up to 64,000 RPM to a CVT [7]. The flywheel is comprised of a steel core wrapped in carbon fiber, with the use of composites necessitated by the radial stresses encountered at such high angular velocity. The flywheel operates in a vacuum inside of a sealed chamber to avoid energy loss to air resistance. The CVT is a toroidal type, also pictured in Figure 1.4. This CVT type uses tilting rollers in traction against concave input and output disks. As the angle of the rollers changes, the contact radius on both the input and output changes to vary the drive ratio.

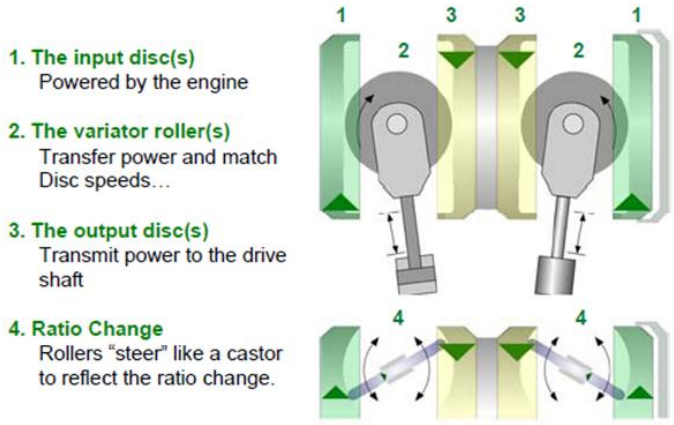

a. Toroidal CVT Operation

b. Composite Flywheel

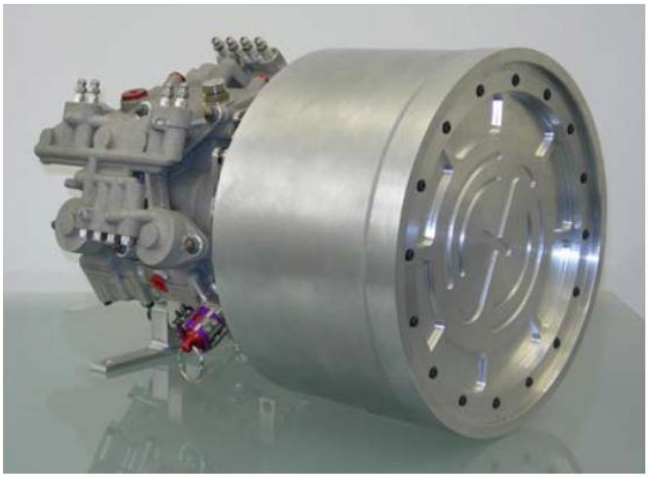

c. Full KERS system with vacuum chamber

Figure 1.4: KERS developed for Formula 1 racing [7]

A limitation of this system is that though the CVT is continuously variable within its range of drive ratios, this range is finite. The flywheel is at highest charge after extreme braking, when the vehicle is at lowest speed. Because the CVT cannot couple this extreme relative velocity, energy must be transferred inefficiently by slipping a clutch, or energy transfer must be delayed until vehicle the vehicle has accelerated to a higher velocity via the engine.

In addition to the Toroidal CVT used in the above KERS, there are many other established CVT types. The primary mechanical CVT architectures are illustrated in simple form in Figure 1.5 [8]. The most common torque transfer method in mechanical CVTs is friction, with either the input, output, or an intermediate component capable of changing shape or position to affect the relative contact radius [8].

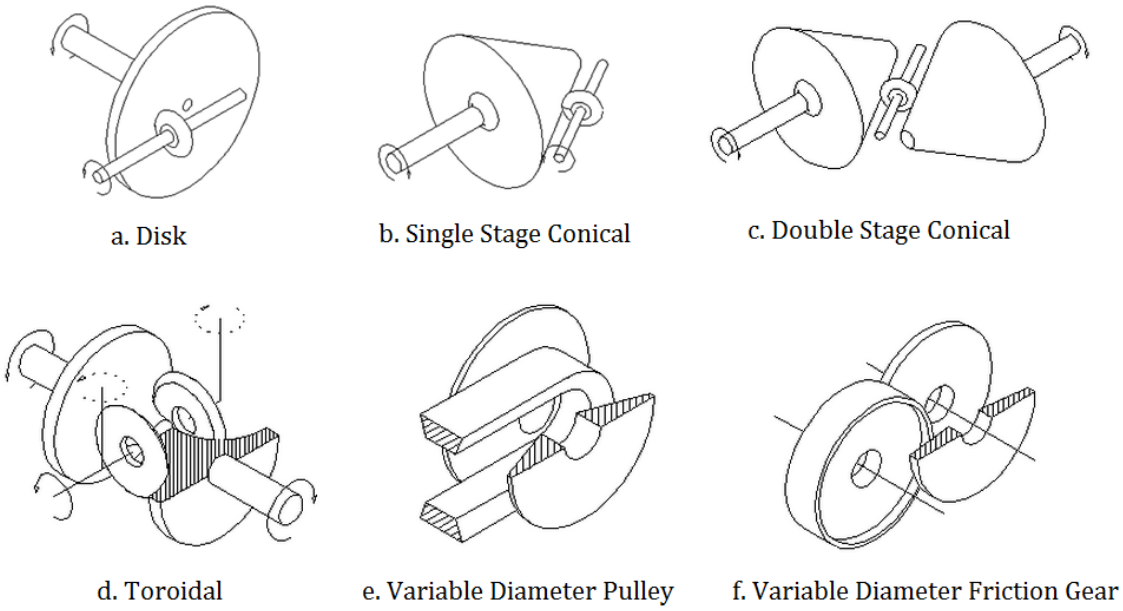

Figure 1.5: Basic mechanical CVTs [8]

CVT's also exist in other energy domains. Hydraulic CVTs use a variable displacement pump and/or motor to vary the flow generated from a mechanical input to drive the output at variable speed and torque [9]. In the electromagnetic realm, the relatively recent technology of passive magnetic gears has been improved to actively control the magnetic exposure between rotors, providing a magnetic CVT [10]. Each embodiment has advantages and disadvantages in terms of efficiency,

complexity, ratio range, weight, torque capacity, etc. The majority of CVT's have a finite range of reduction which is typically less than 10:1 [9]. Given that the difference in velocity between flywheel and vehicle wheel speed may be several orders of magnitude – and indeed infinite when the vehicle is at rest – CVTs are limited in their ability to transmit flywheel energy. Sufficient benefit is provided by existing transmission types to warrant use in dynamic, high performance application such as Formula 1. In a passenger vehicle application however it is desirable to transmit the flywheel energy efficiently to a low or zero speed driveshaft, presenting a further challenge.

Diego-Ayala et al. propose a concept which attempts to increase reduction range step-wise via a planetary gearset, clutch, and brake in addition to a traditional CVT, as seen in Figure 1.6 [11]. The system works in several modes. The planetary gearset provides a reduction between the flywheel and the outer ring, which drives the clutch and the CVT input. A second stage of planetary gears using the same ring drives an output to the vehicle wheels. At the highest necessary reduction (vehicle rest), the clutch is slipped to begin vehicle motion. Once the vehicle and flywheel relative speed has reduced sufficiently, the clutch is fully locked and the CVT begins decreasing the reduction ratio. Once the CVT has reached its lowest reduction, the clutch is disengaged and the brake engages the planetary ring, slowing it to a stop. At this point, the reduction is at minimum, equal to the sum reduction of the planetary gear stages. Regeneration is accomplished by reversing the above steps.

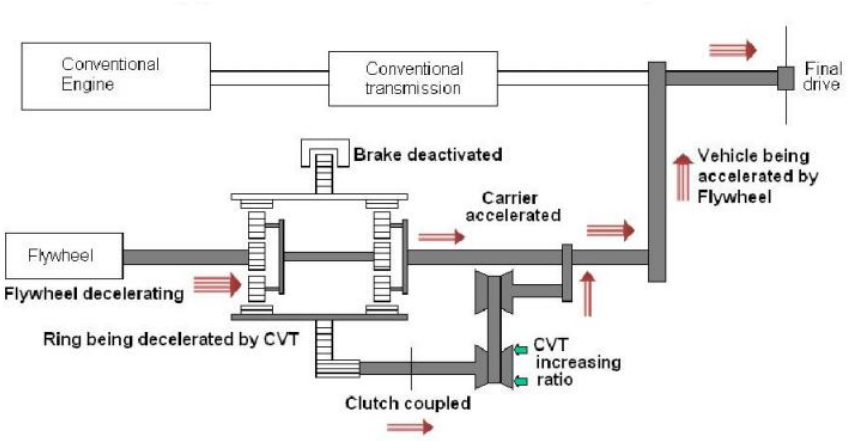

Flywheel Assisted Acceleration with CVT.

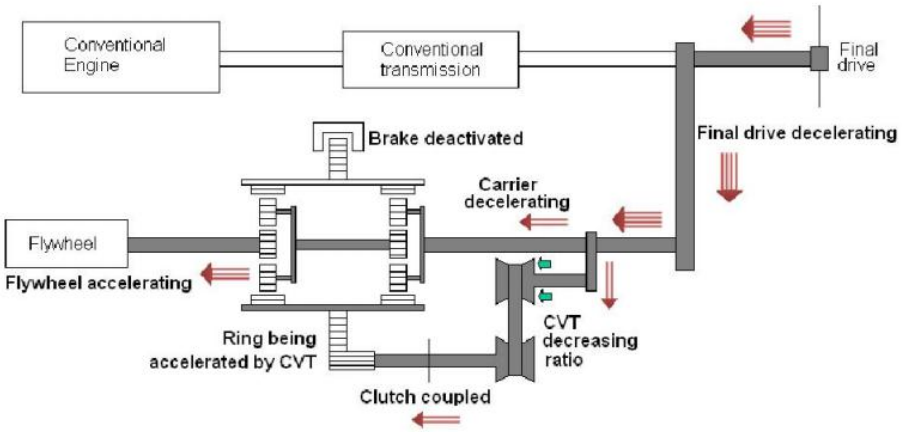

Regenerative Braking with CVT.

Figure 1.6: CVT concept with planetary gearset, clutch, and brake [11]

A disadvantage to this system is that its highest reduction is essentially the same as the CVT alone. An extremely high reduction is needed to take advantage of the high flywheel speed with the vehicle at rest. In the above system, a friction clutch must be used to bleed off energy and reduce the flywheel velocity to a level that may be fully coupled. The transfer from the lowest CVT reduction to the planetary gearset uses a friction brake to transition power, again wasting friction energy.

1.2.3 Switch-Mode Systems

A novel means of approaching flywheel energy transmission is through switch-mode control. Switch-mode systems have long been in use in electrical engineering, where circuits may switch between two or more discrete states to improve functionality and efficiency for tasks such as power transfer [12]. As the most basic properties of electronic components– capacitance, resistance, and inductance – are analogous to those of mechanical systems – stiffness, damping, and inertia – inspiration for mechanical systems may be drawn from electronic power solutions. As an example, one of the most basic switch-mode circuits used for power transfer is the DC boost converter, a type of regulated power supply. This circuit is illustrated in Figure 1.1 of the previous section. Where a linear power supply regulates current and voltage by dissipating excess power as waste heat through a transistor, a boost converter switches the connection between the input and output on and off, with duty cycle of this connectivity regulating the average output voltage. A capacitor is used to store charge and regulate the output voltage and an inductor is used to maintain the input current. This system, which allows for much more efficient power transfer, gives mechanical inspiration to the switch-mode CVT, as detailed in the introduction to this paper.

A major difference between mechanical and electrical systems in the context of switch-mode operation is the time and energy required to change between discrete states. Where a transistor based electrical switch may change state almost instantly and with negligible energy expenditure, mechanical switches – taking the form of clutches in rotary systems – must contend with inertia, stiffness, and

damping when engaging or disengaging. Time and energy are spent in the switching process, decreasing operational resolution and efficiency. As a result of this, switch-mode control of mechanical systems has remained largely unexplored.

The majority of mechanical systems with switching functionality found in the literature use oscillating rotation of an input coupled with a one-way clutch to drive the output in a net forward direction. One-way clutches are also known as indexing clutches, rectifying clutches, freewheeling clutches, sprag clutches, or ratchets, and vary in form. These unidirectional components are the mechanical analog of electrical diodes. A novel concept proposed by W. T. Beale and analyzed by T. Cyders et. al uses a four-bar linkage with a compliant link to modulate speed and torque, illustrated in Figure 1.7 [13]. As the input crank - which may be thought of as the flywheel - rotates, the output link oscillates through positive and negative rotation. The output link pivots about the output shaft, to which it may transmit torque in one direction only via a ratchet and pawl. The output link additionally serves as a torsion spring by use of thin beam bending over a curved restraint surface. For a given output load, as the output link rotates positively, the spring builds torque until it overcomes the output, at which point the output is rotated positively. Once the output finishes its positive rotation, it returns through negative rotation, with the spring load being transferred back to the input, and the output shaft decoupled from the output link via the ratchet. As such, torque is applied cyclically to the output. Depending on the output load, more or less of the output link rotation will be taken up by spring deflection rather than moving the output shaft, increasing or decreasing the speed of the output vs. input. In this way a constant input velocity

and torque is automatically converted to the torque requirement of the output via modulation of velocity with power conserved. To smooth the torque delivered to the output, multiple phase-shifted linkages are used. Though this concept is fairly simple, a drawback – common to all oscillating systems reviewed – is the energy wasted in the cyclic acceleration and deceleration of the oscillating components.

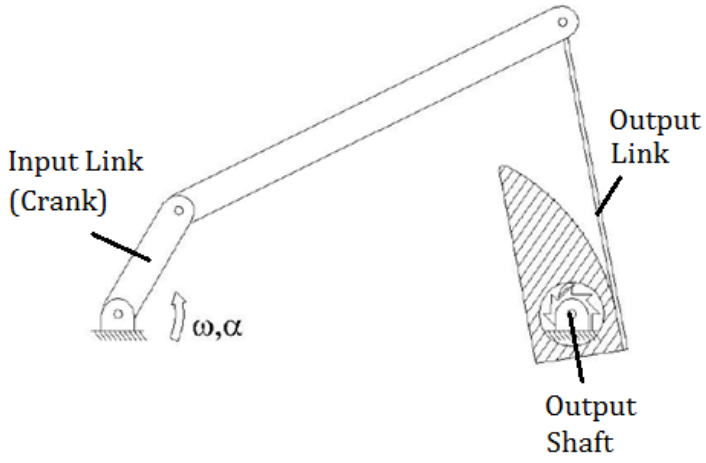

Figure 1.7: Ratcheting CVT utilizing a crank-rocker four bar linkage with compliant output link [12].

Other transmissions using planetary gear systems with oscillatory motion have been proposed. A concept by Lahr et al. uses a cam to induce oscillation, and is illustrated in Figure 1.8 [14]. Though several inversions of this device are possible, the planet carrier as input and sun gear as output is most developed by the authors. As the carrier rotates, followers connected to the planet gears oscillate by following the profile of a grounded cam. Each planet gear may have its own sun gear with a one way clutch, or one way clutches may be used at the planet gears engaging a common sun gear. The sun gear output rotates via the rotation of the carrier plus

the additional rotation of the planet gears due to follower rotation. By shifting the position of the followers along a 3D cam with variable profile, the additional rotation of the planet gears may be regulated, changing the transmission ratio of the system. Though theoretical infinite variability is claimed, in practice restrictions on the cam design limit the range of drive ratios, and prototyping of the system offered only 1:1 to 1:6 in 3 discrete modes.

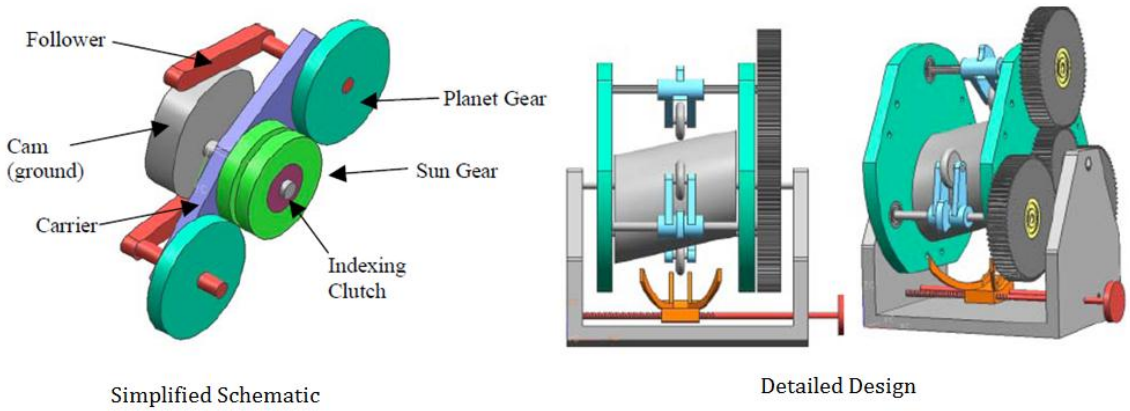

Figure 1.8: Cam-based CVT with rectified oscillating output [14]

Another planetary concept is proposed by Benitez et al, pictured in Figure 1.9 [15]. Fundamentally, this concept is very similar to a typical planetary gear set with the planet carrier as input and sun gear as output. However, instead of fixing the ring gear it is designed to be free to move but of significant mass. A crank-rocker linkage converts constant velocity from a motor or flywheel to oscillatory rotation of the carrier. As the carrier oscillates, power is transferred in phases to kinetic energy in the ring gear and to the output, and from the ring gear to the output. The output is also oscillatory, and must be rectified with a one-way clutch. The ratio of energy put into the ring gear vs. the output, and thus the drive ratio, varies automatically

depending on input velocity and output load. Drawbacks to such a system are wasted oscillation energy, and poor efficiency at low drive ratios. Additionally, the mass of the ring gear must be large to transmit high torque to the output, which is undesirable for vehicular application. The system is intended to function as a velocity amplifier rather than a reducer, and so is not well suited to flywheel transmission.

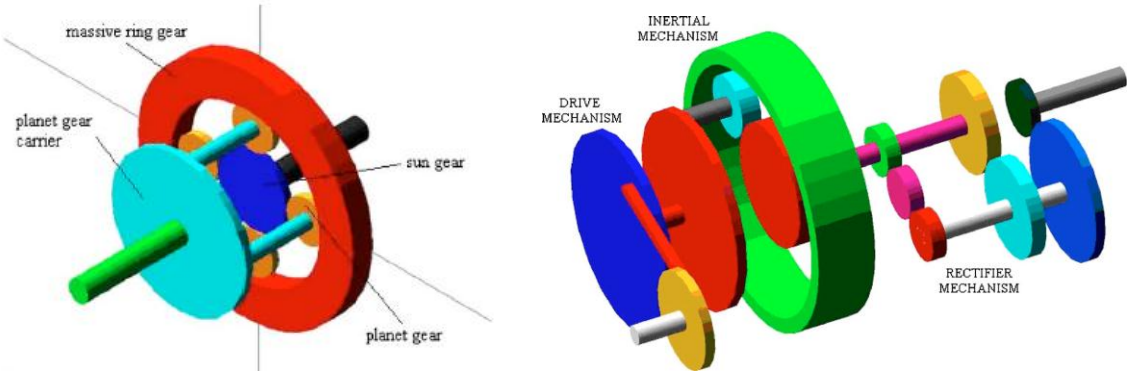

Figure 1.9: Inertial CVT concept [15]

Because of the energy spent on cyclic acceleration, oscillating transmissions in general decrease in efficiency as velocities increase. Because many of the oscillating components must transfer force, potential for reduction of weight is often limited, and this is only made worse as velocities increase. As a flywheel input may have extremely high velocity, these losses can be significant. An advantage to oscillation however is that the switching component, the one way clutch, must only engage and disengage when rotational direction changes and velocity is zero. Very little energy is wasted in the transition from free-wheeling in one direction to torque transfer in the other. Because of this, one-way clutches mimic ideal electrical diodes well. Systems that do not oscillate have more difficulty in switching modes.

A system proposed by Gilbert et. al attempts to use a constant velocity input rather than sinusoidal oscillation, pictured in simplified form in Figure 1.10 [16]. A motor, which may also be thought of as a flywheel, is connected intermittently to a grounded torsion spring via clutch 1. While coupled to the input, the spring deflects, building energy. Once the spring is desirably wound, clutch 1 is disengaged and clutch 2 is engaged, transmitting the stored energy and providing a driving torque. Once the spring has released its energy, clutch 2 is disengaged and clutch 1 engaged to wind the spring again. Clutch 2 may in fact be simply a one way clutch, allowing the spring to be rewound by the flywheel and transfer torque when released. Clutch 1 however must be actively engaged and disengaged, connecting the high velocity flywheel to the counter-rotating spring, which builds torque in opposition to input rotation. Energy is thus spent in slip during engagement of clutch 1. The clutch must also actuate very quickly, as the spring will have only a finite capacity for deflection. The torque output is highly discontinuous, taking the form of a square wave as torque drops to zero during rewinding of the spring and jumps during reengagement. Initial modeling used an idealized clutch with no slip and instant actuation as well as a massless spring. Once the model was expanded to include the limitations of commercial clutches and realistic masses, the system was found to have a limited range of efficient drive ratios, between 1:3.2 and 1.3:1.

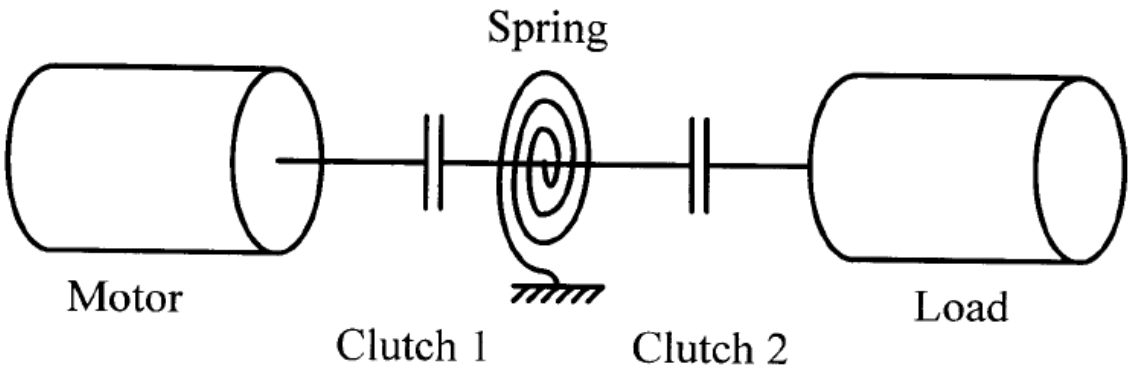

Figure 1.10: Simplified schematic of a double-clutch switching transmission device [16]

The Switch-Mode CVT improves on this concept by eliminating the grounding of the torsion spring. A significant advantage of this is that the output need not be disconnected from the spring while torque is increased through connection to the input. As such, the torque jump with each engagement may be smaller and the output torque profile more smooth. However, the efficacy of the SM CVT, and in reality all mechanisms which hope to use a non-oscillating switch mode functionality, is largely limited by the speed and efficiency of available clutch technology. Initial modeling work by Forbes et al. identified the need for a clutch with a 0.45 ms engagement-disengagement cycle time at maximum duty cycle and 0.01 ms at minimum, with no consideration of slip [1]. Prototype work by Araujo et al. identified commercially available clutches as the primary limiting factor to operation [17]. A clutch that may act more effectively as an ideal switch for systems such as the SM CVT is identified as a gap in available technology. The commercial and academic state of the art of high speed clutch technology is now reviewed.

1.2.4 High Speed Clutches

There are several clutch types across the hydraulic, electric, and mechanical energy domains. These are presented in the following section, organized by the four primary mechanisms of torque transfer: viscous resistance, electromagnetism, interference, and friction. The following section details the state of the art for these four torque transfer types and discusses their suitability for development towards high speed, torque, and efficiency.

Viscous Resistance

Clutches using viscous resistance are called fluid couplings, and use drag features known as vanes to produce torque between an input (pump) and output (turbine). Additionally a grounded stator with additional vanes may be used to affect flow. A typical coupling is pictured in Figure 1.11 [18]. Torque is controlled by the exposure or attitude of the vanes in the fluid, or in the case of magneto-rheological clutches, an electric current changes the viscosity of the working fluid. The input and output are always in slip, so fluid clutches do not truly have an off state. As the primary means of controlling torque is to disperse excess power into the fluid, a fluidic power coupling is not a compelling choice for a high efficiency clutch.

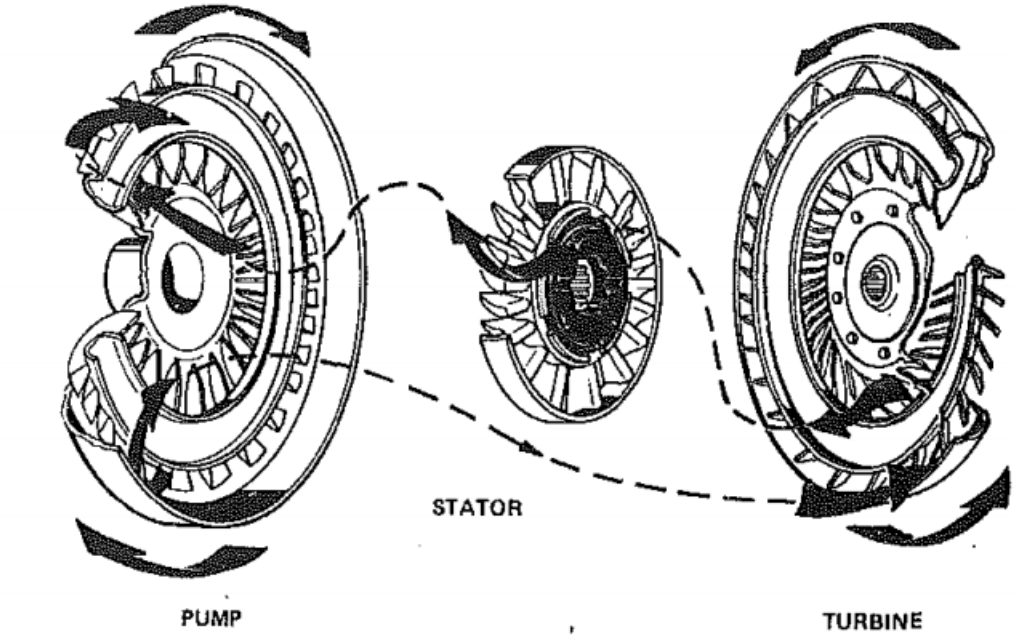

Figure 1.11: Flow paths in a typical fluid coupling. Relative rotation of the pump and turbine causes hydrodynamic drag and resultant torque transfer [18].

Electromagnetism

Clutches using electromagnetism for torque transfer are known as hysteresis clutches. They operate similarly to electric motors, with the polarity of a rotating electromagnet switched such that it is attracted to the advancing pole of a surrounding permanent magnet. In a hysteresis clutch, instead of the permanent magnet being grounded, it is connected to the input shaft, with the electromagnet on the output [19]. This is not to be confused with an electromagnetic clutch, which uses electromagnetism to produce normal force between two friction disks which in turn transmit torque. Use of electromagnetism in this way will be discussed later in the next chapter. Figure 1.12 pictures an example hysteresis clutch.

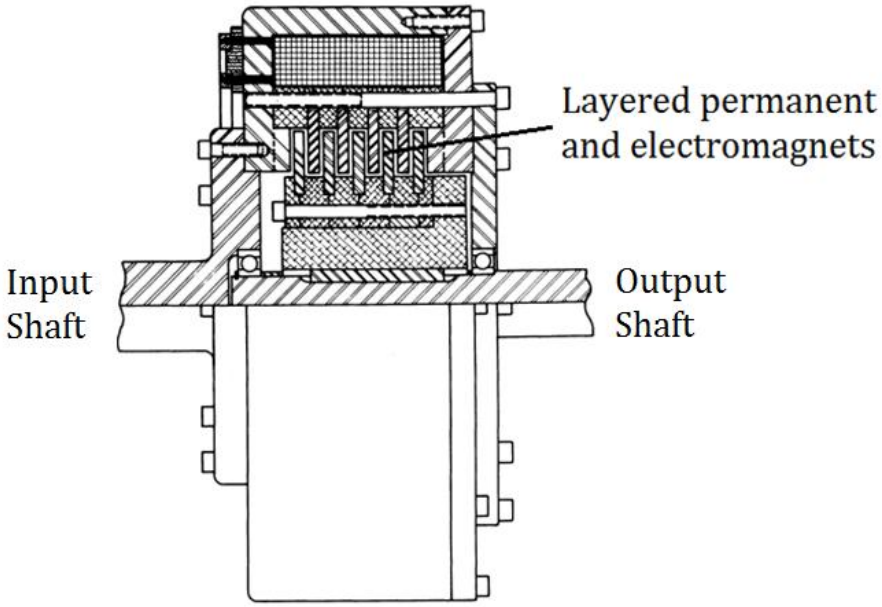

Figure 1.12: Hysteresis clutch cross section [19]

Switching is timed such that as the output shaft is accelerated to the speed of the input, it locks at zero relative angular velocity and 100% torque transfer. Though there is no contact between input and output, energy is still wasted when the clutch is in slip due to eddy currents produced by the electromagnet moving through the magnetic field of the permanent magnet.

Hysteresis clutches have the advantage of near instant full scale torque. However, the weight of the electromagnetic coil and permanent magnet increase as torque requirement increases. To provide a large connecting torque, the clutch must also be heavy and of large moment of inertia. A sampling of commercial hysteresis clutches provides an estimated mass per unit torque of 3 $\frac{kg}{Nm}$ with roughly linear scaling [20, 21]. As will be discussed in the body of this paper, torque in typical passenger vehicle applications is conservatively around 400 Nm. A magnetic clutch

of this capacity would have a mass of 1,200 kg. Because of this weight limitation, magnetic torque transfer is not a promising avenue for a high speed clutch with high torque transfer.

Interference

Interference clutches, more commonly referred to as dog clutches, use interlocking teeth which may be separated to disengage torque transfer [22]. The most common application of dog clutches is in manual automotive transmissions where dog-teeth connect and disconnect the different gears to their respective outputs. A simple example of a dog clutch is illustrated in Figure 1.13.

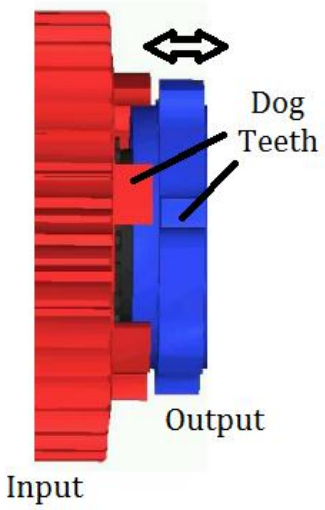

Figure 1.13: Dog clutch example. The blue disk is translated axially to bring the teeth on both disks into and out of interference [22].

Because dog clutches transfer torque via interfering features, no slip occurs and input is coupled to output near instantly. However, differences in input vs. output speed prior to engagement cause the teeth to impact when first coming into

contact, potentially violently. In a manual transmission, the unloaded gear to be engaged is accelerated up to the input speed by a device called a syncromesh utilizing a simple friction clutch. The dog teeth are then used to transmit full torque once there is no velocity difference. The dog clutch itself may only overcome differences in shaft velocity via impact. At the differential velocities typically seen in flywheel transmission applications, these impacts would incur tremendous stresses in the interlocking teeth and vibration throughout the system [22]. Because torque transmission via interference is not well suited to highly mismatched velocities, it is not a promising method for application in switch-mode systems.

Friction

The most common type of commercial clutch is the friction clutch, such as those used in manual automotive transmissions. In a friction clutch, the input is in physical contact with the output via a normal force applied by some actuating mechanism. This normal force may be generated mechanically, electromagnetically, or hydraulically. The friction between the two contacting surfaces, applied at a distance from the rotation axis, transmits torque. Figure 1.14 illustrates this, in a disk configuration.

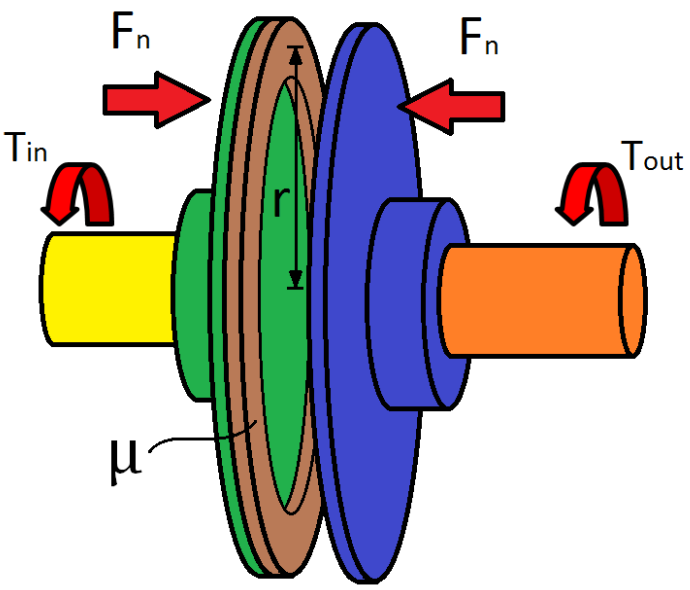

Figure 1.14: Friction disk style clutch

The torque transmitted via friction is given by:

$$T_f = F_n \mu r_f \qquad \text{Equation 1.1}$$

where F_n is the normal force applied to the friction surfaces, μ is the dynamic coefficient of friction between the friction surfaces, and r_f is the effective moment arm of the contact region. Towards the goal of maximizing torque, all three terms on the right side of the equation should be maximized. In practice, high friction composites are used to maximize μ, and r is maximized within packaging allowances of the application. Torque capacity is then limited only to the amount of normal force that can be applied. Efficiency and torque resolution are limited only by the speed at which the actuating mechanism reaches full scale normal force.

The engagement and disengagement speed of a friction clutch is dependent the on its actuation method. Many methods of actuation are employed in

commercially available clutches. However, as will be detailed in Section 2.2, no commercially available friction clutches meet the actuation speed demands of a switch mode system such as the SM CVT. This is identified as a gap in current technology. With a sufficiently high speed actuation mechanism employed, torque transfer via friction has the potential for high torque transfer in a compact, lightweight design.

1.3 Overview

It is the goal of this thesis to develop a clutch which meets the needs of the SM CVT in terms of torque resolution, efficiency, and controllability. Chapter 1 detailed the value of flywheel hybrid technology as an emerging area of research, with switch mode systems such as the SM CVT providing a potential solution to the energy transfer challenges innate to flywheels. A gap in the current performance of switching components – clutches - to meet actuation time needs of such systems is identified. Following in the thesis, Chapter 2 discusses the method of approach taken to develop a clutch to meet these needs in the context of the SM CVT. Derivation of task specifications via the creation of a vehicle-scale design case is described, followed by a review of concepts considered and the basic architecture of the chosen design. Chapter 3 gives detailed design and analysis towards the creation of a benchtop scale prototype. Experimental method and results are presented in Chapter 4, followed by concluding remarks in Chapter 5.

Chapter 2 - Method of Approach

This chapter explains the development of the clutch concept. Functional design requirements are first determined via the creation of a theoretical design case based on the performance needs of a hybrid passenger vehicle. Preliminary and final concepts to meet the defined requirements are then discussed.

2.1 Determination of Task Specifications

The clutch has three main requirements to meet the needs of the SM CVT: fast engagement and disengagement, high efficiency, and a method of duty cycle control. To bound the design space of the clutch, requirements and goals for the performance of the clutch must be determined. The following sections detail the derivation of these performance specifications.

2.1.1 Torque Resolution

An ideal clutch would mimic a theoretical switch, occupying one of two binary states, switching between the two instantly, and operating at infinitely high frequency. A clutch with these properties would allow for infinitely small discrete changes in the torque of the spring, and would approach a truly continuous analog power output. In reality, a physical clutch must contend with dynamics. The stiffness, damping, and inertia of the clutch components and the output load slow the speed with which the clutch can switch the system between its engaged and disengaged states. This results in discrete steps in torque output, and deviation from the intended functionality as a continuously variable transmission. It is therefore necessary to specify a goal for the torque resolution of the system, defined as:

$$R_T = \frac{\Delta T_{ts}}{T_{ts,max}} \qquad \text{Equation 2.1}$$

where ΔT_{ts} is the change in spring torque during a clutch pulse and $T_{ts,max}$ is the maximum torque output of the spring. A maximum torque increase of 5% over one pulse was decided to provide suitable resolution for preliminary research.

It is next necessary to understand the the relationship between the flywheel, spring, and clutch during operation. Figure 2.1 shows the simplified diagram of the SM CVT as introduced in Chapter 1 for reference.

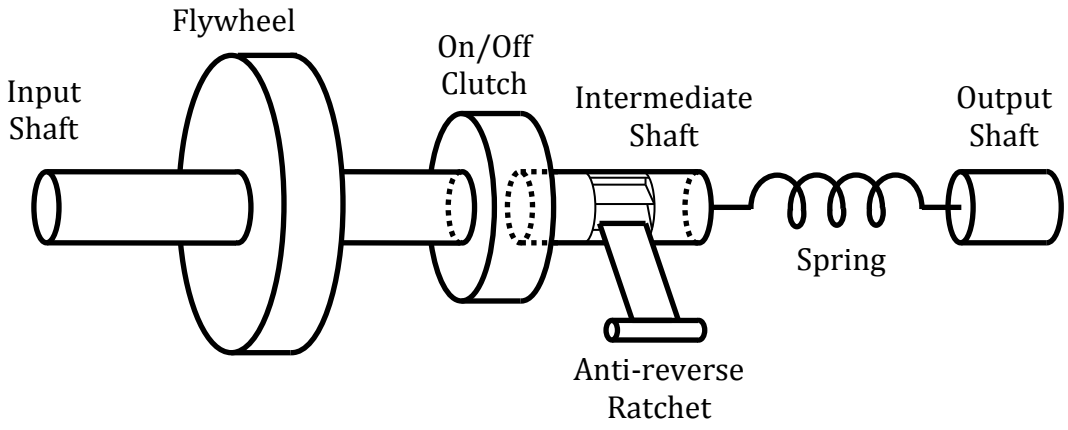

Figure 2.1: Simplified SM CVT Diagram

The change in output torque created by one clutch pulse is given by:

$$\Delta T_{ts} = K_{ts} t_p (\omega_{in} - \omega_{out}) \qquad \text{Equation 2.2}$$

where K_{ts} is the stiffness of the torsion spring, ω_{in} is the input angular velocity, ω_{out} is the output angular velocity, and t_p is the duration of a single clutch pulse. It can be

concluded that the case of highest demand on clutch speed for a given spring design is when the rate of angular deflection is highest, i.e. when the vehicle is at rest and the flywheel is at maximum angular velocity.

Importantly, this model assumes zero slip during engagement and disengagement, i.e. the clutch changes states instantly, but at a limited frequency. Consideration of clutch slip will be discussed later, but this simplified model is conservative for purposes of defining goals for pulse duration, as the spring is advancing at full input velocity for the entirety of the clutch pulse.

From Equation 2.2, the system parameters necessary to define the requirements for the speed of the clutch are apparent. Spring stiffness and maximum deflection, as well as maximum flywheel velocity determine the pulse duration requirements of the clutch. To quantify these parameters, a theoretical design case was considered in which the SM CVT serves as the auxiliary power source in a hybrid passenger vehicle. The design case attempts to assign values to the variables in Equation 2.2, and determine the minimum pulse time necessary to meet the torque resolution goal. The following sections discuss the creation of the theoretical flywheel and spring.

Flywheel

The chief function of the flywheel is to store regenerative energy from events such as braking or descending a grade. It is first necessary to determine a reasonable maximum value for the available energy from such events. For vehicle mass and dimensions, the second generation Toyota Prius was taken as a template. Produced from 2003 to 2009, this Prius model was one of the most commercially

successful hybrid vehicles in the US [23]. This gives a vehicle mass of roughly 1400 kg. The most extreme energy regeneration case is considered to be coming to full stop from highway speed, about 31.3 $\frac{m}{s}$ (70 mph). As all flywheel energy has ideally been spent once the vehicle is at high speed, the kinetic energy available is not considered to be cumulative in successive braking events. Given this mass and velocity, the kinetic energy available for storage is 686 kJ. The kinetic energy stored in a flywheel is defined as:

$$E_f = \frac{1}{2} I_f \omega^2 \qquad \text{Equation 2.3}$$

where I_f is moment of inertia of the flywheel and ω is its angular velocity. It is evident from Equation 2.2 that high angular velocity of the flywheel increases demand on clutch speed. Additionally, parasitic energy loss from the flywheel due to air resistance and bearing resistance is greater at higher speeds. It is therefore desirable to design a flywheel which allows for the lowest angular velocity satisfying the energy storage needs at an allowable space and weight. From Equation 2.3, it follows that moment of inertia should be maximized within fitment constraints which will be discussed.

Given stress considerations and the need for balancing, flywheels designs are typically cylindrical. Where there are limitations on mass and available space, such as the vehicular application of the SM CVT, designs are often hollow cylinders, with lightweight spoke features connecting a rotating ring of mass to a central shaft. Simplified geometry of the two designs is illustrated in Figure 2.2.

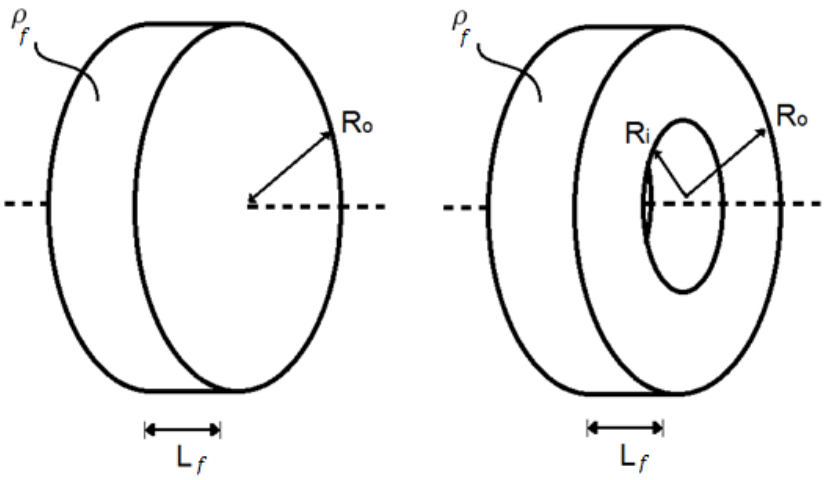

Figure 2.2: Solid and hollow cylindrical flywheels

The moments of inertia of the two designs are given by:

Solid:

$$I_{f,s} = \frac{1}{2} m_f r_o^2 \qquad \text{Equation 2.4}$$

Hollow:

$$I_{f,h} = \frac{1}{2} m_f (r_o^2 + r_i^2) \qquad \text{Equation 2.5}$$

where m_f is the flywheel mass, r_o is the outside diameter, and r_i is the inside diameter of the hollow design. Inspection of these equations shows the advantage of a hollow cylinder geometry. For a prescribed fitment envelope and mass – L_f, r_0, and m_f – the hollow cylinder allows for a larger value of I_f by use of higher density material at a greater distance from the axis of rotation. To quantify these values for a theoretical flywheel design boundaries are needed for mass and size.

From Equations 2.4 and 2.5 it is also shown however that the goal of minimizing ω is in opposition to maximizing energy density of the flywheel. To

make best use of space and weight, high energy flywheels typically operate at very high angular velocities, capitalizing on the higher order of this term. Efficient geometry and high performance composites are employed to keep weight down and increase strength, as material failure due to centripetal forces ultimately limits angular velocity [7]. Because it is the goal of this research to explore novel means of flywheel energy transmission rather than storage, energy density of the flywheel was considered secondary to minimizing the demand on clutch pulse duration while still meeting reasonable criteria for energy storage. To constrain the size of the flywheel towards the goal of maximizing I_f, the Prius was again looked to as an example.

As it is the goal of the SM CVT to be a competitive auxiliary power system for hybrid vehicles, it is desirable to specify a mass of the energy storage medium that is no more than current successful options. The Prius employs a battery for energy storage, with a mass of approximately 45 kg, and this was chosen as the upper bound for the flywheel mass [23]. It should be noted that the energy capacity of the Prius battery is much larger than that of the proposed flywheel, to allow for continued use of the auxiliary system at low speed with the engine switched off. Size should be no greater than can fit in the engine compartment of a typical passenger vehicle alongside the primary power source, and a cylindrical envelope of r_0 = 0.4m and L_f = 0.1m was chosen as a reasonable value. Steel was chosen as a candidate material, having high density (7850 $\frac{kg}{m^3}$), low cost, and good manufacturability. The mass of the hollow ring geometry is given by:

$$m_f = \rho_f L_f \pi(r_o{}^2 - r_i{}^2) \qquad \text{Equation 2.6}$$

It should be noted that this is a simplified design, in a physical execution spoke features would need to be considered in the mass and MOI calculations, but as these may be of small dimension, low density composites, and have mass centers closer to the rotational axis, their contribution was considered negligible. Solving Equation 2.6 for r_i given the chosen design case values gives an inner diameter of 377mm. Solving Equation 2.5 using these values gives a resultant MOI of 6.80 kgm^2. Figure 2.3 illustrates this design roughly to scale against an example vehicle. An important consideration is that flywheels in vehicle applications are most commonly mounted with the rotation axis vertical, to avoid gyroscopic effects when cornering. This requires a 90˚ change in rotation axis to drive the front wheels. This can be accomplished without penalty however via the ring and pinion gears of the differential, which are necessary drivetrain component.

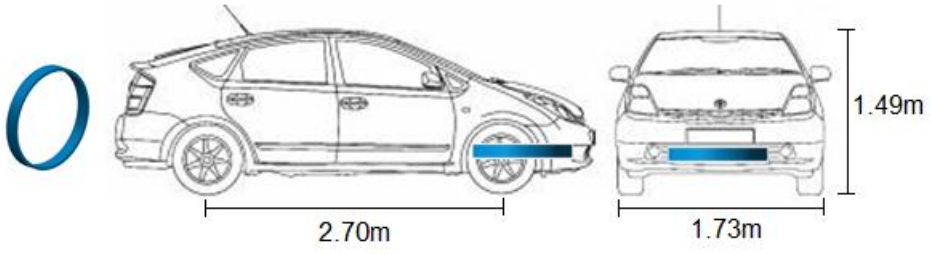

Figure 2.3: Design case flywheel size comparison to a Toyota Prius. Vehicle image and dimensions from [24].

With a flywheel design proposed and a theoretical MOI established, Equation 2.3 can be solved for minimum angular velocity necessary to achieve the specified energy storage. The resulting angular velocity is 449.2 $\frac{rad}{s}$ (4290 rpm).

Spring

The torsion spring of the design case is considered to have constant stiffness and thus the relationship between angle of deflection and applied torque is defined as:

$$T_{ts} = K_{ts}\Theta_{ts} \qquad \text{Equation 2.7}$$

with θ_{ts} representing the angle of deflection of the spring. The primary function of the spring is to provide auxiliary driving torque to the vehicle apart from the ICE. A common method of managing the two power sources used in regenerative braking hybrids is to use the energy storage system to accelerate from rest to a threshold speed (about 15 mph for the Toyota Prius) after which the ICE takes over. This allows the ICE to run in a narrow, efficient power band. It also allows the ICE to be smaller, as it does not need to handle acceleration from rest. A power split device is often used which allows the two power systems to run independently in series, or together in parallel, each providing a complimentary fraction of the total output power [5]. A power split architecture is considered to be employed in the design case.

The torque required of the spring as the auxiliary driver should be competitive in performance with successful hybrid vehicles. The torque output of the Toyota Prius electric motor is approximately 400Nm [23], and this was chosen to be the maximum torque specification of the torsion spring. It is important to note that while the output of the Prius motor is 400Nm, due to the CVT transmission and differential, the motor torque is increased by a drive ratio of up to 3.46:1 at the wheel. Static gearing to increase the final drive ratio of the theoretical vehicle in the design case would be necessary to match this final torque at the wheel, through either the differential or a dedicated reduction gearset. However, as the SM CVT acts as both auxiliary motor and transmission, the output of the Prius motor serves as a benchmark for the output torque prior to static reduction. With this value known, and a torque resolution goal of 5%, the maximum allowable torque increase over one clutch pulse is found to be 20 Nm.

A reasonable maximum deflection capacity of the theoretical spring is not trivial to quantify. There are many possible designs imaginable for a torsion spring for the SM CVT, and this was in fact an area of parallel research by other students [17]. A goal of the spring design is to provide for a high allowable deflection. This is made clear by dividing both sides of Equation 2.1 for torque resolution by the spring stiffness K_{ts}, giving angular resolution:

$$R_\theta = \frac{\Delta\theta_{ts}}{\theta_{ts,max}} \qquad \text{Equation 2.8}$$

where $\Delta\theta_{ts}$ is the change in spring deflection during one clutch pulse and $\theta_{ts,max}$ is the maximum allowable spring deflection. Maximizing the deflection capacity of the spring reduces the percentage change in torque with each pulse, increasing the resolution of the system. It should however also be noted that increasing the total deflection of the spring increases the time for the spring to switch torque states from driving to regeneration for a given vehicle speed, a competing constraint to be considered in future spring design. Early design work by the original SM CVT design indicated that deflections above 2.09 rad (120˚) were difficult to achieve [17]. Though research into high deflection torsion spring options may yield higher values, this was taken as a conservative upper bound for the spring deflection. With these values specified, Equation 2.7 gives a stiffness value of K_{ts} = 191.4 $\frac{Nm}{rad}$.

Clutch Pulse Duration

With the theoretical flywheel and spring created, Equation 2.2 may be solved for minimum necessary pulse duration of the clutch, occurring under the most demanding scenario of maximum flywheel angular velocity and zero vehicle velocity. In this case:

$$\Delta T_{ts} = 20\ Nm$$

$$K_{ts} = 191.4\ \frac{Nm}{rad}$$

and

$$\omega_{in} - \omega_{out} = 449.2\ \frac{rad}{s}$$

The minimum necessary time for the clutch to complete one full engagement and disengagement cycle under worst case conditions while maintaining a 5% torque resolution is then approximately 0.23 ms. As will be detailed in Section 2.2, no commercial clutches were found to achieve nearly this speed of actuation at the required torque.

2.1.2 Efficiency

As stated previously, the model used to determine clutch pulse duration assumes instant change in state of the clutch. This is a conservative model for determining minimum clutch pulse duration, as the spring will advance at full input speed for the entire pulse. However, for consideration of efficiency, this model is invalid. In reality, a clutch cannot couple the input and output shafts instantaneously. Under the common case of the input having greater angular velocity than the output, a period of acceleration is required. In addition to these dynamics, a physical clutch requires a means of actuation to connect the input and output, which is not instantaneous. The connecting torque builds from zero to full scale over some finite time period. As a result of the mismatched input and output dynamics as well as the time required to build full engagement torque, every physical clutch has a slip period where the input and output are interacting but still have relative motion. This relative motion wastes energy to heat. Depending on the type of clutch this may have different physical manifestations, as discussed in Section 1.2.4, but in all cases energy is expended in the transient period where dynamic inequality between input and output is resolved.

In high efficiency systems such as the SM CVT, the energy waste due to clutch slip must be minimized. This can be aided by minimizing accelerated inertia and time to full scale torque, but energy waste cannot be eliminated altogether. Additionally, the flywheel and spring will incur internal losses. However, as loss in these passive components is due to bearing and material damping which can be designed to be very low, clutch loss is expected to be the driving component of total SM CVT efficiency.

Because energy waste can never be eliminated completely, efficiency goals must be specified. Efficiency is considered to be the energy transferred to the output divided by the energy taken from the input. To set a goal for efficiency, the efficiency of current electric regenerative braking systems was looked to as a benchmark. The efficiency of an electric auxiliary system's regeneration cycle varies with operating conditions, but is typically 25-35% [25]. This considers the reused energy after both the energy storage and retransmission processes have occurred in series, and is the product of the efficiencies of both processes individually. To determine the average efficiency of each process, the square root of the median efficiency of 30% was taken, giving a resulting one way transfer efficiency of 55%. Additional losses that will occur in the SM CVT from other components should be small in comparison to the clutch, but unlikely negligible. As such, an efficiency goal of 70% was set for the clutch, to allow for additional system loss while remaining competitive with established hybrid technologies.

2.1.3 Control Method

In addition to operating speed and efficiency, the clutch must afford a method of pulse modulation to control its duty cycle. As previously stated, duty cycle is the fraction of time the clutch is engaged vs. total time. For the SM CVT, controlling duty cycle controls the average angle of advancement of the spring, and thus the average driving torque. The clutch must be capable of 0% duty cycle, in which case it is continuously disengaged, to allow the flywheel to spin freely when connection to the output is not necessary. This occurs when the vehicle is at rest or cruising without need of additional driving torque, and when the flywheel is at rest. Considering the upper bound of duty cycle, the clutch could theoretically operate at 100% duty cycle, where the flywheel is continuously locked to the output. However, this could only occur for a very short duration when the flywheel speed is very near the output speed. As shown in Equation 2.3, the energy storage of the flywheel increases with the square of angular velocity, and so the majority of flywheel energy has been spent once the flywheel slows to speeds approaching the output. As such, maximizing duty cycle maximizes the energy which may be extracted from the flywheel, but has diminishing returns with higher duty cycles. The clutch should have a duty cycle range from 0% to at least 50% to make use of the highest energy range of flywheel velocity.

Given the duty cycle control needs, two pulse modulation techniques typically employed in the electronics world offer viable solutions, pulse width modulation (PWM) and pulse position modulation (PPM). Figure 2.4 illustrates the two.

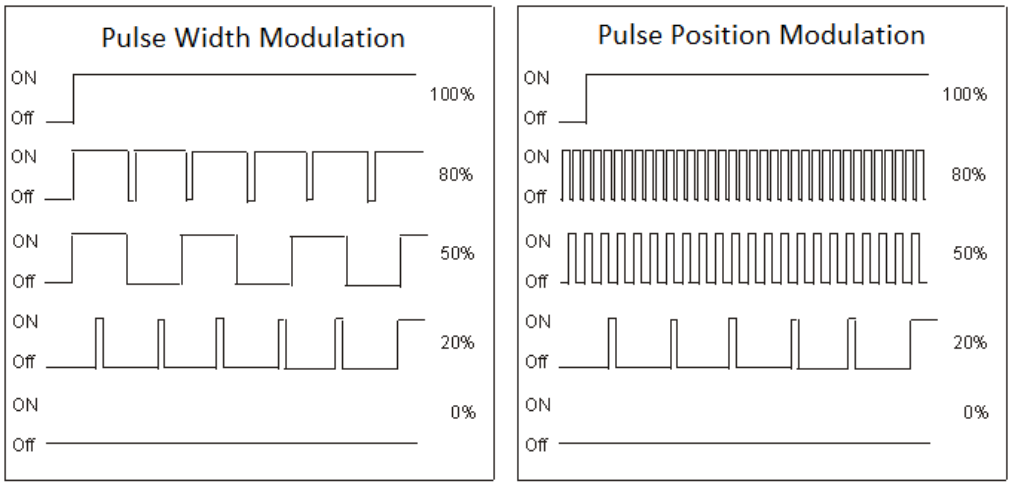

Figure 2.4: Pulse Width and Pulse Position Modulation comparison across a range of duty cycles. Adapted from [26]

In PWM, the frequency of pulse events remains constant, and the duration of time spent "on" within a single period is varied to control duty cycle. In PPM, the duration of all pulses is constant, and the frequency of pulses is varied to control duty cycle [12]. Because energy loss occurs during switching, it is desirable to minimize the number of pulses necessary while still maintaining the goal torque resolution. Which method utilizes the least pulses depends on the application. For a given PWM frequency and PPM pulse duration, there will be a single duty cycle at which the two methods give the same response. In the arbitrary signals of Figure 2.3, this occurs at a duty cycle of 20%. At duty cycles above this point of similarity, PWM requires fewer pulses, while at lower duty cycles, PPM requires fewer. Depending on the achievable frequency and minimum pulse duration of a clutch concept, either method may be valid. If possible, both should be considered to find the control method which offers the least possible switching of states.

2.2 Concepts

With performance specifications for efficiency, torque resolution, and method of control defined, concepts for the physical execution of the clutch were explored. As discussed in Section 1.2.4, friction was identified to be the most promising method of torque transfer in high speed, high torque, and low weight applications. Commercial friction clutches are primarily differentiated by the method used to produce the connecting normal force between the friction surfaces. This is the actuation method of the clutch. This section discusses the methods of clutch actuation considered across the fluid, electromagnetic, and mechanical energy domains, and details the basic architecture of the chosen concept.

2.2.1 Fluid

Hydraulic and pneumatic actuators produce force by exposing a piston travelling in a sealed cylinder to the pressurized fluid. Double acting actuators switch which side of the cylinder is pressurized to allow for both pushing and pulling, allowing for engagement and disengagement in a clutch application. In a pneumatic or hydraulic clutch, high pressure fluid chambers apply closure force to friction disks, working very similarly to an actuator. Though they are capable of very high torque transfer, movement of the fluid through inlet and evacuation passages tends to limit actuation speed, with pneumatic actuators typically faster than hydraulic due to lower fluid inertia and viscosity. Commercial pneumatic actuators typically have a response time - defined as the time elapsed from receiving a control signal to reaching full pressure - of greater than 0.1s [27 , 28]. This value increases in applications where large force and thus piston areas are needed. Due to this

latency in pressure buildup, fluid actuation - mature in industry - is not promising for this application.

2.2.2 Electromagnetic

Electromagnetic solenoids produce force via attraction and repulsion of a permanent magnet to an electromagnet. Electromagnetic clutches use this attraction and repulsion to engage and disengage friction disks. Due to the large coil sizes needed to produce normal force, electromagnetic clutches require on the order of 10ms to reach full current even with optimization [29]. Coupled with the time taken to accelerate the moving friction disk and close the air gap, time to full friction may take on the order of 50ms [30]. These benchmarks come from clutches with lower torque capacity than that required of the SMCVT. Because of this latency, electromagnetic actuation, also mature in industry, was deemed an undesirable method for this application.

2.2.3 Mechanical

In the mechanical domain, springs are used to provide force. As this force is proportional to deflection, controlling spring force becomes a problem of controlling displacement. Steel springs can be designed to be extremely stiff, with large force generated by only a small displacement. This allows for a smaller package size, and more importantly reduced travel needed of moving parts, increasing actuation speed. Friction clutches with mechanical actuation are employed in most manual vehicle transmissions, where springs are used to connect the friction disks and the operator may disconnect the disks via a cable or linkage attached to the clutch

pedal. Use of displacement controlled spring force in a high speed, cycling clutch however is largely unexplored.

Because clutches must often be engaged at irregular intervals due to system feedback or human input, the flexibility of pneumatic or electromagnetic actuation with electronic signaling is often advantageous. However, where consistent, high speed, high precision, and / or high force motion is required such as in industrial assembly applications, mechanical actuation via either cams or linkages offers unmatched performance [31]. The drawback, however, is that mechanical actuation, often relying on a constant speed rotating input and contending with significant inertia, offers limited flexibility to vary timing or respond to an irregular control signal. Developing a means to actuate the clutch with the speed and precision of a cam or linkage, while incorporating a means to quickly change duty cycle, offers a potential solution.

Because a clutch is by nature mounted to a rotating input shaft, there is potential to capture this rotation as the input to the actuating mechanism. In the context of the SM CVT, the flywheel can be used to provide timing and energy for the clutch pulses. As the energy used to compress the spring is stored as potential energy, it may also be transferred back to the flywheel during disengagement depending on the design of the displacement producing mechanism. Additionally, by utilizing the flywheel to provide energy for both vehicle motion and spring compression energy, the need for an auxiliary power source for the clutch – a battery, fluid pump, or motor - is avoided.

To provide normal force with a variable duty cycle, the actuating mechanism must control the period of time spent in “dwell” – defined as the portion of the mechanism’s cycle where the end effector has no motion - with the clutch spring at full compression. Several concepts were considered to achieve this. A common method to achieve dwell in a linkage design is to utilize a four-bar mechanism with a coupler curve having a portion which is of near constant radius, a “pseudo arc”, and adding an additional dyad connected to the coupler point [32]. Figure 2.5 illustrates an example linkage and the coupler curves associated with several points on the coupler link (a), and the creation of a dwell mechanism by adding a crank-slider type dyad (b).

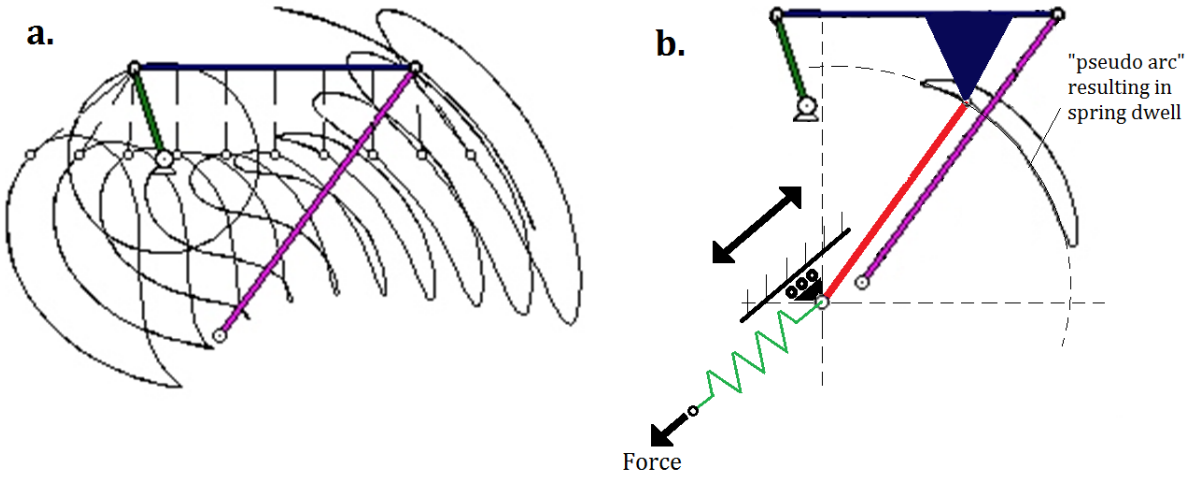

Figure 2.5: Example four bar coupler curves generated from various control points on the coupler, illustrating near constant radius portions (a). Dwell mechanism created by adding a crank-slider type dyad to the coupler point of a desired curve (b). [33]

To control the duration of the dwell and thus the duty cycle, the length of the near constant radius portion of the coupler curve must be modified during operation. This could possibly be done by changing the position of the coupler point or changing the pivot position of a link via a translation stage, or using a telescoping link to achieve a variable link length. It is likely however that designing the “pseudo

arc" to change length while maintaining the same center point would be difficult, especially in consideration of the need for a large range of duty cycles. Though this concept was seen to have some potential, the logistical difficulties warranted exploration of other actuation concepts.

In addition to linkages, cams are commonly used for precise, high speed mechanical actuation. Cams are not typically used in applications which require variability, as the cam profile is machined into solid material, and does not easily facilitate in-use changes. A notable exception to this is a type of variable valve timing employing a cam profile which varies along the cam's rotation axis. The camshaft is shifted back and forth, changing the profile seen by the follower, and varying the position, duration, and amplitude of valve opening. This is illustrated in Figure 2.6.

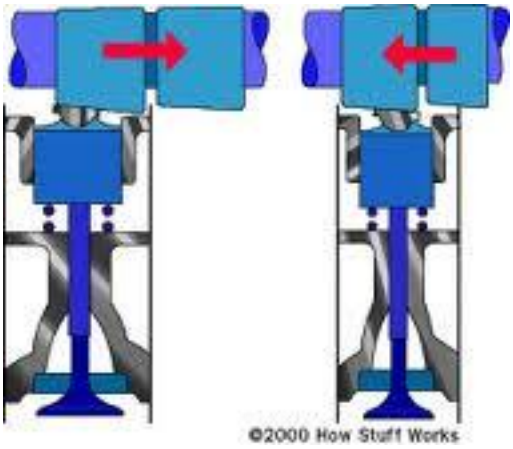

Figure 2.6: Variable valve timing example [34]

For purposes of the SM CVT clutch, a variable profile cam with a short high dwell duration at one end and a long high dwell duration at the other could be employed. The operator would then shift the position of the follower along the cam's length to control duty cycle. However, if a radial cam such as that used in the valve timing example were employed, the direction of motion would be orthogonal

to the shaft axis. Because the desired direction of normal force used to engage the clutch is parallel to the rotation axis, per Figure 1.14, an additional linkage would be required to redirect the displacement from the cam. However, this is avoided by instead using an axial cam, which produces follower displacement parallel to the rotation axis. Figure 2.7 shows an example double dwell axial cam. An additional advantage of an axial cam is that it allows the input shaft to serve as the cam shaft, with cam rotation provided by the flywheel.

Figure 2.7: Double dwell axial cam [35]

To vary duty cycle of an axial cam, the duration of the high dwell must change radially. The operator would correspondingly shift the position of the follower radially. In order to have a linear relationship between radial follower position and duty cycle, the length of the high dwell must increase following a spiral curve of the form $r = \theta$. Thus, a 10% increase in radial position of the follower corresponds to a 10% increase in duty cycle. Figure 2.8 illustrates such a cam design. The follower travel and cam rotation axes are normal to the page plane. Several radial positions of the follower are shown in red, at 10%, 25%, and 50% duty cycle. As the cam rotates, the follower rises to high dwell at the green line, and falls to low dwell at the

blue line. It should be noted that a transition section is necessary between the high and low dwells which is not represented in the figure; the design of the transition profiles will be discussed in the following chapter.

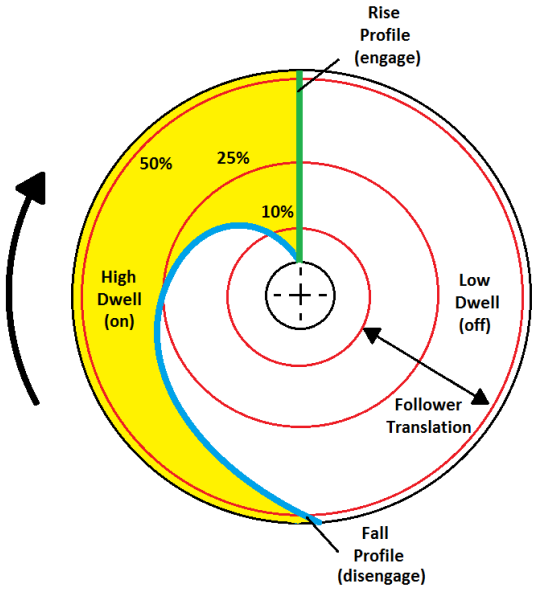

Figure 2.8: Variable duty cycle axial cam diagram

Use of a cam which rotates with the flywheel offers an important control advantage in that there is implicit mechanical timing. If an electromagnetic or pneumatic clutch with an auxiliary power source were used, controlling the advancement of the torsion spring with each pulse would require active sensing and computation to ensure proper clutch engagement duration at a given flywheel speed. This adds additional complexity and failure modes. In a cam driven design, because and the clutch is engaged only when the cam is in high dwell, the advancement of the torsion spring is known directly, and is equal to the high dwell duration at a given radial follower position. The duty cycle of the clutch is controlled by a single degree of freedom, the radial translation of the follower.

A clutch using friction disks and a variable profile axial cam for actuation has the potential for high speed actuation, high force generation, and high efficiency. Additionally, variable profile axial cams and mechanical duty cycle control via cams are promising and largely unexplored areas. For these reasons, this method of actuation was pursued. Figure 2.9 illustrates the basic architecture of the final clutch concept.

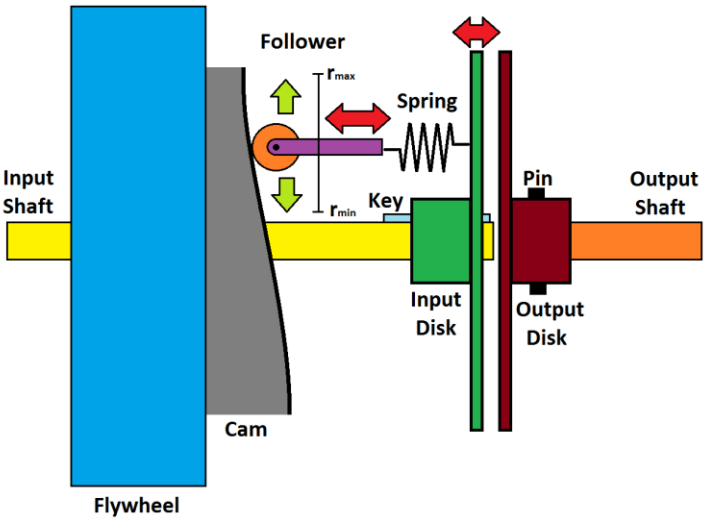

Figure 2.9: Final clutch concept

The following chapter presents the detailed design and analysis of this concept towards the creation of a scaled prototype.

Chapter 3 - Detailed Design and Analysis

This chapter describes the design of the clutch towards the goal of a scaled benchtop prototype. The power scale of the prototype is defined, followed by description of the components and operation of the system. Analysis informing the design is also detailed. Part drawings are presented in Appendix A.

3.1 Prototype Scale

For benchtop experimental testing, a prototype of less power than a full scale vehicle application was desirable in consideration of cost, time, and safety. A maximum speed of 105 $\frac{rad}{s}$ (1000 rpm), approximately 24% of the design case, was chosen to provide a good basis for investigating the dynamics of the clutch. A maximum torque of 70 Nm, approximately 18% of the design case, was chosen as a good basis to investigate the effect of torque load on clutch slip and overall efficiency.

An important additional factor in choosing the maximum torque capacity was the relationship between torque, normal force, and overall size of the prototype. As given in Chapter 1, the torque transmitted by a friction disk style clutch is:

$$T_f = F_n \mu r_f \qquad \text{Equation 1.1}$$

where F_n is the normal force applied to the friction surfaces, μ is the dynamic coefficient of friction between the friction surfaces, and r_f is the effective moment arm of the contact region. Increasing torque is accomplished by increasing any of

the parameters on the right side of the equation. Following inquiries of high friction composite material vendors, a maximum value dynamic coefficient of μ = 0.49 against steel was seen among materials with capacity for machining. The exact material chosen will be detailed later in this chapter. Increasing the contact radius r_f is an effective means of increasing torque, but also incurs increases in the size of the input and output disk, as well as other components that will be detailed in this chapter. This increases the MOI of the output which must be accelerated during engagement, and also the mass which must be displaced by the cam. Additionally, the limited available space in the engine compartment of a vehicle - and in the lab - dictates that the disks should be of reasonably small radius. A contact surface with an outer radius of 76.2mm (3") and inner radius of 63.5mm (2.5") was chosen as a compromise, and a convenient size for lab scale testing. This gives a mean contact radius of r_f = 69.85mm (2.75").

With the friction coefficient and radial size of the clutch constrained, the torque which may be produced is limited only by the normal force which is created through spring compression. For safety reasons, and to limit the structural demands on the components of the prototype, the amount of stored spring energy must be practical. A torque value of 70Nm gives a total spring force of 2045 N (460lb) through Equation 1.1, considered to be a good compromise of safety, component loading, and torque range to be investigated. The following sections detail the design of the clutch's individual components to meet the defined performance goals.

3.2 Cam

This section describes the creation of the prototype axial cam with radially varying profile. Definition of the follower transition profiles is detailed, as well as the modeling of the cam.

3.2.1 Profile Definition

It is the function of the cam to provide compressive spring displacement, forcing the input disk against the output disk. Conveniently, the compressive spring used to provide normal force for the friction disks serves a second purpose by providing the closure force between the follower and the cam. An issue arises in that a single follower and spring acting at a varying radius from the central shaft would provide imbalanced force to the input disk, creating localized engaging normal force and potential binding as the disk translates along the shaft (Figure 3.1a). Ideally, an evenly spaced array of springs with equal radial position would act on the input disk, approximating a uniform distributed loading (Figure 3.1b). In compromise, three followers and springs are used to constrain planar motion of the input disk and distribute normal force (Figure 3.1c).

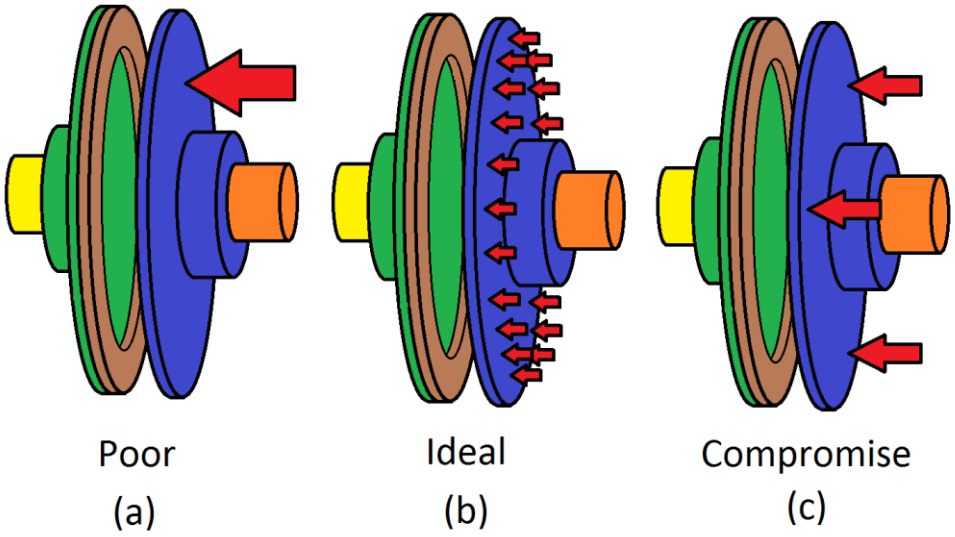

Figure 3.1: Follower and spring locations

Use of three followers necessitates a cam with three high dwells per revolution. The cam function is a "double dwell", in which the cam profile has 4 sections: a low dwell, rise transition, high dwell, and fall transition. Figure 2.7 of the previous chapter illustrates an axial cam of this type. Figure 3.2 illustrates these features on an example profile.

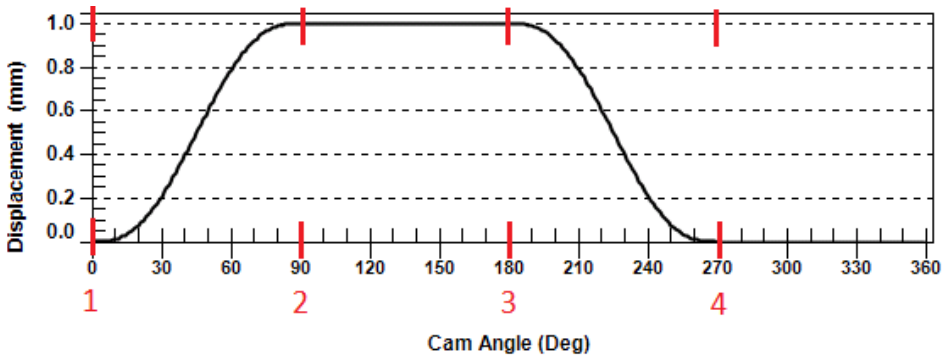

Figure 3.2: Double dwell cam profile. Section 1-2 is the rise transition, 2-3 the high dwell, 3-4 the fall transition, and 4-1 the low dwell. In this example, each section is 90˚, and the rise height is 1mm.

With 3 followers, the actual cam has 12 sections, 3 identical double dwell sets. In the dwells, the position is either high or low, and the velocity and acceleration of the follower is zero. The transition profiles must increase or decrease the position of the follower between these dwells. The motion of the follower is prescribed by the geometric profile of the transition section, and must maintain continuity through the second derivative of position. There are several methods for defining a double dwell cam profile [31]. Simple harmonic, modified sine, modified trapezoid, and cycloidal profiles all start by defining a continuous acceleration profile and modifying amplitude to reach the desired position change. Each method has benefits and drawbacks with respect to maximum acceleration and velocity occurring within the transition. A different technique, which is a good compromise of peak acceleration and velocity amplitude, is defining a high order polynomial based on the boundary conditions necessary for smooth follower motion. This method was employed in the design of the prototype cam.

Given that the transition sections must join to the zero velocity and acceleration dwells, the boundary conditions for the defining polynomial are:

Rise:

$$s_1 = 0, s_2 = h$$

$$v_1 = 0, v_2 = 0$$

$$a_1 = 0, a_2 = 0$$

Fall:

$$s_3 = h,\ s_4 = 0$$

$$v_3 = 0,\ v_4 = 0$$

$$a_3 = 0,\ a_4 = 0$$

Where s is the follower displacement, v is the follower velocity, a is the follower acceleration, and h is the total rise height of the cam, the maximum value of s. The subscripts correspond to the start and end points of the profiles, per Figure 14. These conditions are met by a fifth order polynomial, known in cam design as a "3-4-5" polynomial [31]. The displacement definitions for the rise and fall profiles are given by:

Rise:

$$s = h[\ 10\left(\frac{\theta}{\beta}\right)^3 - 15\left(\frac{\theta}{\beta}\right)^4 + 6\left(\frac{\theta}{\beta}\right)^5\ ] \qquad \text{Equation 3.1}$$

Fall:

$$s = h[1 -\ 10\left(\frac{\theta}{\beta}\right)^3 + 15\left(\frac{\theta}{\beta}\right)^4 - 6\left(\frac{\theta}{\beta}\right)^5\ ] \qquad \text{Equation 3.2}$$

where θ is the angular position within the rise section and β is the total angular duration of the rise section. During rise, as θ approaches β from start to end of the section, the term $\frac{\theta}{\beta}$ increases from 0 to 1, and the displacement increases from 0 to h. Conversely, the fall decreases from h to 0. To minimize slip, the duration of the transition section β should be as short as possible. However, three factors limit the

minimum length of the transition. For a given rise height h, decreasing β has the following effects, illustrated in Figure 3.3.

1. The acceleration, a, required to displace the follower increases, leading to potential "jump", where the follower leaves the cam surface due to inertial forces. This occurs in the case that return spring force is less than required to decelerate the follower train to its rest position in the high dwell. Designing a follower train of small mass aids in mitigating this.
2. The minimum radius of curvature in the cam profile, ρ, decreases. The follower cannot be of larger radius than the minimum radius of curvature of the profile it follows. This leads to a small follower with high contact stress, increased wear, and reduced structural capacity to carry spring load.
3. The maximum pressure angle, ϕ, the angle between the direction of follower travel and the contact force vector normal to the cam surface, increases. This reduces the useful force component compressing the spring and increases the bending load on the follower. A guideline for cam driven machinery is to design for pressure angles below 30° [31].

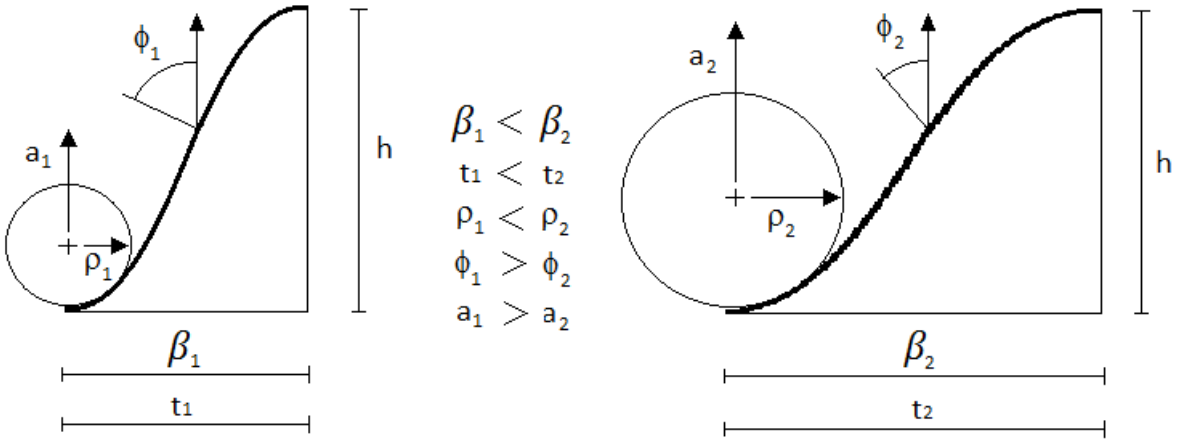

Figure 3.3: Effect of transition length β on duration t, acceleration a, minimum radius of curvature ρ, and pressure angle Φ

These relationships also hold true when β is held constant and h increases, however the value of h does not affect slip as the time to full spring compression and decompression is dependent only on transition length and angular velocity. The value of h can in theory be extremely small, coupled with extremely stiff springs to achieve the required normal force. In reality, several factors limit the minimum value of h. Firstly, an air gap is needed to provide clearance between the clutch disks in the disengaged state. Secondly, in practice, small deflections and stiff components amplify manufacturing error, leading to performance that can deviate from the design intent. Large travel and softer components allow for a more compliant system with less sensitivity to build tolerances and operational variation. Additionally, as the springs increase in stiffness, they will eventually approach the stiffness of other system components. The springs will no longer be the driving component of normal force, making tuning difficult. For purposes of the prototype, ability to adjust the system via the springs is advantageous, and so a compromise

between large spring travel and small rise height was needed. A rise height of 3.175mm (0.125”) was chosen as a reasonable value based on available springs. This is comprised of 2.54mm (0.1”) of compressive spring travel and 0.635mm (0.025”) of disk clearance. External constraints also bound the design of the follower tip radius. A follower tip that is too small will be incapable of supporting the normal forces required and will cause high wear on both the follower and cam, and so a compromise between minimum ρ and large follower tip radius was needed. A follower tip radius of 3.175mm (0.125”) was chosen as a reasonable value. Spring and follower design will be further detailed in the following section.

Minimum radius of curvature and maximum pressure angle of the profile are affected by the size of the cam in addition to h and β, however dynamics are not. Reducing the radius of an axial cam has the same geometric effect as reducing β, “compacting” the profile as in Figure 3.4. However, at the same angular velocity, the transition sections will have the same time duration regardless of radius from the rotation axis, and so follower dynamics are unchanged.

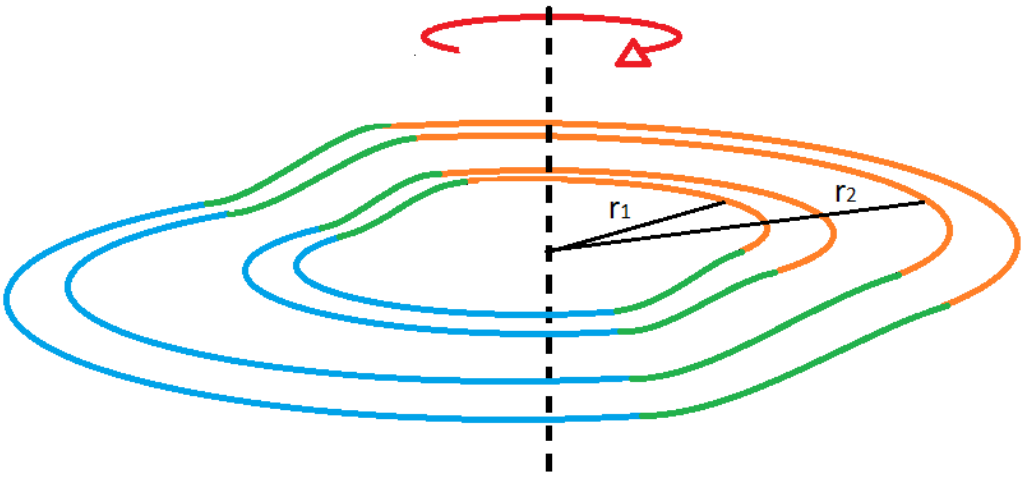

Figure 3.4: Cam profile at differing radii. At smaller radii (r_1), the transition sections (green) have an effectively shorter length, decreasing minimum radius of curvature and increasing maximum pressure angle. However, for a given angular velocity, the time taken to traverse the transition profile at any radius is constant, and so acceleration and resultant follower train dynamics are also constant.

A typical axial cam profile is designed at a single, specific radius from the rotation axis. The prototype axial cam with varying profile is designed to have a continuous range of radii between a minimum and maximum value r_{min} and r_{max}. As illustrated in Figure 3.4, the worst case values of ρ and ϕ occur will occur at r_{min}. Therefore, increasing r_{min} allows for a shorter transition duration β for the same constraints on ρ and ϕ. Additionally, radial space must be allowed for the input shaft and follower bearing components, which will be detailed in later sections. However to increase the linear travel resolution - and thus duty cycle resolution - of the followers as they move between r_{min} and r_{max}, and also decrease total package size of the cam, a large value of r_{min} is undesirable. As such, compromise is again needed. A value of 30.16mm (1.1875") for r_{min}, and 80.96mm (3.1875") for r_{max} were chosen as reasonable dimensions for the prototype design.

With these values known, the cam design software Dynacam was used to determine a minimum transition length β which meets the design constraints. A value of $\beta = 20°$ gives:

1. Minimum radius of curvature ρ = 6.30mm (0.25”). This allows for the desired follower tip radius of 3.175mm.
2. Maximum pressure angle ϕ = 28.2°. This is within the recommended maximum of 30°.
3. Maximum acceleration a = 1.61E^6 $\frac{mm}{s^2}$ occurring at $\frac{\theta}{\beta}$ = 0.75 and s = 2.38mm. As will be detailed in Section 3.8 on system stiffness, this magnitude of acceleration will not cause the follower to leave the cam surface.

3.2.2 Modeling and Manufacture

To model the rise section of the cam, several planar profiles were created in Solidworks at even intervals, centered on a straight line from r_{min} to r_{max}, with each profile corresponding to the increased radius at each interval. The complete three dimensional rise profile was created via a “loft” feature through the template profiles.

The fall section employed a similar method, however instead of the template profiles being centered on a straight line, it is centered on a spiral curve defined in polar coordinates r and θ by:

$$r = r_{min} + (r_{max} - r_{min})\left(\frac{\theta}{\beta_{dwell,max}}\right) \qquad \text{Equation (3.3)}$$

where the term $\beta_{dwell,max}$ indicates the maximum high dwell duration. Figure 3.5 illustrates the resulting shape of the fall segment, as well as the 2 dimensional profiles used to create both the rise and fall. By centering the fall profile on this curve, as the followers are translated radially from r_{min} to r_{max} the duty cycle of the clutch increases linearly from minimum to maximum. It should be noted that the template profiles would ideally follow the curvature of their given radial position, however limitations in the CAD software allowed only planar profiles to be created, leading to minor chordal error.

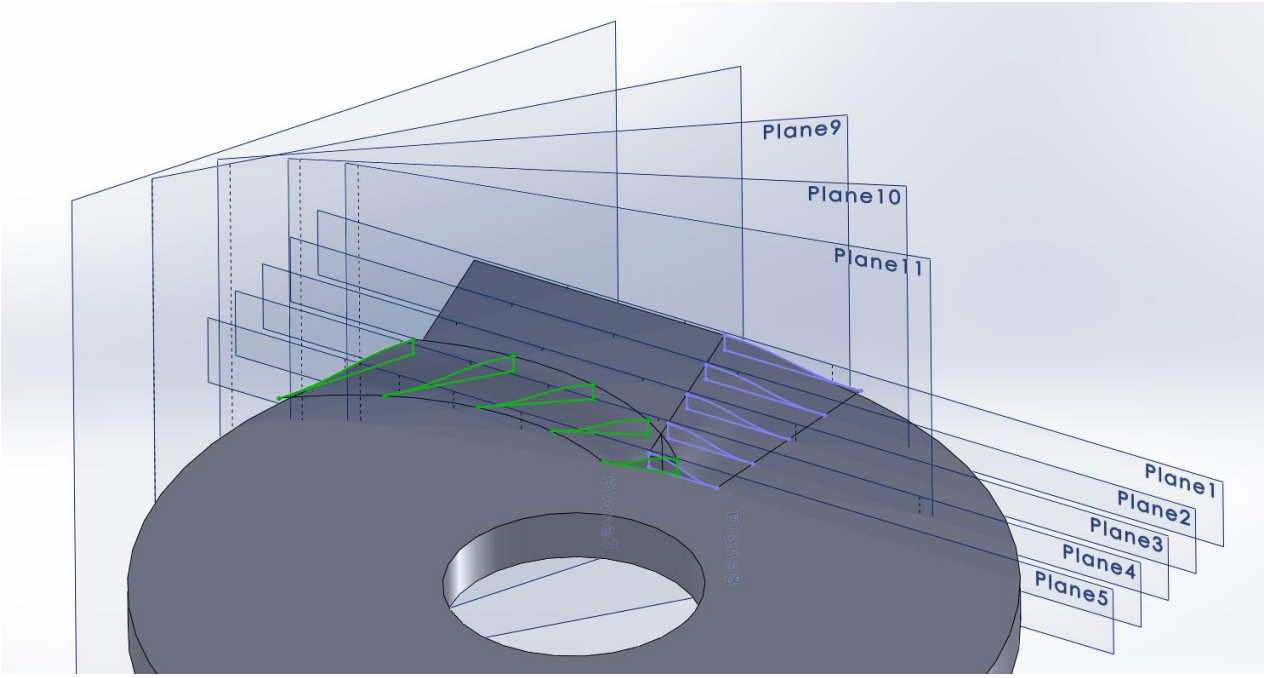

Figure 3.5: Modeling of rise (blue) and fall (green) sections. The full three dimensional profiles are created by connecting planar template profiles at evenly spaced radial positions. The blue rise profiles follow a straight radial line, while the green fall profiles follow a spiral to increase high dwell duration with radial position.

Given that there are 3 high dwells per rotation of the cam, the maximum duty cycle will be equal to $3\beta_{dwell,max}$ / 360°. As can be seen in Figures 3.5 and 2.10, as $\beta_{dwell,max}$ increases, the direction of the tangent vector to the spiral becomes closer to

circumferential. This creates an additional force on the follower tip in the radial direction, in addition to the axial force and circumferential forces present in a typical axial cam. This additional force limits the maximum duty cycle that may be achieved by the cam. A duty cycle of 50% was chosen as a compromise between capturing flywheel energy as detailed in Section 2.1.3 and limiting the radial force on the follower. This duty cycle corresponds to a maximum dwell duration of $\beta_{dwell,max} = 60°$. In addition, because load on the follower is less during fall than rise, applying the spiral curve to the fall section serves to further minimize the radial force component.

As the profiles have an associated length, an overlap between rise and fall occurs as dwell length and duty cycle approach zero. This can be seen in Figure 3.5 as the profiles approach the cam center. In this overlap region, planar rise and fall sections with zero intermittent dwell were created, with the rise height h transitioning to zero as the radius approaches r_{min}. Figure 3.6 shows the modeling of this overlap region. This allows the follower to gradually transition from the 0% duty cycle where the cam profile is flat into the outer radial positions with full rise height. The transition of rise height from 0 to h follows a "3-4-5" polynomial similar to the rise and fall profiles, with a length chosen such that the same criteria are met for maximum pressure angle and minimum radius of curvature. Because the radial translation speed of the control linkage will be very slow compared to the effective velocity from cam rotation, the inertial force caused by this profile is negligible.

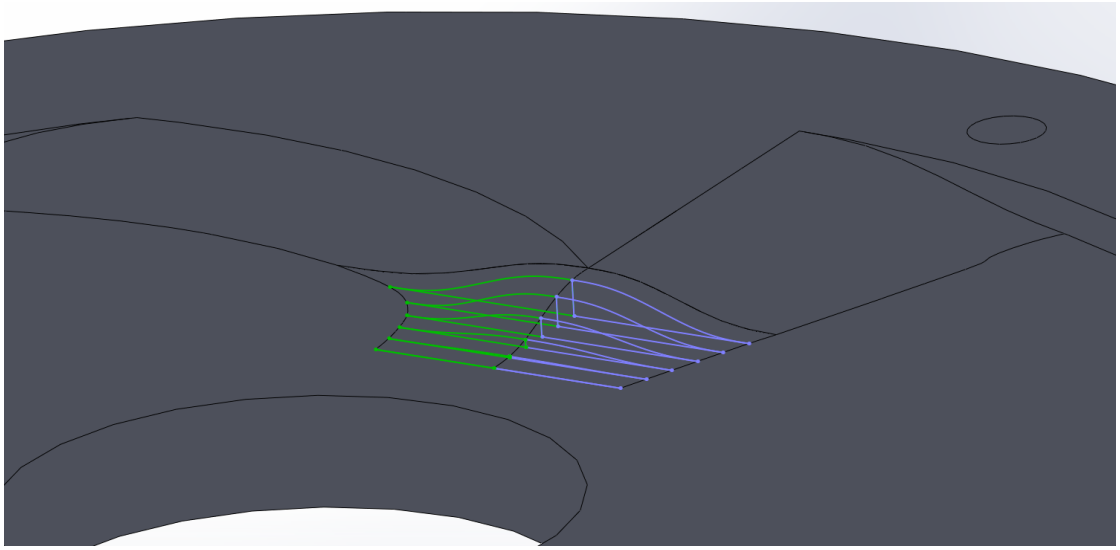

Figure 3.6: Transition section from inner cam radius. There is zero dwell between rise and fall, and rise height is gradually transitioned from 0 to h following the same polynomial as the rise section.

A bolt pattern around the outside of the cam allows for mounting to the flywheel. An existing flywheel from the original SM CVT prototype was reused for the clutch prototype. Figure 3.7 shows the final cam model and flywheel mounting position, with the finished components pictured in Figure 3.8.

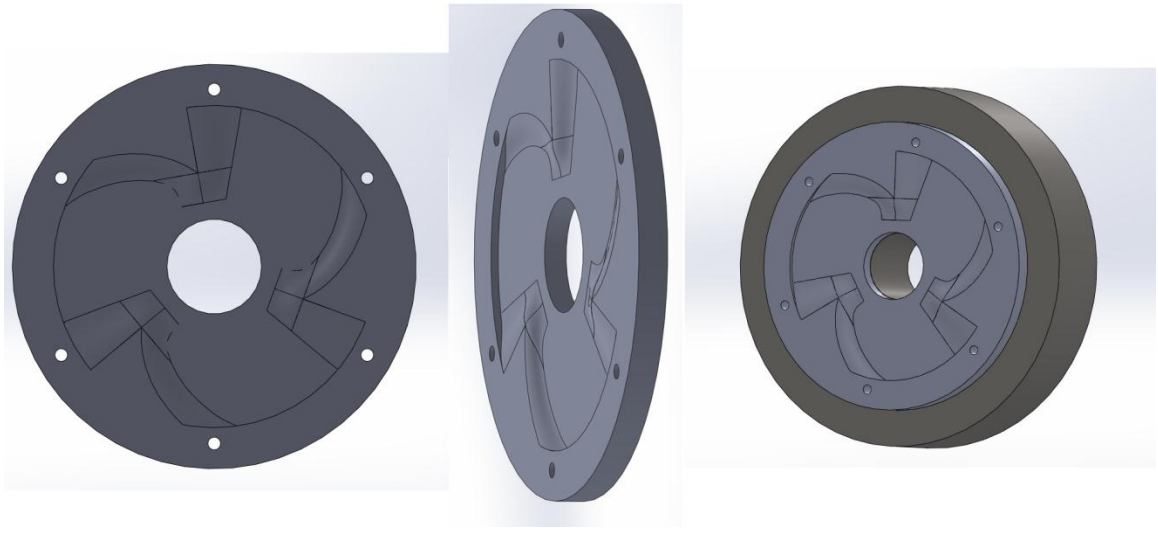

Figure 3.7: Final cam design

Figure 3.8: Finished cam and flywheel

The cam was machined from AISI 4140 steel on a 3 axis CNC mill. Because of the compound curvature, a ball end mill was used to create the polynomial surfaces. The tool diameter was 6.35mm (0.25”), below the minimum radius of curvature of the cam profile. A circular tool path was used starting at the inner radius. Each radial position was cut to the full necessary depth at a 0.002” vertical step, and 0.002” increment between radial positions. This resolution was chosen as a compromise between machining time and fidelity to the original geometry.

3.3 Followers and Springs

This section describes the design of the cam followers and compression springs used to generate closure force.

3.3.1 Followers

Because of the spiral shape of the fall profiles of the cam, point contact of the follower is necessary. As such, a traditional cylindrical roller-follower is not an option. The follower must be either spherical, or crowned to a degree approaching a torus. Given the small allowable follower radius of the prototype cam, no commercial options were available, and so a simple spherical tipped follower in sliding contact was designed. In a production setting, a custom spherical roller follower of small diameter - similar to a ball point pen - could be employed to minimize friction, but this was outside the scope of the project. Though sliding point contact incurs significant component wear, follower lifetime was expected to be sufficient for proof of concept testing. Figure 3.9 illustrates the follower design.

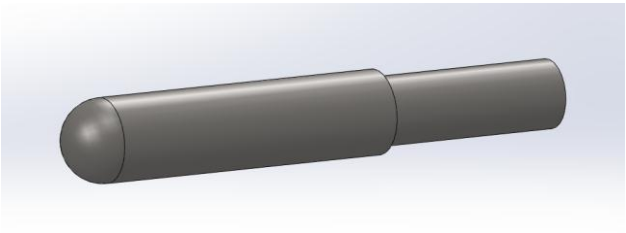

Figure 3.9: Follower design, with sliding spherical tip.

The cylindrical body of the follower allows it to travel axially in a sleeve bearing, facilitating displacement from the cam. The end of the follower is stepped down in diameter, providing a mounting feature for the spring. Due to the high expected wear, 4140 steel was chosen as the material for the followers.

3.3.2 Springs

The requirements for the springs are high stiffness, small size, and adjustability for purposes of tuning and experimental flexibility. Disk, or "Belleville" springs are well suited to this type of application. Figure 3.10 illustrates this spring type:

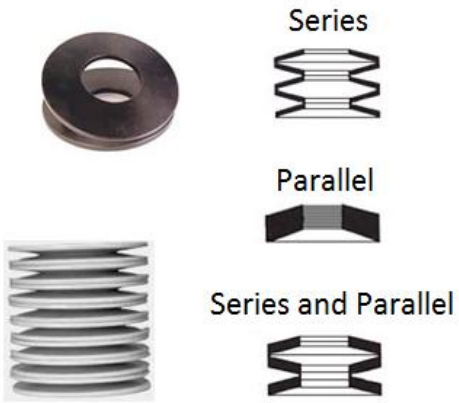

Figure 3.10: Disk spring illustration. By stacking disk springs in series, parallel, or a combination of both, a range of effective stiffnesses can be achieved. Adapted from [36]

A particular advantage of disk springs is that by stacking them in different series and parallel configuration, a wide range of effective stiffnesses can be achieved. The choice of individual springs and stacking configuration will follow in Section 3.8, which details the stiffness analysis of the clutch assembly as a whole. Figure 3.11 shows the follower with disk springs mounted.

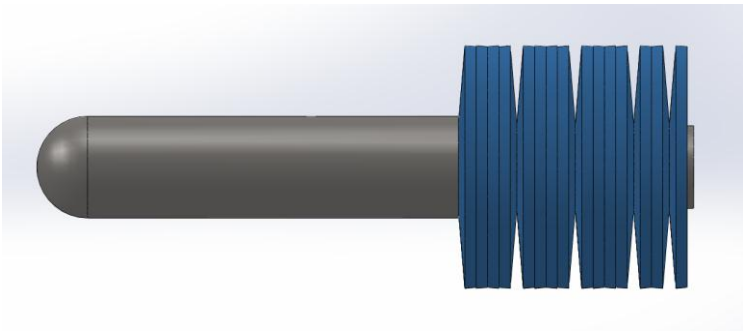

Figure 3.11: Follower with stacked disk springs

3.4 Control Linkage

A mechanism was required to translate the followers from inner to outer cam radius. For simplicity and to ensure synchronized motion, it is desirable for a single input to control the position of all three followers. Two concepts were considered. The first, pictured in Figure 3.12, uses a closed-form cam profile to control the radial position of the followers. By rotating the closed-form cam, the radial position of the followers is controlled. A disadvantage to this concept is that the entire assembly – the guides, rails, and center hub - must all oscillate with the motion of the axial cam.

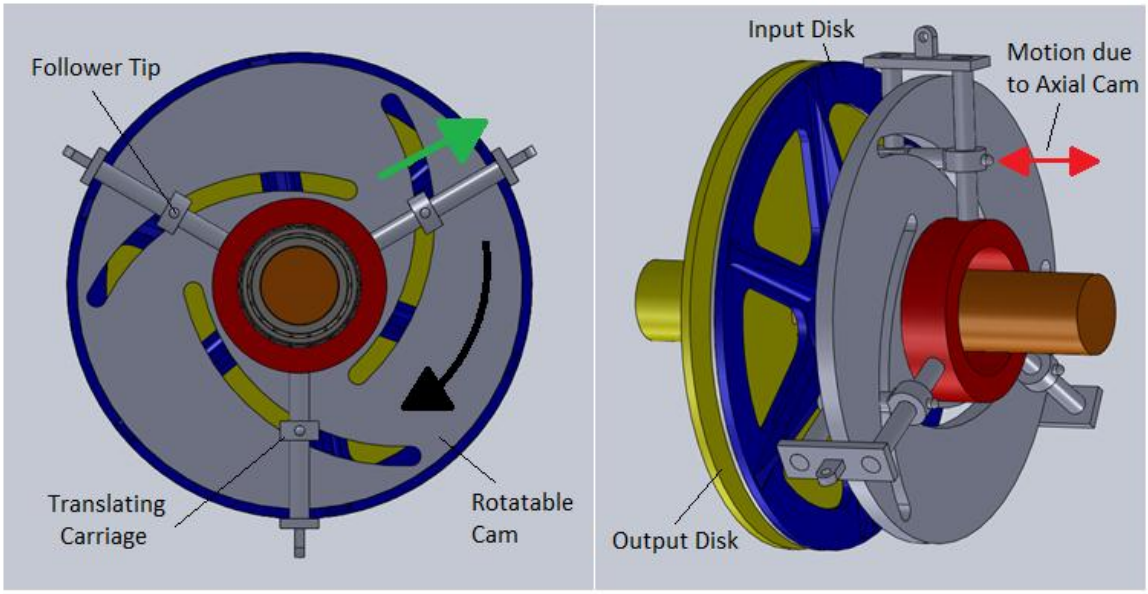

Figure 3.12: Cam concept to control radial follower position. As the cam is turned clockwise, the followers move outward radially on linear guides. The guides, rails, and center hub all undergo the oscillatory displacement the axial cam, pushing the input shaft against the output.

A second option, which minimizes the oscillating mass to only the followers, uses identical four-bar slider linkages sharing a common input link. Figure 3.13 illustrates this concept. Sliding links translate radially and house brass sleeves in which the followers displace due to the axial cam motion. Radial translation is facilitated by "mini-rail" linear slides manufactured by PBC Linear. Rotation of the input link is accomplished via a pivot mounted electric linear actuator. The input link is mounted via a sliding fit onto a hollow center hub pressed into the ground plate, and captured via a spring clip. Inside the hub is a needle bearing supporting the input shaft. The minimum radius from the shaft axis to the follower tips, corresponding to the minimum operating radius of the cam profile, is limited by the size of features surrounding the shaft, as can be seen in Figure 3.13. The radial dimension of the shaft, bearing, hub, center link, carriage, follower bearing, and

follower all add to the minimum radius the followers can occupy from the rotation axis. As such, these dimensions were minimized as much as possible, by design and use of compact features such as a needle bearing.

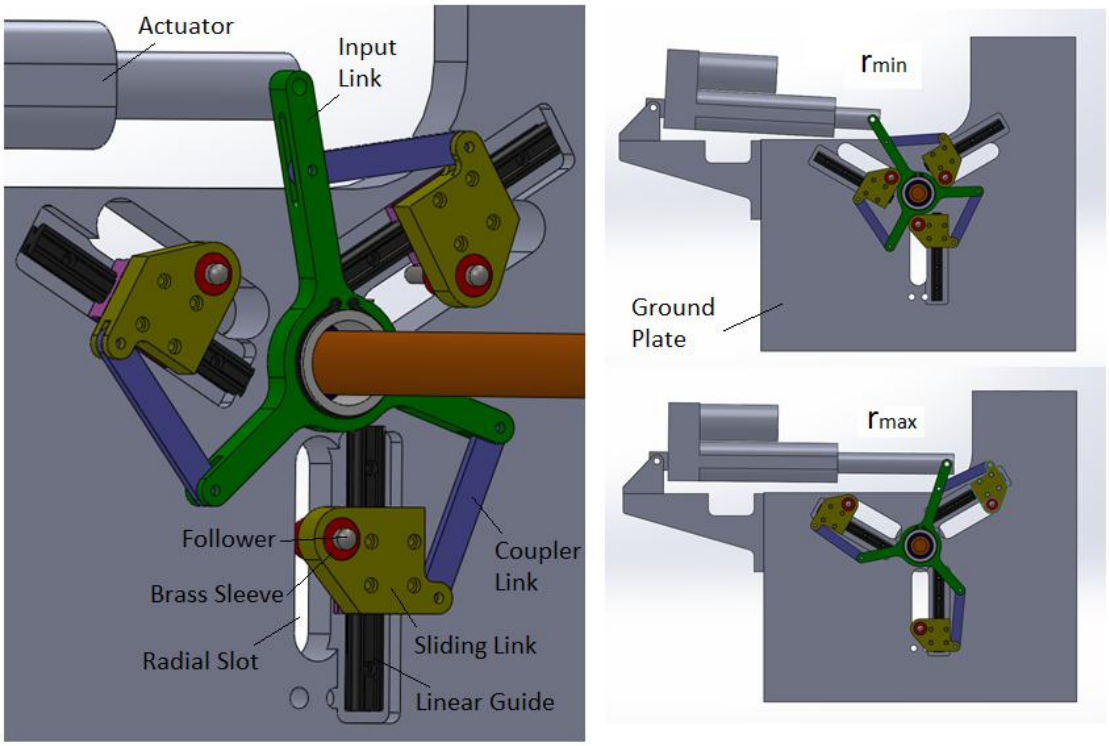

Figure 3.13: Control linkage concept. Follower sleeves (red) are housed in radially translating guides (yellow), mounted to a ground plate. Rotation of the input link (green) by an electric linear actuator synchronously translates the followers from inner to outer cam radius. Slots in the ground plate allow the followers to act against the input disk on the opposite side.

Figure 3.14 shows the finished linkage.

Figure 3.14: Finished control linkage

A force analysis, detailed in Appendix B was performed to verify the structural adequacy of the relatively small components and also to ensure the moments applied to the linear slide were within the manufacturer's recommended limits.

3.5 Input Disk Assembly

The function of the input disk is to receive normal force from the springs and engage the output disk, transferring energy from the flywheel. It must be capable of transferring input torque, but also capable of translating along the input shaft to engage and disengage from the output. Additionally, it must allow for relative motion between its own rotation and the grounded springs. To accomplish these functions, an assembly of four components was designed, illustrated in Figure 3.15. The assembly consists of the input disk with a friction facing, a large diameter thrust

bearing, and a slotted “follower guide” component that interfaces with the translating springs.

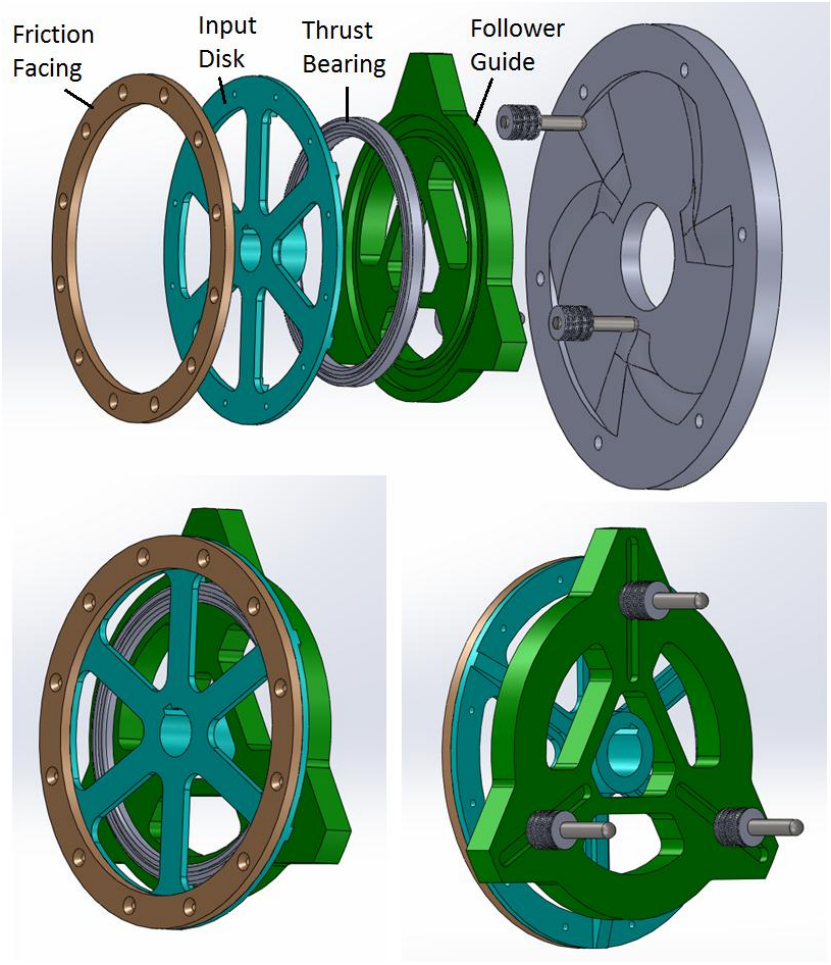

Figure 3.15: Input disk assembly. Control linkage and ground plate not shown in exploded view.

As the followers are displaced by the axial cam, the disk springs are compressed between the face of the follower guide and the stepped diameter of the follower. The end of the follower is allowed to continue travel into slots cut in the guide while the springs compress against the guide, transmitting force. The slots extend radially, facillitating the translation of the followers and springs due to the linkage motion. A

thrust bearing is mounted to the opposite side of the guide, via a press fit of the inner race of the bearing.

The bearing and guide are mounted to the input disk via a press fit on the outer race of the bearing. In this way, there can be relative rotation between the guide and input disk while still allowing spring force to be transmitted through the thrust bearing. The input disk is mounted on the input shaft via a sliding fit to allow for axial translation, but is keyed to allow torque transmission. Thus the thrust bearing and guide are supported by the input disk.

A friction facing is used to maximize the coefficient of friction between the disks. Both the material and machining were provided by Cleveland Oak Inc. The material chosen was a proprietery composite "HB1" with dynamic coefficient of friction μ = 0.49, against steel. Per the manufacturer recommended minimum, a thickness of 4.76mm (3/16") was used. The inner and outer diameter correspond to the intended moment arm of the friction surface as described in Section 1.2, at 76.2mm and 63.5mm respectively. A countersunk 12 bolt pattern mounts the facing to the input disk, providing distributed support.

Because the input assembly undergoes oscillating displacement from the cam, minimizing weight was desirable. Towards this end, both the input disk and follower guide are made of aluminum. Figure 3.16 shows the finished input disk assembly.

Figure 3.16: Finished input disk assembly

3.6 Output Disk

The function of the output disk is to react the normal force from the input disk, and transmit the generated torque to the output shaft. To reduce the inertial torque demands on the clutch, the MOI of the output disk should be as low as possible while having the strength to meet the torque and normal force requirements. Mass optimization of the output disk and other components is described in Section 3.8. Though the clutch is not active in the regeneration process of the SM CVT as diagramed in Figure 1.3 of the introduction, provisions for regeneration in future prototypes of the SM CVT were included. A one-way bearing, serving as the over-running clutch allowing the spring to drive the flywheel during braking, is housed in the output disk. The input disk extends into the one-way bearing, spinning freely while the velocity of the input is greater than the output, but locked when the output overruns the input. The output disk design is pictured in Figure 3.17.

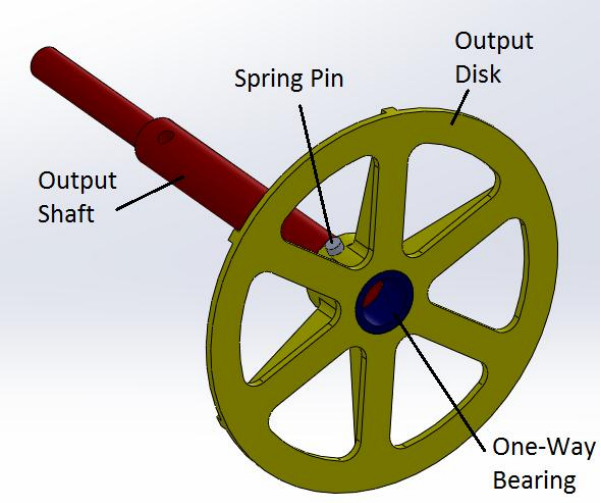

Figure 3.17: Output disk design

The output disk is mounted to the output shaft via a spring pin which supports the axial force from the input disk and also transmits torque to the output shaft. Because of the high force transmission and expected wear, the output disk is made of AISI 1020 steel. Figure 3.18 shows the finished output disk assembly.

Figure 3.18: Finished output disk

3.7 Enclosure and Test Equipment

To support the system components, an enclosure was designed, pictured in Figures 3.19 and 3.20. At far left is a post supporting a flange mounted spherical bearing for the input shaft. The center post mounts the control linkage and actuator as well as a needle bearing for the input shaft. The flywheel and cam are mounted between these two supports via two wedging shaft collars which are compressed between the input shaft and the inner diameter of the flywheel. Radial slots in the center post discussed in Section 3.4 allow the followers to engage the cam surface and pass through to the follower guide on the opposite side.

The input disk mounts on and is keyed to the input shaft on the right side of the center post. The input shaft continues into the one-way bearing inside the output disk. As previously mentioned, this allows torque transfer back to the flywheel, but also serves to support the left end of the output shaft. At far right is another post with spherical bearing to support the right end of the output shaft. The spherical bearings permit minor angular misalignment of the shafts, and are mounted with oversized clearance holes to permit axial alignment during assembly. The flange bearings are spherical, permitting angular misalignment. A base plate and top plate position the support posts.

When the springs are compressed, the force generated must be reacted by the posts at either end. To transmit this load, shaft collars on the input and output shaft are mounted against the flange bearings, preventing translation of the shafts along their axes. Lexan covers shield the sides of the enclosure to prevent escape of any high energy components in the event of a structural failure.

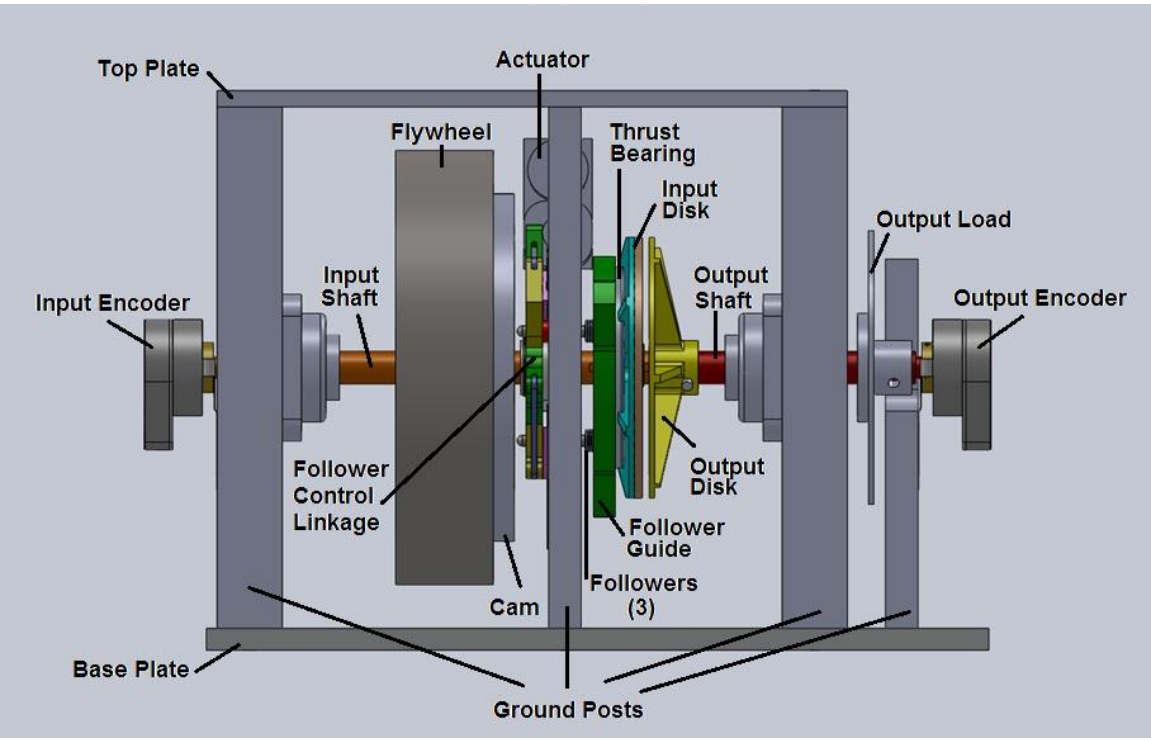

Figure 3.19: Full System diagram.

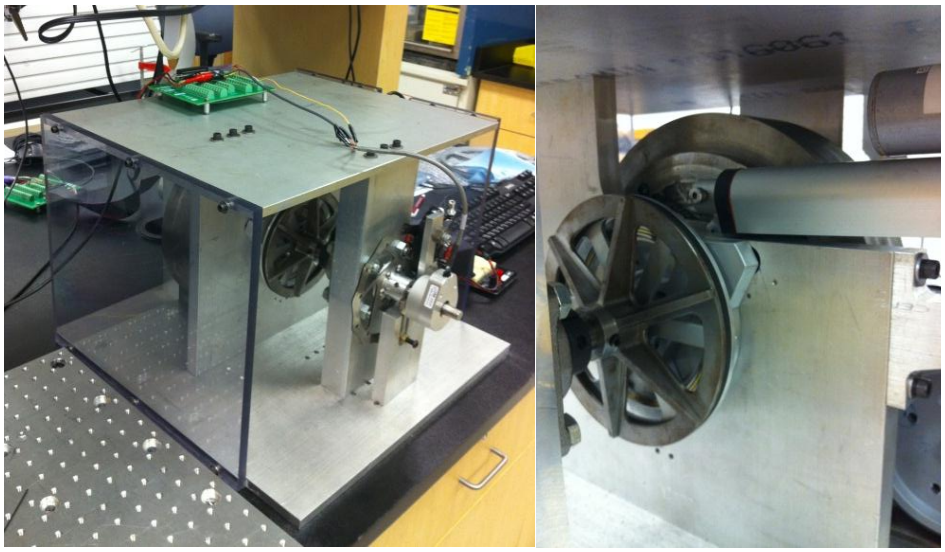

Figure 3.20: Clutch prototype

Also included in addition to the functional components of the clutch are several fixtures for experimentation including encoders and a friction brake serving

as the output load. These will be detailed in the following chapter on Experimental Procedure.

3.8 Stiffness Analysis

Ideally, the force generated due to follower displacement would be dependent on the stiffness of the disk springs only. In reality, all of the clutch components have stiffnesses dependent on their material and geometry, and contribute to the force-displacement relationship of the system as a whole. To determine the necessary stiffness of the disk springs, the stiffness of the other components must be known, as well as the role of each component in an equivalent spring system. Figure 3.21 illustrates this equivalent spring system.

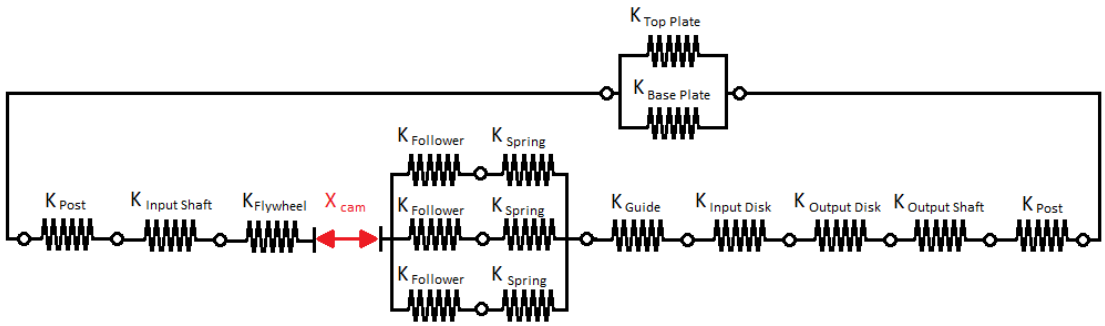

Figure 3.21: Equivalent spring system diagram. The top and bottom plate as well as the three spring and follower pairs act in parallel, and these parallel sets act in series with all other springs. Displacement between the cam and followers builds force in the system, which is equal at all points between springs in series.

With the series and parallel configuration of the system components defined, an equation for the effective stiffness of the system as a whole may be written, by combination of the equations for springs in series and parallel. The stiffness of the total spring system is given by:

$$\frac{1}{K_{System}} = \frac{1}{K_{Top\ Plate}+K_{Base\ Plate}} + \frac{1}{2K_{Post}} + \frac{1}{K_{Input\ Shaft}} + \frac{1}{K_{Flywheel}}$$

$$+\frac{1}{3K_{Follower}} + \frac{1}{3K_{Spring}} + \frac{1}{K_{Guide}} + \frac{1}{K_{Input\ Disk}} + \frac{1}{K_{Output\ Disk}} + \frac{1}{K_{Output\ Shaft}} \quad \text{Equation 3.4}$$

The spring stiffness must be chosen such that the system builds the desired normal force under the displacement of the cam. As both the compressive spring travel and required normal force have been defined, at 2.54mm and 2045N respectively, the desired system stiffness is then 805 $\frac{N}{mm}$. By determining the stiffness of all system components, Equation 13 may be solved for K_{Spring} to find the necessary spring stiffness.

Component stiffness was determined through Finite Element analysis. Each component was fixed via boundary conditions representative of the constraints in the real world clutch assembly. The full intended load of 2045N was applied to each component at the appropriate surfaces, and displacement was observed. Approximate linearity over small displacement was assumed.

A further purpose of this analysis was to investigate the structural integrity of each component by observing the magnitude and location of peak stresses. Several components including the disks and follower guide were improved by removal of unnecessary structural material or addition of reinforcement. Figure 3.22 shows several components in their deformed states. Further details of the FEA procedure are presented in Appendix C.

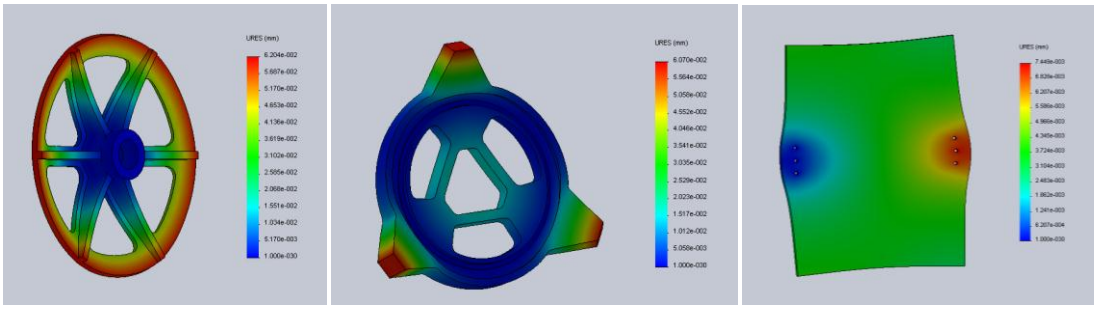

Figure 3.22: Stiffness simulation results of the output disk, follower guide, and top plate. Deformations are scaled for visibility.

Table 1 lists the stiffnesses computed for each component.

Component	Stiffness Coefficient K (N/mm)
Posts	1.75E+5
Top Plate	2.63E+5
Base Plate	4.38E+5
Flywheel	2.80E+6
Followers	4.21E+5
Guide	3.51E+4
Input Disk	9.80E+4
Output Disk	3.49E+4
Input Shaft	1.79E+6
Output Shaft	3.58E+6

Table 3.1: Component Stiffnesses

Entering these values into Equation 3.4 and solving for K_{spring} gives a desired stiffness of 286 $\frac{\text{N}}{\text{mm}}$ for each spring and 858 $\frac{\text{N}}{\text{mm}}$ for all three in parallel. All other components together have an effective stiffness of approximately 13600 $\frac{\text{N}}{\text{mm}}$, and so the softer springs are the dominant compliant element. The springs are responsible for 94% of total system compliance, affording easy adjustment of the clutch by changing springs.

A disk spring was sought which could be stacked in a series and parallel configuration to achieve the desired stiffness of 858 $\frac{\text{N}}{\text{mm}}$ while having an inner

diameter which could engage the follower per Figure 3.11, and at least 2.54mm of compressive travel. A disk spring was chosen with an inner diameter of 5.2mm, outer diameter of 15mm, thickness of 0.71mm, travel of 0.41mm, and stiffness of $1731\frac{\text{N}}{\text{mm}}$, manufactured by Belleville Springs Ltd. Fifteen springs are stacked as illustrated in Figure 3.23, with 3 springs in series individually with 6 sets of parallel pairs.

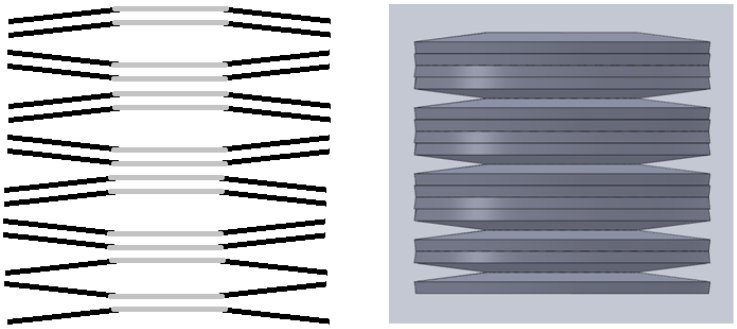

Figure 3.23: Disk spring stack configuration

Using the equations for springs in series and parallel, the effective stiffness of the stack of springs is $288.5\ \frac{\text{N}}{\text{mm}}$, with a travel of 3.66mm. Per the manufacturer specification, only 75% of full spring travel should be used before the spring stiffness becomes nonlinear. This leaves 2.75mm of usable travel, adequate to accommodate the cam displacement. With 3 stacks compressing in parallel, the effective stiffness of all follower springs together is $865.5\frac{\text{N}}{\text{mm}}$, within 1% of the desired stiffness.

Because the disk springs must not only provide the normal force for the friction disks but also the closure force to keep the followers in contact with the cam profile, it is necessary to confirm that the inertial forces caused by acceleration of

the follower train will not overcome the springs. The follower train is considered to be all components which are displaced by the cam: the followers, springs, follower guide, thrust bearing, input disk, and friction facing. The mass of these components was determined via CAD software to be 0.694 kg. As was stated in Section 3.2.1, the peak acceleration magnitude of the follower train is 1.61E^6 $\frac{mm}{s^2}$. With this mass and acceleration, the inertial force of the follower train is 1115N. The peak acceleration occurs at a displacement value of 2.38mm. This displacement represents 1.75mm of compressive spring travel after the 0.635mm air gap between the disks has been closed. At this displacement, the follower springs exert 1515N of force on the follower train. As such, the spring force is adequate to overcome the inertial forces of the accelerating mass, and contact between the follower and cam will be maintained.

Because the disk springs are not compressed until the friction disks make contact, there is no closure force to keep the followers against the cam surface when the cam displacement is less than 0.635mm, the length of the air gap. Fortunately, the inertial forces in this displacement range from both the rise and fall transitions act to maintain follower contact. However, to avoid free motion of the follower train while in low dwell, a small amount of closure force is desirable. To achieve this, a low stiffness “wave” spring manufactured by Smalley Steel Ring Company was used, pictured in Figure 3.24. The spring is mounted on the input shaft between the input and output disks, providing approximately 10N of closure force in low dwell. When the disks are in contact, the thickness of the friction facing prevents the spring from being fully compressed.

Figure 3.24: “Wave” spring used to secure the follower train in low dwell.

The following chapter details the experimental testing carried out to investigate the performance of the design described in this chapter.

Chapter 4 - Experimental Procedure

This chapter explains the experimental methods used to verify the operation of the clutch. The experimental design and equipment setup will be detailed, followed by a presentation and discussion of results.

4.1 Test Equipment

To prove the concept of the clutch as well as quantify performance, empirical testing of the prototype is presented. Of chief concern in the experimental design is the ability to identify the flow of energy in the system, both in losses and useful transmitted energy. By examining these energy components the efficiency of the prototype can be determined. Additionally, torque capacity and resolution of the angular advancement of the output should be validated against the design intent. Finally, these performance characteristics should be quantified vs. the variable operating conditions of angular velocity, output load, and duty cycle.

To derive this information, the rotational state of the input and output must be known vs. time. By attaching angular encoders to both the input and output shafts, angular position vs. time may be measured directly. Velocity and acceleration may then be calculated as the first and second derivative of this data. Because of the short duration of the pulse events being examined, high resolution is required. A US digital HB6M angular encoder with 10,000 pulses per revolution was used, offering an angular resolution of 0.036˚. With the cam transition length and resulting pulse duration being 20˚, the encoders can provide up to 333 position data points within a

single engagement or disengagement profile. Actual number of data points is limited by sampling rate however, as will be explained later.

To study the effects of output load on the system response, a means of producing a controllable resistive torque on the output was desirable. This was achieved via a friction brake. An Avid BB7 bicycle brake caliper is mounted to ground, with a brake rotor mounted to the output shaft via a custom flange. This assembly is pictured in Figure 4.1(a). The brake cable is run through a hollow screw, on which a jam-nut is tightened or loosened against the caliper body to control clamping force. Because torque produced under dynamic rather than static friction is of interest, it is necessary to calibrate the output torque with the shaft in motion. To do so, a pulley of known diameter is mounted to the output shaft, and a wrapped wire is pulled by an actuator. This setup is pictured in Figure 4.1(b). An Omega LCR S-beam type load cell is mounted in-line between the wire and the actuator to measure the pulling force as the actuator rotates the pulley. With pull force and moment arm known, the dynamic friction torque of the brake may be calibrated to test the clutch at a specified load. As dynamic friction coefficient is independent from velocity, use of a brake for the output load offers a consistent resisting torque across operating conditions, though dynamic torque due to acceleration of the output inertia must also be considered, as will be explained later in this chapter.

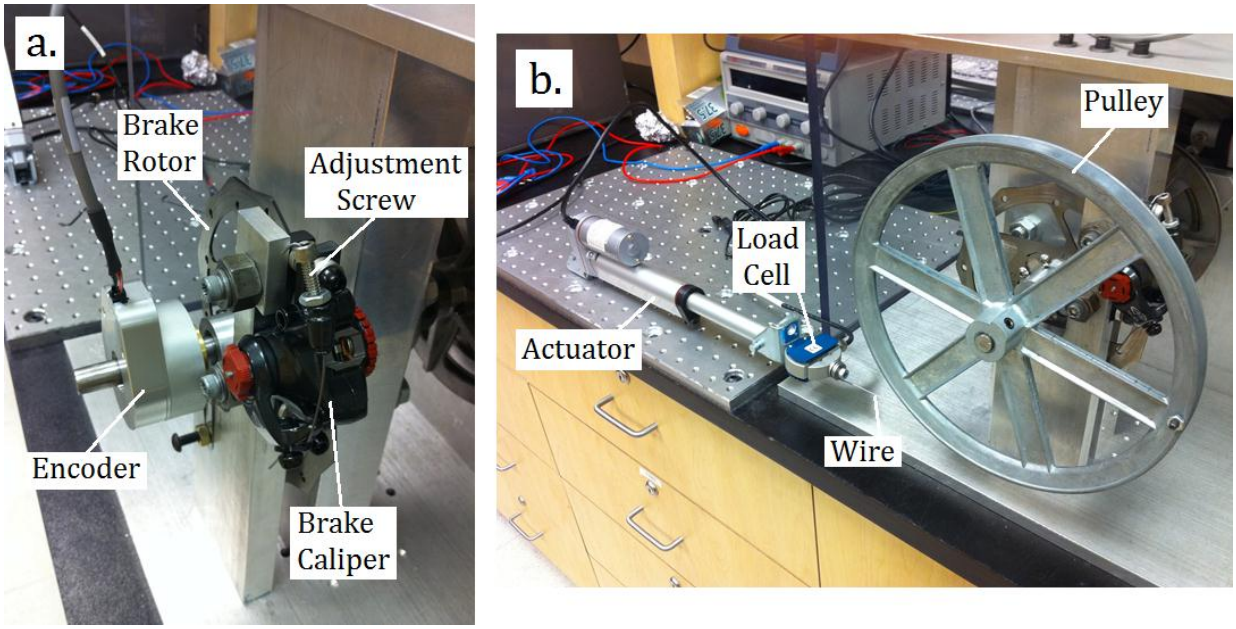

Figure 4.1: Output load components – bicycle brake assembly (a.), and dynamic torque calibration setup with actuator, load cell, and pulley (b).

To charge the flywheel, an electric motor with a mounted rubber wheel is used. The input flywheel is driven up to high angular velocity prior to data acquisition. Once the flywheel has reached the desired angular velocity, the drive motor is decoupled, and the actuator driving the control linkage of the clutch is switched on. This moves the followers outward radially, initiating clutch pulses and torque transfer to the output. A regulated power supply powers both actuators and the electric motor. Figure 4.2 shows the motor, linkage actuator, and input encoder.

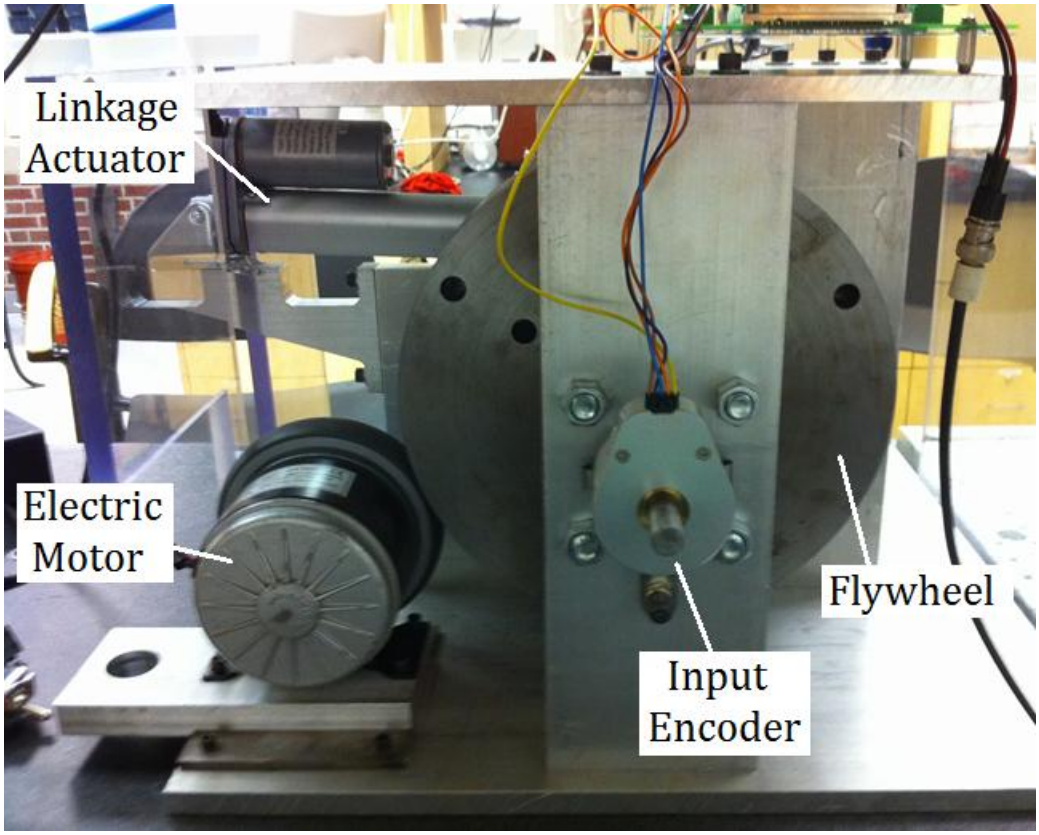

Figure 4.2: Input side of the clutch experimental setup

Data acquisition from the encoders and load cell is accomplished through a National Instruments PCI-6601 I/O card and a Labview interface. This card is equipped with an onboard counter, allowing for a sampling frequency independent of the pulse frequency of the encoders. Sampling rate and timing were set via a reference signal from a signal generator. With the flywheel at maximum test velocity of 105 $\frac{rad}{s}$, a single 20˚ engagement or disengagement transition will last only 3.3ms. At this speed, a sampling frequency of 50kHz will produce 166 data points within one engagement or disengagement profile, a reasonably large data set for examination. This sampling rate was used for the majority of testing, though lower

rates were used in some cases at low angular velocity where such high time resolution was not necessary. The full test setup is shown in Figure 4.3.

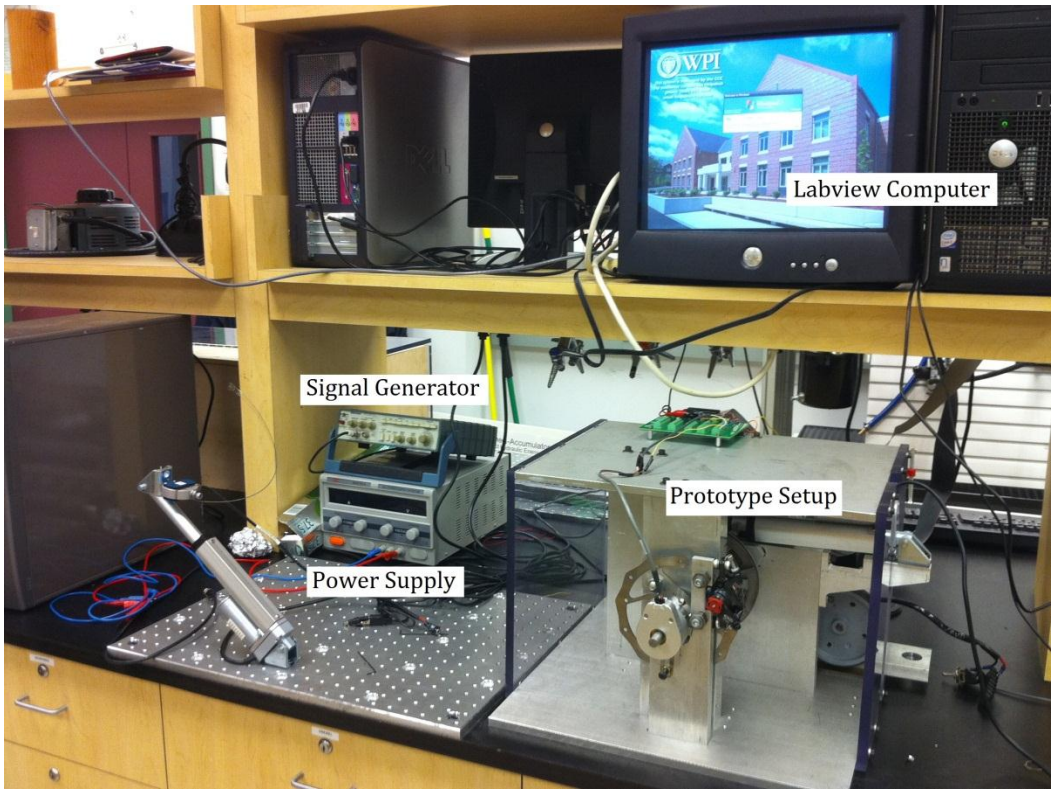

Figure 4.3: Full experimental setup

4.2 Laboratory Procedure

During operation of the clutch, the variables of most interest towards performance are input angular velocity, output torque load, and duty cycle. The ranges and testing intervals for these experimental factors are:

Input Angular Velocity – because the clutch transfers energy from the input to output, the flywheel will slow to a stop during each test run. By bringing the

flywheel to the maximum intended test velocity, clutch pulses will be observed across a full range of velocities between zero and the initial flywheel velocity. As described in Section 3.1, the maximum test velocity intended is 105 $\frac{rad}{s}$ (1000 rpm). To maximize the number of pulses observed before the flywheel comes to a stop, a low brake load of 10 Nm is to be used for this test, as well as a low duty cycle which brings the followers out into the full rise height of the cam but no farther.

Output Torque – the torque capacity of the clutch will be tested by varying the brake torque from 10 Nm to the full intended torque capacity of 70 Nm at 10 Nm intervals. To maximize number of pulses observed before the flywheel comes to a stop, the maximum angular velocity will be used, as well as a low duty cycle which brings the followers to the full rise height of the cam but no higher. As such, the 10Nm torque test and the angular velocity test described above will be the same.

Duty Cycle – Duty cycle will be tested from 10% to the maximum of 50% at 10% intervals. To maximize number of pulses observed, maximum flywheel velocity will be used, as well as a low brake torque of 10 Nm. For all testing, to avoid coupling the effects of varying duty cycle with output torque and input velocity, data will not be recorded until the actuator is switched off and the control linkage is at rest.

A test run consists of the following steps:

1. Set / verify air gap
    a. Measure air gap at several points around the circumference of the friction disks using calipers or feeler gage

b. If the air gap is not at the desired distance, remove the output shaft collar and bearing set screw. Slide the output shaft in the spherical bearing until the air gap is as intended.
c. Replace the shaft collar such that it is in contact with the bearing, tighten bearing set screw.

2. Set brake torque
    a. Remove output encoder from output shaft via set screw
    b. Mount pulley on output shaft, tighten set screw
    c. Rotate pulley by hand until wire is taught
    d. Adjust control screw on brake caliper to increase or decrease brake torque
    e. Begin recording load cell data
    f. Switch actuator on to rotate pulley
    g. End data recording once pulley has finished travel
    h. Calculate average torque during rotation from load cell data
    i. If torque is not as desired, tighten or loosen the control screw on the brake caliper to adjust. This requires some trial and error. Repeat steps e. through i. until brake torque is as desired
    j. Remove pulley and replace encoder
3. Bring flywheel to full angular velocity
    a. Press electric motor and rubber wheel against flywheel. Motor is mounted on a sliding block
    b. Switch on motor

c. Observe angular velocity readout calculated from the input encoder via Labview interface

d. Once the flywheel has reached 105 $\frac{rad}{s}$, switch off electric motor and remove

4. Engage clutch and record data

    a. Switch on the control linkage actuator

    b. Allow actuator to travel to desired duty cycle. This is estimated via marks on the ground plate. Some trial and error is required here as well. Duty cycle may be verified via the collected data as will be detailed later.

    c. Once desired duty cycle has been reached, begin recording encoder data.

    d. End data recording once flywheel has come to rest.

    e. Run Matlab code to post process the recorded data. Details of the post processing method are presented in the following section.

This laboratory procedure and range of experimental parameters define the experimental method desired prior to testing. The next section details certain difficulties that were encountered during operation of the clutch and the limitations that were imposed on the range of parameters which could actually be tested, followed by presentation of results.

4.3 Experimental Results

During testing, limitations of the prototype setup were encountered which should be noted. The limited energy content of the flywheel posed the primary restriction on the range of parameters which could be tested. The flywheel, reused from the original SM CVT prototype, was bounded in size by safety concerns in case of a mechanical failure. Its energy content was 1.02 kJ at the maximum test velocity of 105 rad/s. This energy content, coupled with the relatively low speed of the actuator driving the control linkage allowed for a maximum of approximately 20% duty cycle before the flywheel came to rest, even at low output torques. Because of this, testing across the full range of duty cycles was not possible. Additionally, as data were not recorded until the control linkage had moved the followers into the full high dwell and come to rest, significant flywheel energy was expended during the period of follower translation. This limited the maximum flywheel velocity data to approximately 50 rad/s. Finally, tests run with a brake torque above 20Nm yielded few observable pulses for comparison of trends, and so the majority of data was recorded at 10 and 20Nm. In spite of these limitations, valuable data was obtained.

Due to the discrete nature of the encoder data, a low pass filter was needed to smooth the high frequency noise resulting from the finite position and time increments. Using Matlab, a second order Butterworth filter with a cutoff frequency of 500 Hz was applied. These data were then differentiated twice to obtain angular velocity and angular acceleration. The Matlab code used for post processing the data

is presented in Appendix D. Figure 4.4 shows the filtered position, velocity, and acceleration data from a sample test run.

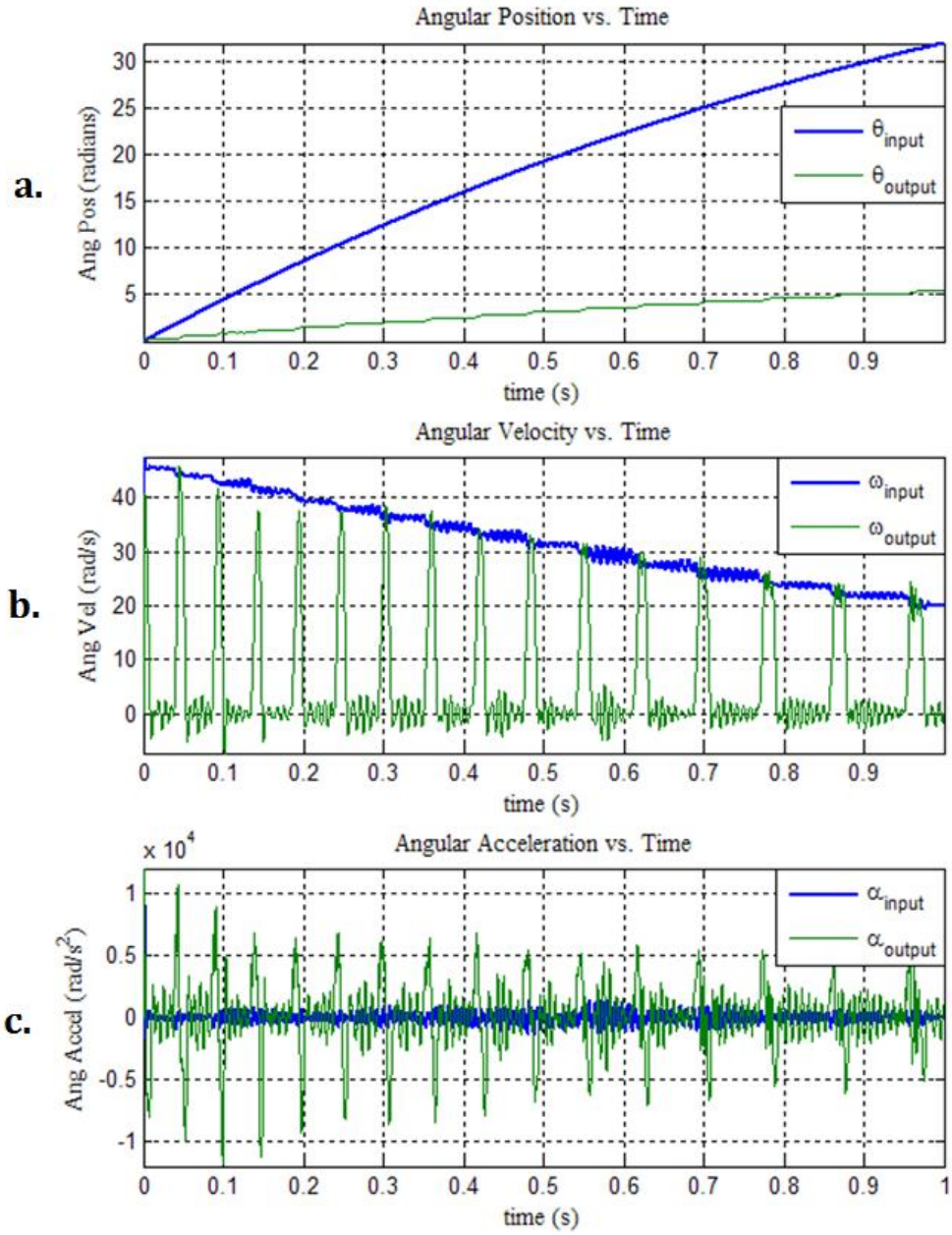

Figure 4.4: Angular position, velocity, and acceleration from a sample run.

To examine pulses individually, Matlab code was written to identify the engagement and disengagement profiles. A threshold angular velocity value is used

to separate the rise and fall profiles from the minor oscillations seen during full engagement and full disengagement. Figure 4.5 illustrates the identification of individual profiles.

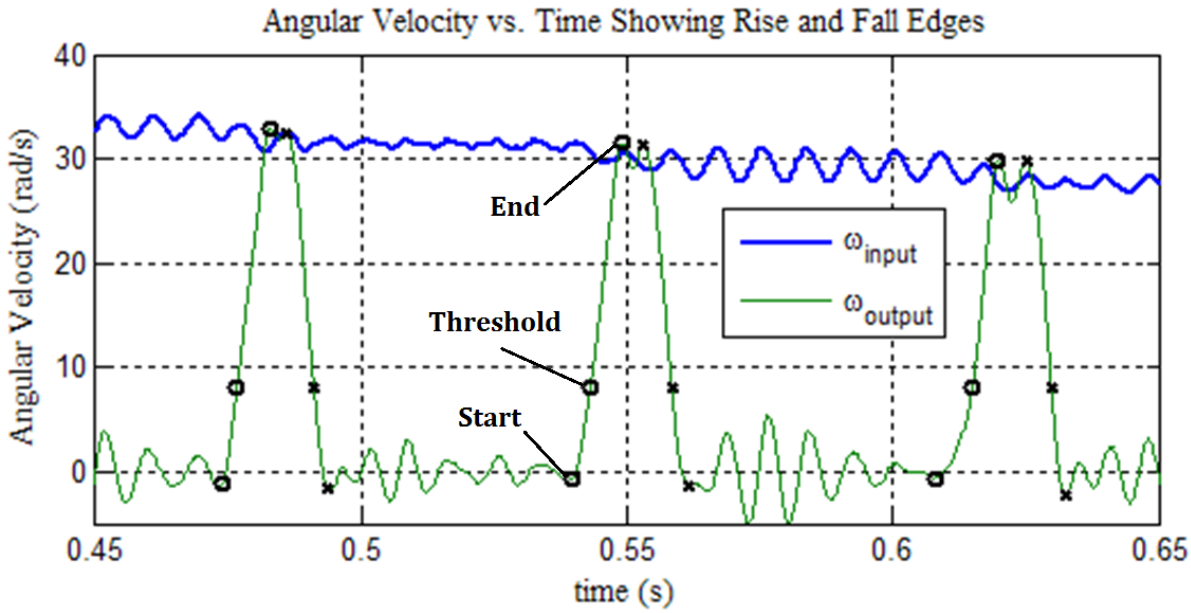

Figure 4.5: Identifying rise and fall profiles. Once the threshold angular velocity is reached, a rise profile is searched backward to find the beginning of velocity increase and forward to find the end. The fall is treated similarly, though with velocity decrease.

To determine the torque transferred by the clutch, the torque applied by the bicycle brake and the inertial torque incurred by accelerating the output assembly must be considered. The total torque transferred by the clutch as a function of time is calculated as:

$$T_c(t) = T_b + T_i(t) = T_b + I_{out}\alpha_{out}(t) \qquad \text{Equation 4.1}$$

where T_b is the static torque provided by the brake per calibration prior to testing, $\alpha_{out}(t)$ is the measured angular acceleration of the output shaft, and I_{out} is the

moment of inertia of the entire output assembly. Determined via the CAD design software, the inertia of the output assembly – including the output disk, output shaft, shaft collar, brake rotor, mounting flange, and rotating components of the encoder and spherical bearing – is 0.0026 Nm^2.

Considering α_o to be the peak positive angular acceleration averaged across all clutch pulses of a test run, the maximum transmitted clutch torque may be calculated from the recorded data via Equation 4.1. Initial testing of the clutch was performed at half of intended torque capacity to minimize risk of component failure early in experimentation. To accomplish this, the air gap between the friction disks was increased from 0.635mm to 1.91mm (0.025" to 0.075"), resulting in 1.27mm of compressive spring travel rather than the full 2.54mm (0.05" rather than 0.1"). Table 4.1 Shows the torque transmitted under half capacity settings.

Brake Torque (Nm)	Inertial Torque (Nm)	Total Clutch Torque (Nm)
10	13.1	23.1
20	5.8	25.8
30	0	< 30

Table 4.1: Torque components with clutch at half capacity.

At 30Nm, the static friction of the brake was not overcome by the clutch. To test higher torque loads, the air gap was reduced to the intended 0.635mm for full torque capacity. Table 4.2 shows the torque transmitted at full scale settings. At 50 Nm, the static friction of the brake was greater than the torque capacity of the clutch.

Brake Torque (Nm)	Inertial Torque (Nm)	Total Clutch Torque (Nm)
30	14.2	44.2
40	6.5	46.5
50	0	< 50

Table 4.2: Torque Components with clutch at full capacity.

To calculate the system efficiency, the flow of energy must be determined from the measured data. The input energy is considered to be the kinetic energy lost by the flywheel and additional rotating input assembly components with each clutch pulse. Because the inertia of all rotating input components act together as an energy storage device, the entire input inertia will be hereafter referred to as the flywheel. The energy lost with each clutch pulse is computed via the change in average angular velocity before and after a pulse. This is illustrated in Figure 4.6.

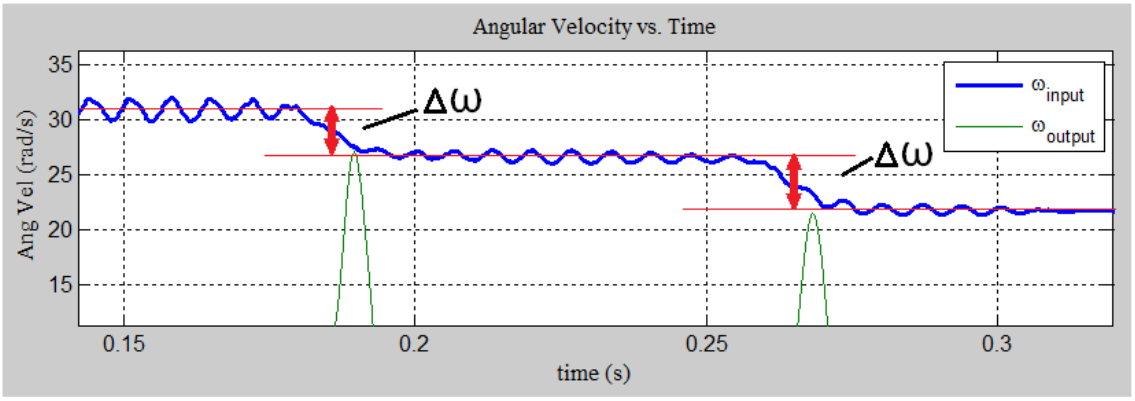

Figure 4.6: Angular velocity lost by the flywheel with each clutch pulse.

With the change in angular velocity known, the energy lost by the flywheel from a clutch pulse is calculated as:

$$\Delta E_f = \frac{1}{2} I_f (\omega_{in,1}{}^2 - \omega_{in,2}{}^2) \qquad \text{Equation 4.2}$$

where I_f is the flywheel moment of inertia and ω_{in1} and $\omega_{in,2}$ are the average flywheel velocity before and after the clutch pulse, respectively. Determined via CAD software, the moment of inertia of the input assembly – including the flywheel, cam, input shaft, input disk, shaft collar, and rotating components of the encoder and spherical bearing – is 0.2013 kgm^2. Figures 4.7 and 4.8 show the kinetic energy lost during individual pulses by the flywheel vs. angular velocity at 10 Nm and 20 Nm of brake torque, respectively.

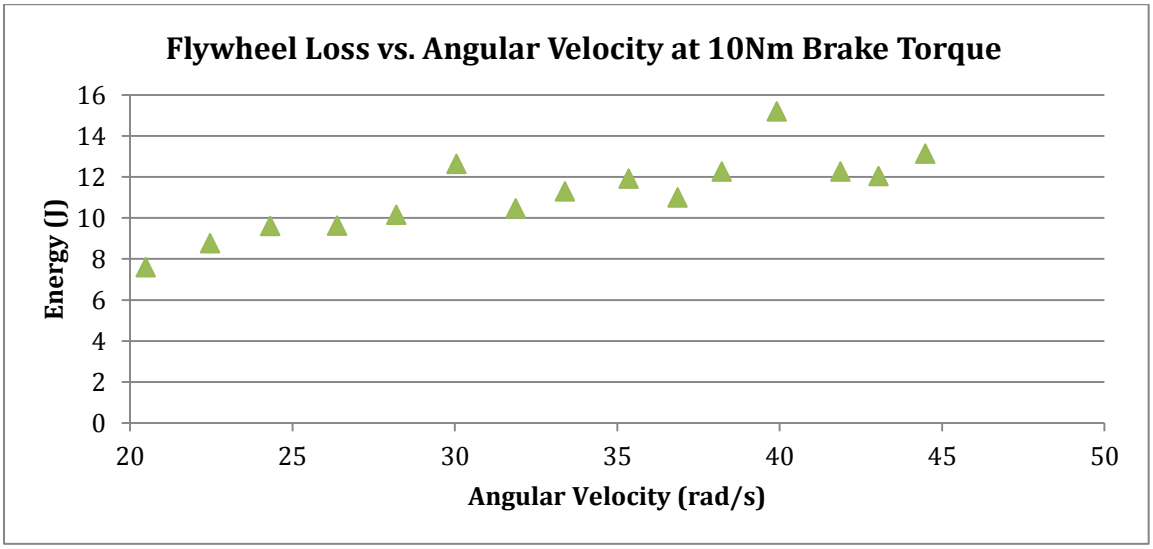

Figure 4.7: Flywheel loss vs. angular velocity, brake torque = 10Nm

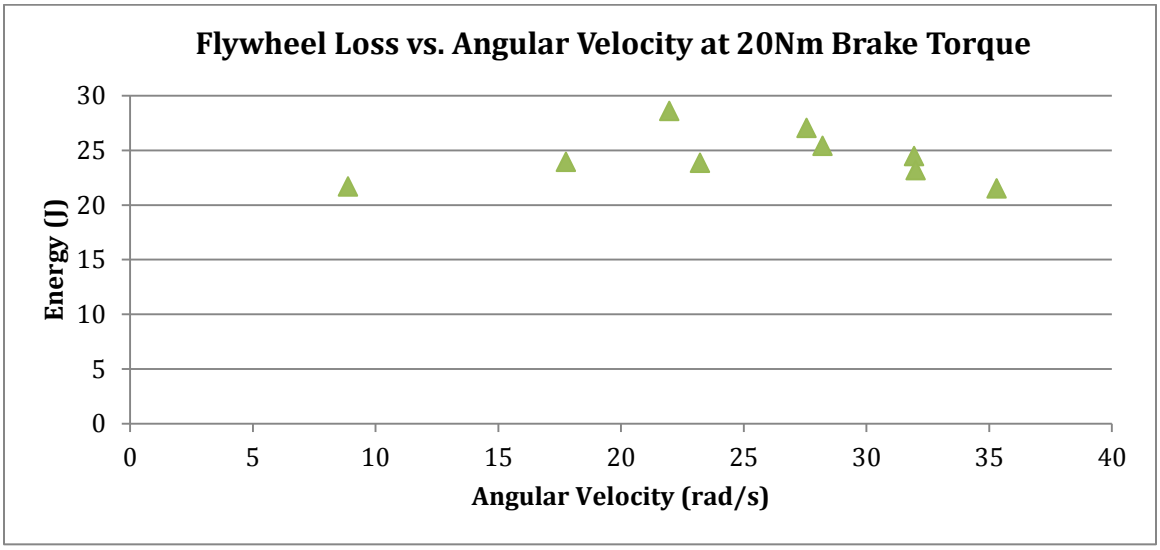

Figure 4.8: Flywheel loss vs. angular velocity, brake torque = 20 Nm

The energy transmitted to the output is computed as:

$$E_{trans} = T_b(\Theta_{out,2} - \Theta_{out,1}) \qquad \text{Equation 4.3}$$

where $\theta_{out,1}$ and $\theta_{out,2}$ are the angular position of the output before and after the clutch pulse, respectively Figures 4.9 and 4.10 show the transmitted energy during single pulses plotted against angular velocity of the input, with data collected at brake torques of 10Nm and 20Nm, respectively.

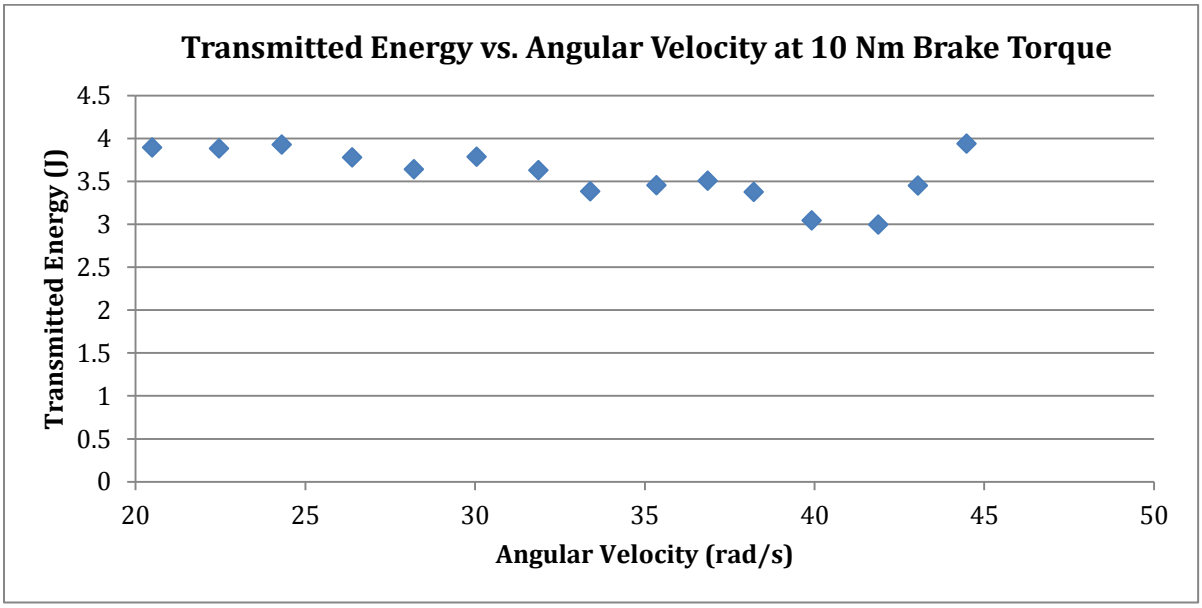

Figure 4.9: Transmitted energy vs. angular velocity at brake torque = 10Nm

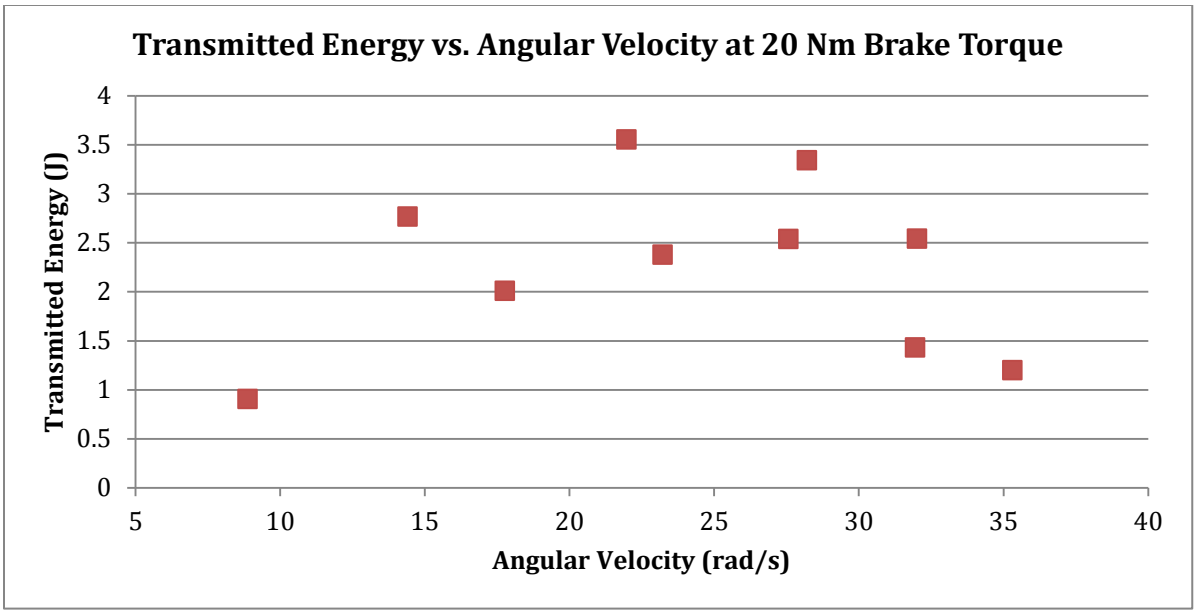

Figure 4.10: Transmitted energy vs. angular velocity at brake torque = 20Nm

Finally, the loss energy is considered. There are two primary energy loss mechanisms: heat energy expended by clutch slip, and heat energy expended by parasitic losses present in the system. Energy lost to clutch slip can be calculated from the data as:

$$E_{slip} = \int_{t1}^{t2} T_c(t)[\omega_{in}(t) - \omega_{out}(t)]\, dt \qquad \text{Equation 4.4}$$

where ω_{in} and ω_{out} are the input and output angular velocities, respectively, and the integral limits t_1 and t_2 correspond to the start and end of a clutch pulse, respectively. Figures 4.11 and 4.2 plot the energy lost to clutch slip during single pulses vs. angular velocity at brake torques of 10Nm and 20 Nm respectively.

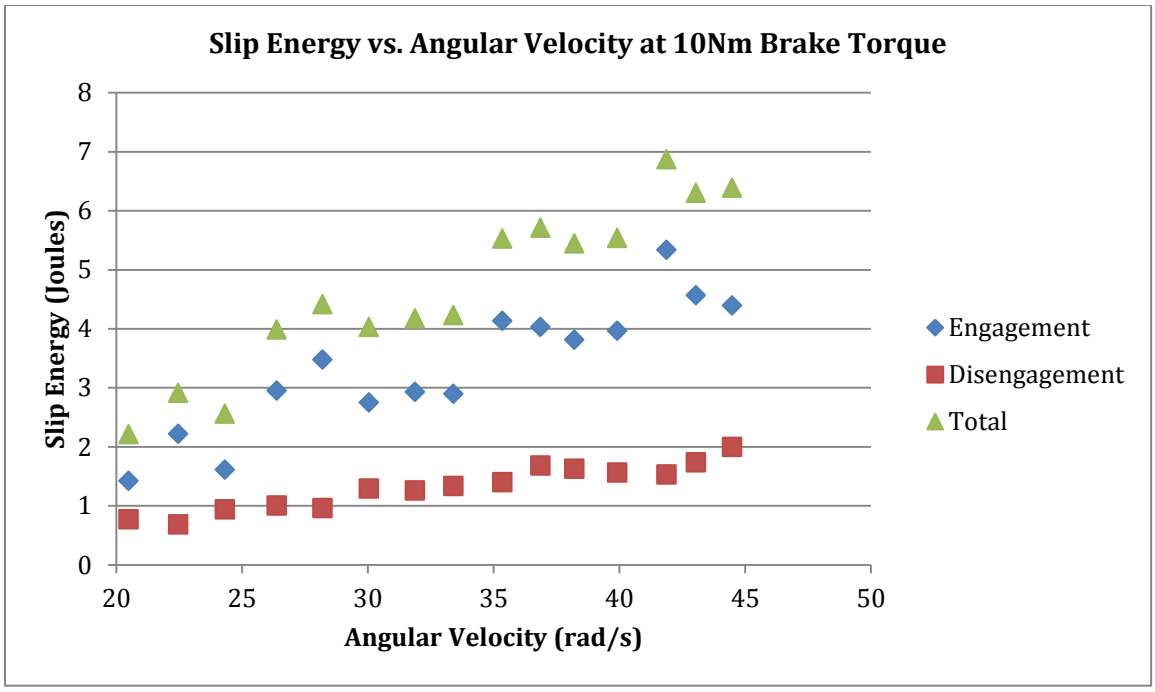

Figure 4.11: Slip energy vs. angular velocity of the input at brake torque = 10Nm. Components of total slip energy shown are engagement, where the output is accelerating, and disengagement, where the output is decelerating.

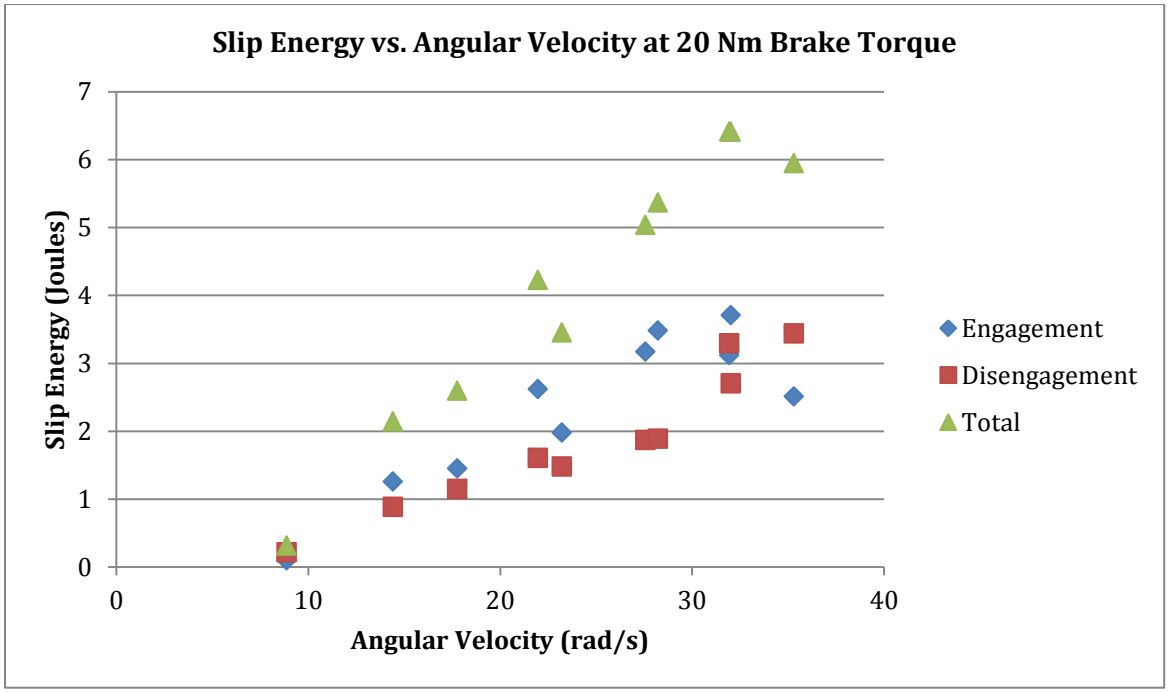

Figure 4.12: Slip energy vs. angular velocity of the input at brake torque = 20Nm

Parasitic losses in the system are then represented as the difference between the energy taken from the flywheel and transmitted to the output or lost to clutch slip. Figures 4.13 and 4.14 plot all of the single pulse energy components together as a function of angular velocity, at brake torques of 10Nm and 20 Nm respectively.

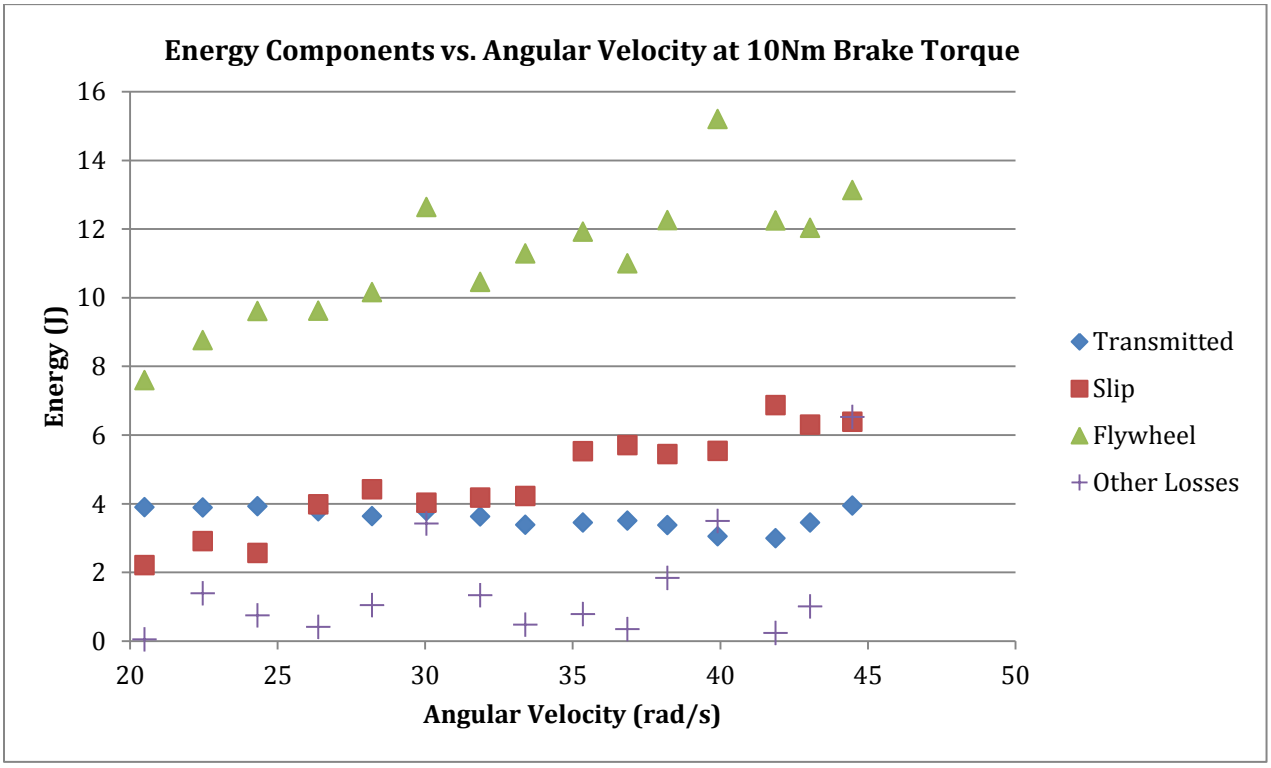

Figure 4.13: Components of energy vs. angular velocity at brake torque = 10Nm. Other Losses is computed as the difference between the transmitted and slip energies and the total flywheel energy, and represents the energy lost to parasitic resistances in the system.

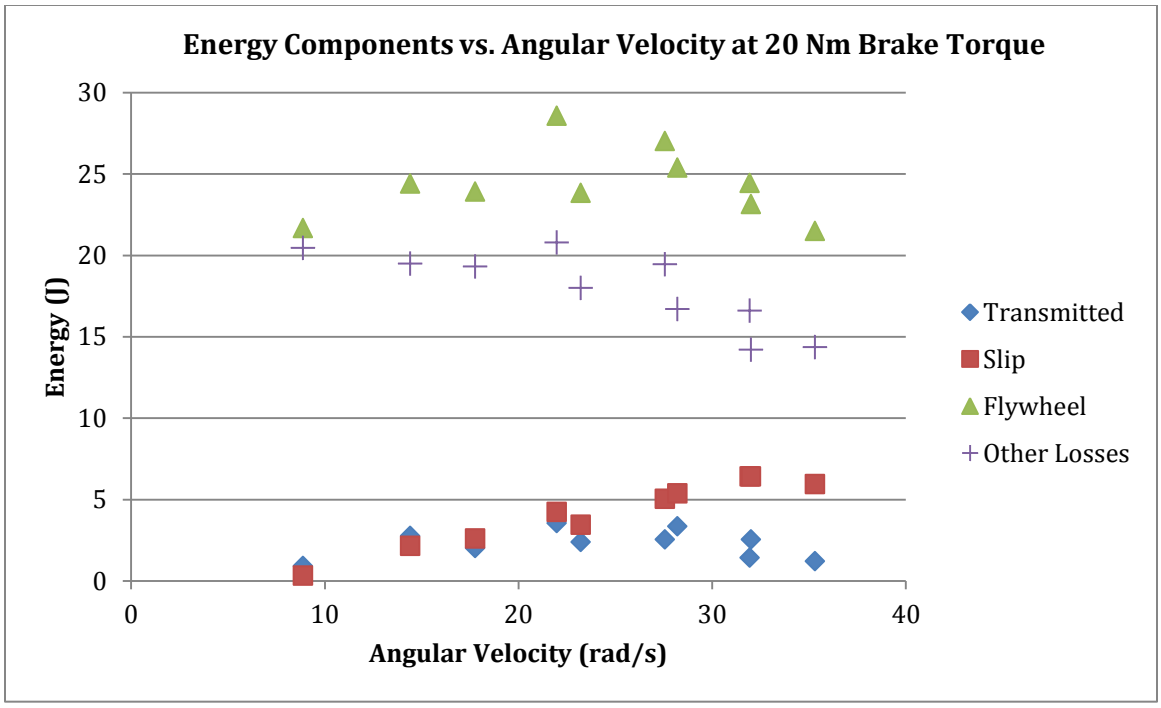

Figure 4.14: Components of energy vs. angular velocity at brake torque = 20Nm.

To calculate efficiency, the transmitted energy is divided by the total flywheel energy spent. Figures 4.15 and 4.16 plot the efficiency of single pulses vs. angular velocity at 10Nm and 20 Nm brake torques, respectively.

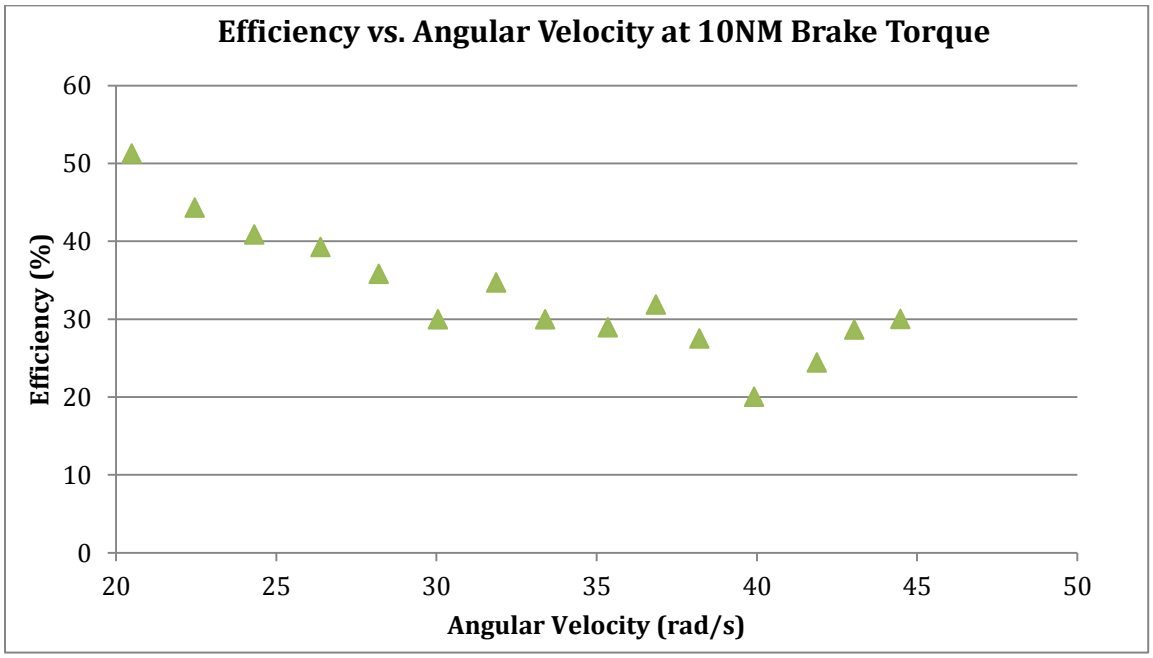

Figure 4.15: Clutch efficiency vs. angular velocity at brake torque = 10Nm

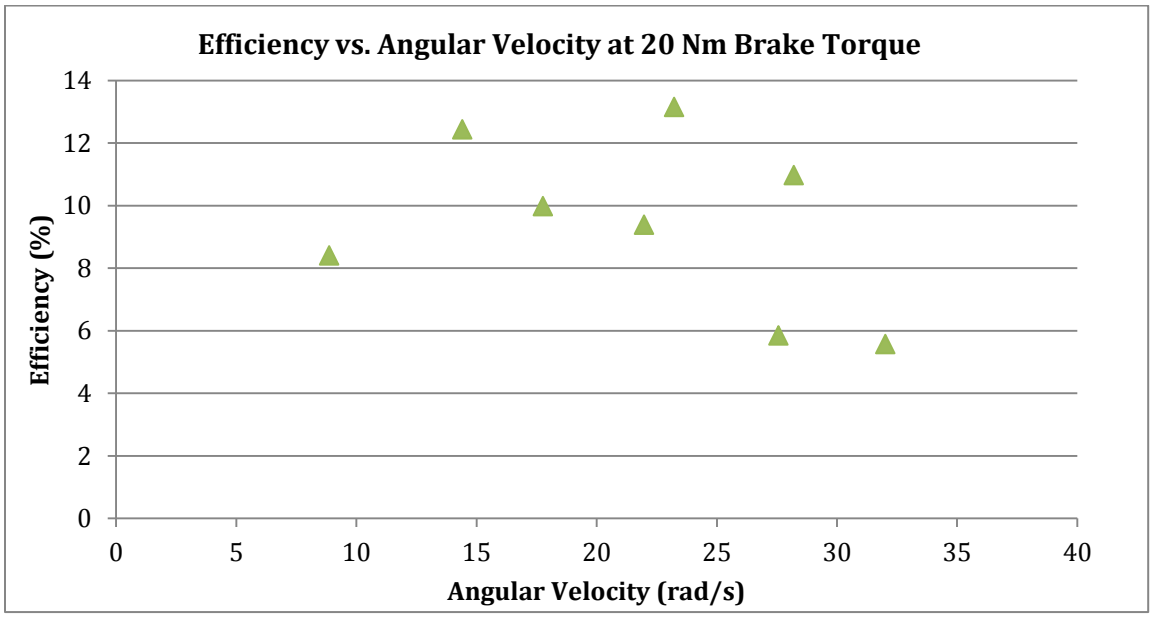

Figure 4.16: Clutch efficiency vs. angular velocity at brake torque = 10Nm

4.4 Experimental Results Discussion

Observation of these data shows that the macroscopic operation of the clutch is as intended. Discrete steps in position of the output shaft are seen with each clutch pulse. Applied to the SM CVT, these increases in rotational position would correspond to increases in torque. The velocity plot shows the flywheel stepping down in speed with each pulse, transferring its kinetic energy to the output load. The output is shown to alternate between a state of rest around zero velocity and a connected state where its speed matches the input.

Oscillation of the input and output shafts can be seen in Figure 4.4 when the clutch is either fully disengaged or fully locked. This was not expected, though in consideration of the torsional compliance innate to the system, it is a sensible

behavior. Following the high accelerations and decelerations of an engagement and disengagement, a “ringing” of the rotating inertia is incurred. On the input side, this is likely attributable to the torsional compliance of the length of shaft between the flywheel and the encoder. Because of the high inertia of the flywheel, such high frequency oscillations would not occur through the entire input assembly as a whole. Instead, it is likely that the encoder experiences local oscillation at the end of the shaft. On the output side, which is of significantly lower inertia, the oscillation at the friction disks may not be negligible, though it is likely smaller than at the far end of the shaft where the encoder is mounted and data is recorded. Some amount of torsional compliance is unavoidable, but this may be improved in the future by employing a larger diameter, possibly hollow shaft to increase torsional rigidity. Additionally, mounting the encoders closer to the flywheel and friction disks would eliminate extraneous lengths of shaft. For purposes of energy calculation, the small positive and negative oscillations in each direction over a large time period cancel, having small effect on the primary, designed mechanisms of energy transfer. In addition to the torsional compliance, manufacturing error in the cam and computational error in processing the data may also contribute to the oscillatory noise.

The maximum torque transmitted, shown in Table 4.2, was approximately 45.3Nm, 65% of the design goal of 70Nm. A likely cause of this limitation in torque capacity is the compressibility of the high friction facing. It was assumed during design that the friction facing would be ceramic or of similar hardness. Combined with the small thickness of the part, the contribution of the friction facing to total

stiffness of the system was considered negligible. Once received, it was apparent that the proprietary HB1 material was a softer, fibrous composite. This increased compliance decreases the total stiffness of the clutch assembly, and reduces the normal force produced by the displacement from the cam. Another possible factor was wear of the follower tips. Though the test setup was "reset" several times so that the air gap was at the intended value, the spherical contact surface of the followers incurred significant wear which would increase the effective air gap over time, reducing compressive travel. Other factors, such as error in the coefficient of friction of the facing or stiffness of the disk springs vs. the manufacturer reported nominal, error in the component stiffness simulations, and error in measurement may as well contribute to the discrepancy in predicted vs. measured performance torque capacity.

The kinetic energy taken from the flywheel has visible trends at both 10Nm and 20Nm that agree with the trends of the slip and transmitted energies of the clutch, as will be discussed shortly. Overall, the energy taken from the flywheel with each pulse was fairly consistent. The energy loss per pulse at 20Nm was approximately double the loss at 10Nm, as would be expected.

The transmitted energy at 10Nm was largely independent of angular velocity. This agrees with expectation, as the mechanism of energy transfer, friction, is also velocity independent. This independence is however not seen at 20Nm. At torques of 20Nm and higher, it was found that significant slipping occurred at high velocities, such that there was no output rotation until the flywheel had slowed to approximately 35-40 $\frac{rad}{s}$. The reason for this increased slipping at a combination of

high torque and high velocity is not clear. It is possible that the dynamic friction coefficient of the chosen friction facing material chosen may have a dependence on level of compression, and future testing of the clutch with other friction materials is recommended.

Slip energy is shown to increase with increasing angular velocity at both 10NM and 20Nm, as shown in Figures 4.9 and 4.10. This is sensible when looking at Equation 4.4, in which acceleration of the output inertia is equal to clutch torque minus brake torque, both theoretically constant. This results in an acceleration of the output which is also constant. As such, the time required for the output to reach the velocity of the input is greater at higher input velocity, resulting in increased slip. It is important to note that since each pulse is identified via the motion of the output, no slipping which occurs prior to output motion is captured in the data processing. In reality, significant slipping may occur when the clutch torque has not yet overcome the brake torque. It is recommended that in future testing the absolute position of the input shaft be recorded, such that pulses may instead be identified via the relative angular position of the cam to the followers.

In Figure 4.11, it is shown that the slip and transmitted energy of the clutch account for the majority of energy taken from the flywheel, and additional losses within the system are comparatively small. However, in Figure 4.12, there is a significant gap between the energy expended by the clutch and taken from the flywheel. This is likely attributable to slip occurring before the clutch has overcome the brake torque, which is unaccounted for. It can also be seen that the slip energy of disengagement is lower than engagement at both 10Nm and 20Nm. The inertia of

the output acts against the clutch during engagement, however during disengagement, it acts with the clutch, attempting to continue the forward motion of the output shaft against the brake. As such, the angle of slip during disengagement is reduced.

The efficiency of the clutch at 10Nm averages 33%. At 20Nm this value drops to 10%. The efficiency goal of 70% was not met. It is however believed that significant improvements can be made to the performance of the clutch in future testing, as will be detailed in the following chapter. Valuable understanding of the clutch concept was gained via experimental testing, and the prototype was successful in demonstrating the functionality of the design.

Chapter 5 - Conclusion

This chapter reviews the information that has been presented and discusses the conclusions the author has drawn. Based on these conclusions, recommendations for future work are also presented.

5.1 Review

The case for flywheels as a promising alternative power source for hybrid vehicles has been presented, as well as the potential for tackling the energy transfer hurdles via the emerging field of mechanical switch mode control. A gap in the performance of clutches to meet the output resolution requirements of such systems was identified. To address this gap, a novel clutch concept was sought, with design constraints drawn from the theoretical application of the Switch-Mode CVT to a full scale hybrid passenger vehicle.

Several design directions were considered, with a final concept chosen which utilized a cam rotating with the flywheel to produce and time the engagement force of friction disks connecting input to output. Detailed design and analysis was performed to create a scaled prototype of the clutch for baseline testing. The experimental procedure and gathered data were presented, with a comparison of the empirical results to the design goals. The overall operation of the clutch was shown to be as intended, but most of the performance goals were not fully met.

5.2 Conclusions

The clutch prototype was successful in demonstrating the functionality of the proposed concept. The clutch delivered discrete torque pulses resulting in a controlled advancement of the output. Use of a cam mounted to the flywheel offers implicit mechanical timing, a unique advantage over typical high speed clutches which use electronic triggering and would necessitate active sensing and processing for control. This direct link between flywheel position and clutch state allows for the advancement of the output to be controlled by the geometry of the design and the position of single input degree of freedom, rather than a time based computational synchronization. Torque transfer via mechanical means – friction and spring force – allowed for high torque transfer in a small and lightweight package.

Additionally, the axial cam with varying profile was the first of its kind that could be found in the literature, and was successful in expanding the use of cams in applications requiring a variable output. It is the hope of the author that the design approach taken in this research will inform future designs of variable profile cams. Additionally, the design considerations presented to optimize the cam for minimal switching time will inform future research of cams meant to drive mechanical switch-mode systems.

Though the clutch was successful in many ways, there are significant improvements necessary to advance the design. The experimental testing of the prototype showed that the performance goals were not met for torque transfer and

efficiency. Additionally, the test setup did not allow for testing across full intended range of operating parameters. In the following section recommendations are presented on how to improve both testing and performance in future work.

5.3 Recommendations

The size of the flywheel and speed of the control linkage actuator posed a significant limitation on the maximum duty cycle that could be reached. The energy content of the flywheel was quickly expended at its current size, limiting the maximum tested duty cycle to approximately 20%. It is expected that clutch efficiency will increase with increasing duty cycle, as the slipping transitions are a lower percentage of each pulse. Use of a larger flywheel with proper safeguards, or possibly replacement of the flywheel with a motor which could produce a controllable, non-decaying torque and velocity would allow for higher duty cycle testing. A higher speed actuator would also improve the maximum duty cycle which could be reached in a flywheel setup. Additionally, the actuator used offered no position feedback from which to calculate duty cycle directly via the control linkage geometry, necessitating that it be calculated in post processing from the recorded data. An actuator with a positional input or feedback would allow a specific duty cycle to be chosen for a test run.

The capacity of the clutch was lower than expected. As was discussed in Chapter 4, the most likely reason for this was the use of a compliant friction facing. It is likely that a stiffer, possibly ceramic facing would improve the torque performance of the clutch. In addition to the structural properties of the friction

material, understanding the effect of temperature, humidity, and other environmental factors on friction performance would benefit the design. Additionally, testing of a variety of friction facings would allow investigation of the impact of material on the increased slipping of the clutch at a combination of high torque and high velocity.

The importance of minimizing output inertia was made clear in testing. Inertial work was a significant component of total transmitted energy. Though the kinetic energy transferred to the output is useful work, the addition of the transient acceleration load leads to increased slip and energy waste during engagement. Optimization to maximize stiffness at minimum moment of inertia would benefit the design. It is likely that increasing the torque capacity of the clutch through stiffer springs or increased cam travel in a higher power prototype can be achieved with a proportionally smaller increase in output inertia through proper design.

Further optimization of the cam and follower train would also be beneficial. Transitioning quickly from low to high dwell is key to reducing slip and increasing efficiency. As discussed in Section 3.2, the inner radius of the cam was chosen as a compromise between follower travel resolution and overall package size vs. minimizing the transition duration. In future designs where a larger flywheel may be employed, increasing the inner radius of the cam would allow for a shorter transition length from low to high dwell within the constraints of minimum radius of curvature, maximum pressure angle, and maximum acceleration. Increasing the overall size of the cam however also incurs increased size of the follower control components, both the linkage and guide, so care must be taken in design. Decreasing

the rise height of the cam, in conjunction with use of stiffer springs, would allow for a shorter transition as well. However this increases the sensitivity of the system to manufacturing variation, so higher tolerances may be needed as the cam travel becomes smaller. Lastly, at the speeds encountered in testing, the linear acceleration of the follower train was small enough that the spring force was more than enough to maintain contact. At higher speeds, it will be important to optimize the translating components for minimum mass while maintaining necessary stiffness to keep inertial force below spring force.

Furthermore, because minimizing the transition duration β was constrained by the conditions at the innermost radius, it is conservative at higher radii. A dwell duration which increases with radial position could take advantage of the reduced pressure angle and increased radius of curvature at larger radii, so long as acceleration requirements are met.

The followers themselves could be significantly improved from the current sliding contact design. Inspection of the followers after testing showed that the spherical tips had been noticeably flattened, and grooves were visible in the cam in areas of high use. A design similar to a ball point pen, or perhaps a torus with a pivoting axis, would allow for rolling contact. This would reduce component wear and also energy loss from follower friction.

Several improvements to the test setup are also recommended. A torque transducer at the output, though higher cost, would allow for direct measurement of torque. This would greatly reduce error both from calculated inertia values and derivation of acceleration from position. Use of accelerometers in parallel with

angular encoders would allow the recorded data to be checked from both measurements, and allow for more accurate acceleration data of the input and output shafts. As discussed in the previous chapter, mounting the encoders at the ends of both shafts, a significant distance from the axial points of interest, incurred increased torsional oscillation. Mounting sensors closer in line to the flywheel and output disk would help to mitigate this.

In conclusion, the first prototype of a cam driven high speed clutch successfully demonstrated the potential of the concept, but more research and development is necessary to advance the design. There is significant opportunity for improvement of performance, primarily in the areas of torque capacity, switching efficiency, and component life.

References

[1] Forbes, T. and Van de Ven, J., 2008, “Switch-Mode Continuously Variable Transmission with Flywheel Energy Storage.” ASME International Mechanical Engineering Congress and Exposition 2008

[2] Demetriou, M. A., Van de Ven, J. D., 2011, “Switch-Mode Continuously Variable Transmission: Modeling and Optimization.” Journal of Dynamic Systems, Measurement, and Control, Vol. 133, May, 2011

[3] 2012, "Department of Energy, Annual Energy Review 2011." *DOE/EIA-0384*, Energy Information Administration (EIA), Washington, D.C.

[4] www.fueleconomy.gov, 2012, website: http://www.fueleconomy.gov/feg/hybridtech.shtml

[5] Carrasco, J. M., Franquelo, L. G., Galvan, E., and Lukic, S. M., Sergio Vazquez, E10, “Energy Storage Systems for Transport and Grid Applications.” IEEE Transactions on Industrial Electronics, Vol. 57, No. 12, December 2010

[6] Krejnin, G. V. and Krivts, I. L., 2006, “Pneumatic Actuating Systems for Automatic Equipment : Structure and Design.” CRC/Taylor & Francis, Boca Raton

[7] Cross, D. and Brockbank, C., 2009, "Mechanical Hybrid System Comprising a Flywheel and CVT for Motorsport and Mainstream Automotive Applications." SAE Technical Paper 2009-01-1312

[8] Johns, W. E., 2003, “Notes on Continuously Variable Transmissions.” website: http://www.gizmology.net/cvt.htm

[9] Beachley, N. H. and Frank A. A., 1979, “Continuously Variable Transmissions: Theory and Practice.” University of Wisonsin, Madison, WI

[10] Clark, R., 2009, “New Drive System Takes Gears Out of the Equation.” *Industrial Technology*, June 2009, p. 28

[11] Diego-Ayala, U., Martinez-Gonzalez, P., and Pullen, K. R., 2008, “A Simple Mechanical Transmission System for Hybrid Vehicles Incorporating a Flywheel.” Hybrid and Eco-Friendly Vehicles Conference 2008

[12] Erickson, R. W. and Maksimovic, D., 2001, *Fundamentals of Power Electronics, Second Edition*, Kluwer Academic Publishers, Secaucus, NJ

[13] Cyders, T. and Williams, R. L. II, “Analysis of a New Form of Intrinsically Automatic Continuously Variable Transmission.” DETC2010/MECH-28729, ASME International Design Engineering Technical Conferences & Computers and Information in Engineering Conference, August 15-18, 2010

[14] Lahr, D. F. and Hong, D. W., 2006, “The Operation and Kinematic Analysis of a Novel Cam-Based Infinitely Variable Transmission.” DETC2006-99634, ASME International Design Engineering Technical Conferences & Computers and Information in Engineering Conference, September 10-13, 2006

[15] Benitez, F. G., Centeno, G., Morales, F., and Perez, F. B., 2010, “Continuous Variable Transmission With an Inertia-Regulating System,” ASME Journal of Mechanical Design, Vol. 132, May 2010

[16] Gilbert, J. M., Oldaker, R. S., Grindley, J. E., and Taylor, P. M., 1996, "Control of a Novel Switched Mode Variable Ratio Drive." *UKACC International Conference on Control*, **1**, University of Exeter, UK, pp. 412-417.

[17] Araujo, J. M., DeMalia, M. A., Lambusta, C. M., Morocco, A. J., Van de Ven, J., 2009, “Switch-Mode Continuously Variable Transmission”, Worcester Polytechnic Institute

[18] Brennen, C. E., Brennen D., and McKinnon C. N., 2001, “Hydraulic Analysis of a Reversible Fluid Coupling,” ASME Journal of Fluids Engineering, Vol. 123, June, 2001

[19] Brown, L. R., 1956, “The Principle Mechanical and Electrical Features of a Hysteresis Clutch.” IRE Transactions on Industrial Electronics, Vol. 3

[20] Ogura Industrial Corporation, 2012, “HB Electromagnetic Hysteresis Brake.” website: http://www.ogura-clutch.com/products.html?category=2&product=84

[21] Magtrol Incorporated, 2012, “Hysteresis Clutches.” website: http://www.magtrol.com/brakesandclutches/hysteresis_clutches.html

[22] Hofer Powertrain GmbH, 2009, “Potentials and Development Methodology for Transmissions with Dog Clutches.” website: www.hofer.de

[23] Reynolds, K., 2004, “Motor Trend 2004 Car of the Year Winner: Toyota Prius.” Motor Trend Magazine, January, 2004

[24] Prius image and dimensions from: http://www.the-blueprints.com/index.php?blueprints/cars/toyota/20845/view/

[25] Bharathan, D., Cao, J., Emadi, A., 2007, "Efficiency and Loss Models for Key Electronic Components of Hybrid and Plug-in Hybrid Electric Vehicles' Electrical Propulsion Systems." IEEE Vehicle Power and Propulsion Conference 2007

[26] Pulse Width Modulation / Pulse Position Modulation comparison adapted from: http://www.cs.unca.edu/~bruce/Fall11/255/Labs/Lab13AnalogInput.html

[27] Brown, M. D., Plummer, A. R., Richardson, R., 2001, "Self-Tuning Control of a Low-Friction Pneumatic Actuator Under the Influence of Gravity." IEEE Transactions on Control Systems Technology, Vol. 9, No. 2, March, 2001

[28] Misra, S., Peerdeman, B., Plettenburg, D., Smit, G., Stramigioli, S., 2012, "Evaluation of Pneumatic Cylinder Actuators for Hand Prostheses." IEEE International Conference on Biomedical Robotics and Biomechatronics, Roma, Italy, June 24-27, 2012

[29] Ding, C., Yang, Y., 2008, "Analysis and Improvement Method of the Dynamic Response of Electromagnetic Clutch Used in the Tufted Carpet Jacquard." International Conference on Computer and Electrical Engineering, 2008

[30] Book, J. W., Swanson, D. K., 2000, "Torque Feedback Control of Dry Friction Clutches for a Dissipative Passive Haptic Interface." Proceedings of the IEEE International Conference on Control Applications, Anchorage, AK, September 25-27, 2000

[31] Norton, R. L., 2002, "Cam Design and Manufacturing Handbook." Industrial Press, Inc., NY, NY

[32] Norton, R. L., 2008, "Design of Machinery: An Introduction to the Synthesis and Analysis of Mechanisms and Machines", McGraw Hill, Boston

[33] Four bar coupler curve image from: http://www.mhhe.com/engcs/mech/norton/norton/ch3/coupler_curve_atlas/coupler_curve_atlas.htm#info

[34] Variable valve timing image from: http://auto.howstuffworks.com/camshaft2.htm

[35] Axial cam image from: http://www.e-star.com.sg/services_cam.html

[36] Disk spring images adapted from: http://www.circlip.net/disc-washers.html

Appendices

Appendix A contains the part drawings for the custom machined clutch components.

Appendix B details the force and stress analysis for the control linkage.

Appendix C details the FEA procedure used to determine component stiffness and structural integrity.

Appendix D contains the Matlab code used to post process the experimental data.

Appendix A: Part Drawings

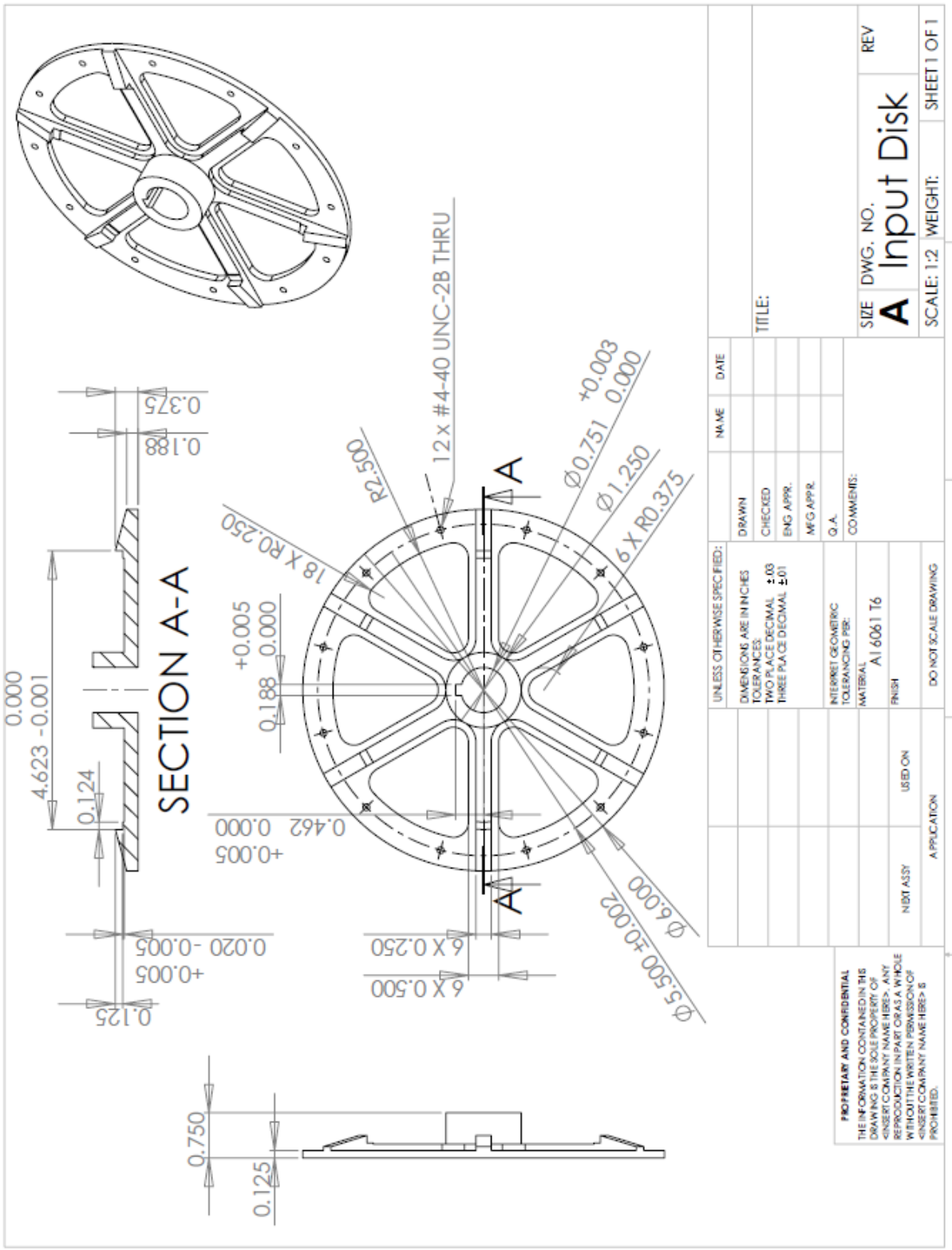

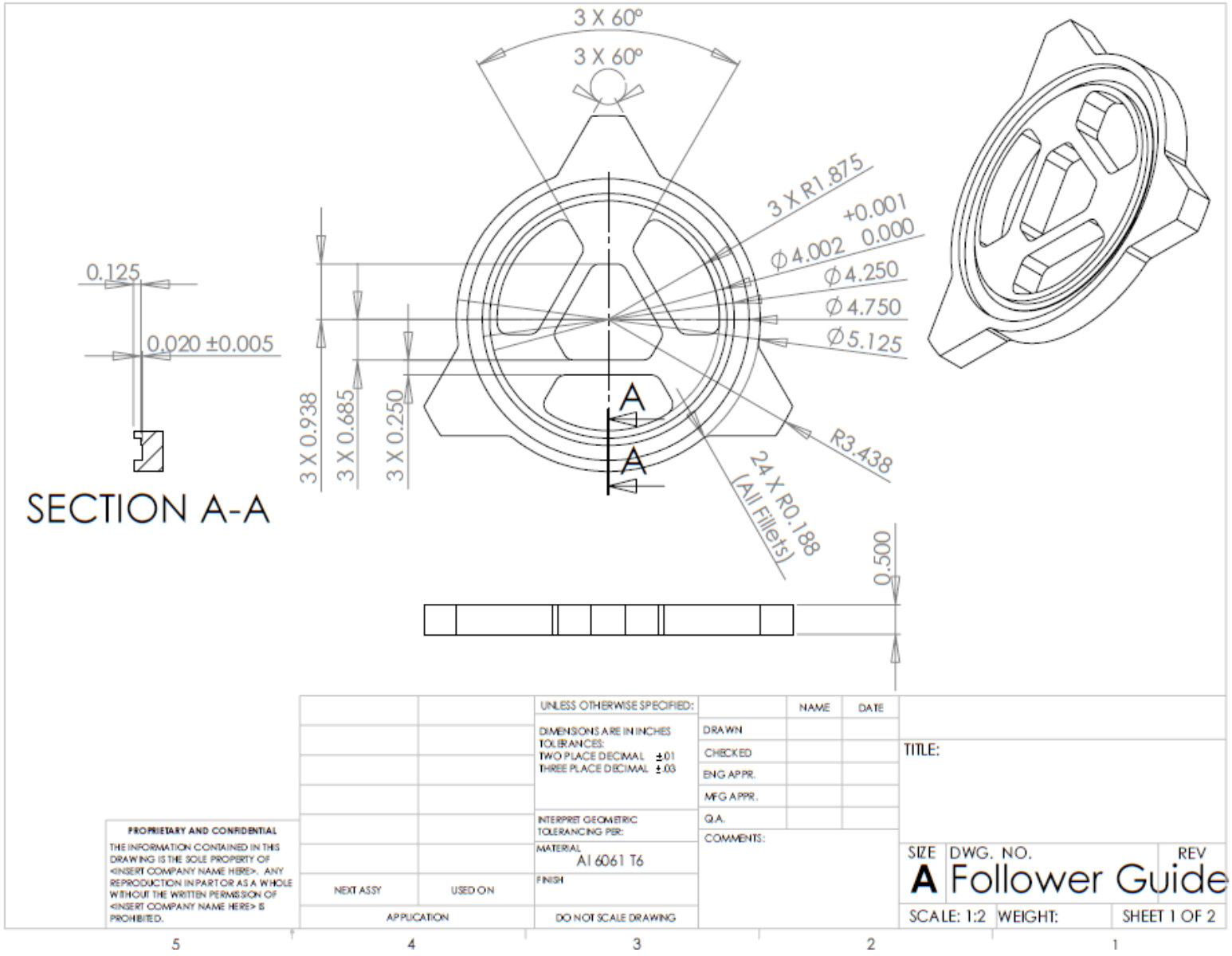
3 X 60°
3 X 60°
3 X R1.875
+0.001
Ø4.002 0.000
Ø4.250
Ø4.750
Ø5.125
R3.438
24 X R0.188
(All Fillets)
0.500
3 X 0.938
3 X 0.685
3 X 0.250
A
A
0.125
0.020 ±0.005
SECTION A-A
UNLESS OTHERWISE SPECIFIED:
DIMENSIONS ARE IN INCHES
TOLERANCES:
TWO PLACE DECIMAL ±.01
THREE PLACE DECIMAL ±.005
INTERPRET GEOMETRIC TOLERANCING PER:
MATERIAL
Al 6061 T6
FINISH
DO NOT SCALE DRAWING
NEXT ASSY
USED ON
APPLICATION
DRAWN
CHECKED
ENG APPR.
MFG APPR.
Q.A.
COMMENTS:
NAME
DATE
TITLE:
SIZE
DWG. NO.
REV
A
Follower Guide
SCALE: 1:2
WEIGHT:
SHEET 1 OF 2
PROPRIETARY AND CONFIDENTIAL
THE INFORMATION CONTAINED IN THIS DRAWING IS THE SOLE PROPERTY OF <INSERT COMPANY NAME HERE>. ANY REPRODUCTION IN PART OR AS A WHOLE WITHOUT THE WRITTEN PERMISSION OF <INSERT COMPANY NAME HERE> IS PROHIBITED.
5
4
3
2
1

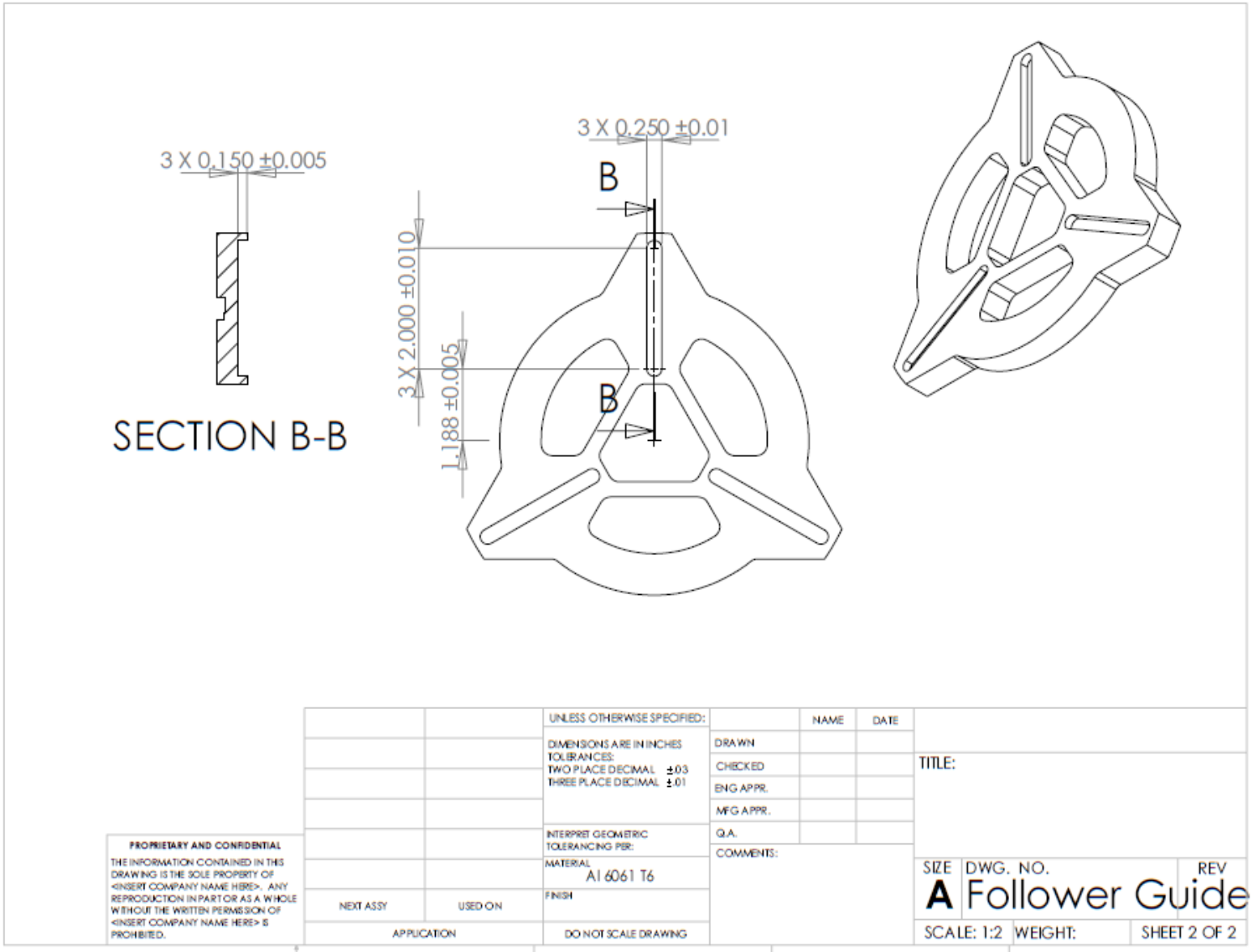
3 X 0.150 ±0.005
SECTION B-B
3 X 0.250 ±0.01
B
3 X 2.000 ±0.010
1.188 ±0.005
B
UNLESS OTHERWISE SPECIFIED:
DIMENSIONS ARE IN INCHES
TOLERANCES:
TWO PLACE DECIMAL ±.03
THREE PLACE DECIMAL ±.01
INTERPRET GEOMETRIC TOLERANCING PER:
MATERIAL
Al 6061 T6
FINISH
DO NOT SCALE DRAWING
NAME
DATE
DRAWN
CHECKED
ENG APPR.
MFG APPR.
Q.A.
COMMENTS:
TITLE:
SIZE
DWG. NO.
REV
A
Follower Guide
SCALE: 1:2
WEIGHT:
SHEET 2 OF 2
NEXT ASSY
USED ON
APPLICATION
PROPRIETARY AND CONFIDENTIAL
THE INFORMATION CONTAINED IN THIS DRAWING IS THE SOLE PROPERTY OF <INSERT COMPANY NAME HERE>. ANY REPRODUCTION IN PART OR AS A WHOLE WITHOUT THE WRITTEN PERMISSION OF <INSERT COMPANY NAME HERE> IS PROHIBITED.
5
4
3
2
1

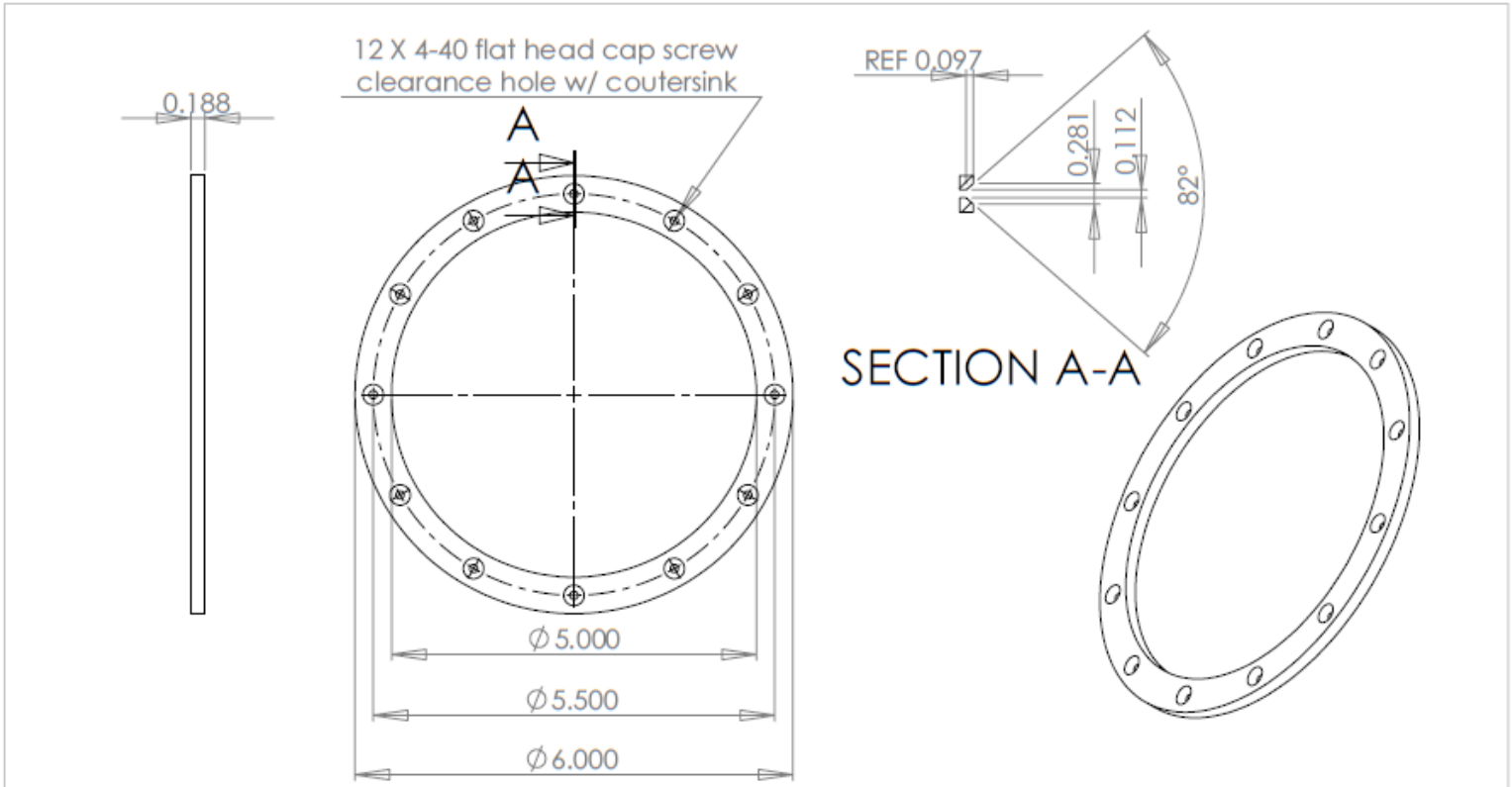

		UNLESS OTHERWISE SPECIFIED:		NAME	DATE
		DIMENSIONS ARE IN INCHES TOLERANCES: TWO PLACE DECIMAL ±.03 THREE PLACE DECIMAL ±.01	DRAWN		
			CHECKED		
			ENG APPR.		
			MFG APPR.		
		INTERPRET GEOMETRIC TOLERANCING PER:	Q.A.		
		MATERIAL NF 780	COMMENTS:		
NEXT ASSY	USED ON	FINISH			
APPLICATION		DO NOT SCALE DRAWING			

PROPRIETARY AND CONFIDENTIAL

THE INFORMATION CONTAINED IN THIS DRAWING IS THE SOLE PROPERTY OF <INSERT COMPANY NAME HERE>. ANY REPRODUCTION IN PART OR AS A WHOLE WITHOUT THE WRITTEN PERMISSION OF <INSERT COMPANY NAME HERE> IS PROHIBITED.

TITLE:

SIZE	DWG. NO.	REV
A	FrictionFacing	

SCALE: 1:2	WEIGHT:	SHEET 1 OF 1

5 4 3 2 1

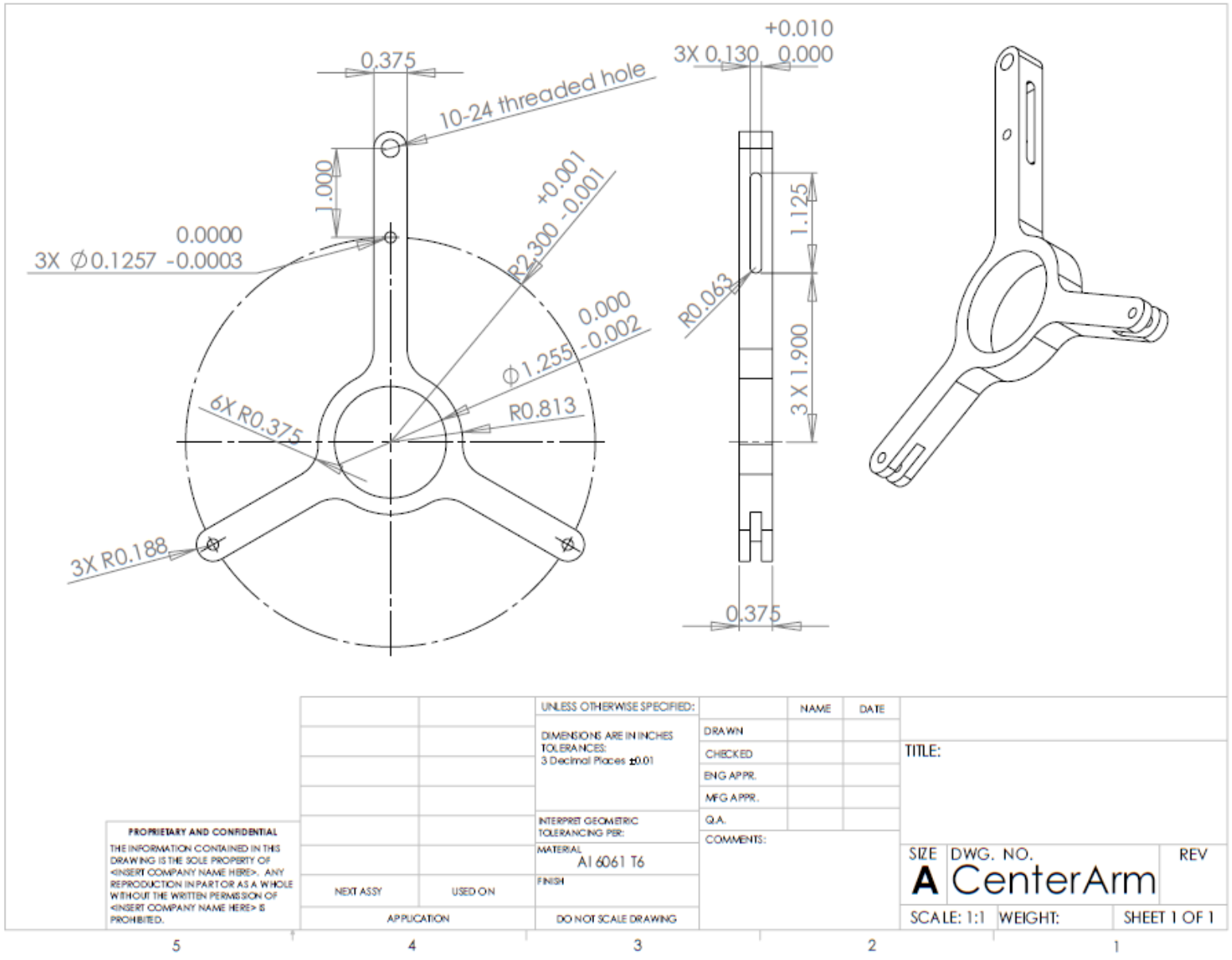
0.375
10-24 threaded hole
1.000
+0.001
R2.300 -0.001
0.0000
3X ∅0.1257 -0.0003
0.000
∅1.255 -0.002
6X R0.375
R0.813
3X R0.188
+0.010
3X 0.130 0.000
1.125
R0.063
3 X 1.900
0.375
UNLESS OTHERWISE SPECIFIED:
DIMENSIONS ARE IN INCHES
TOLERANCES:
3 Decimal Places ±0.01
INTERPRET GEOMETRIC TOLERANCING PER:
MATERIAL
Al 6061 T6
FINISH
NEXT ASSY
USED ON
APPLICATION
DO NOT SCALE DRAWING
NAME
DATE
DRAWN
CHECKED
ENG APPR.
MFG APPR.
Q.A.
COMMENTS:
TITLE:
SIZE
A
DWG. NO.
CenterArm
REV
SCALE: 1:1
WEIGHT:
SHEET 1 OF 1
PROPRIETARY AND CONFIDENTIAL
THE INFORMATION CONTAINED IN THIS DRAWING IS THE SOLE PROPERTY OF <INSERT COMPANY NAME HERE>. ANY REPRODUCTION IN PART OR AS A WHOLE WITHOUT THE WRITTEN PERMISSION OF <INSERT COMPANY NAME HERE> IS PROHIBITED.
5
4
3
2
1

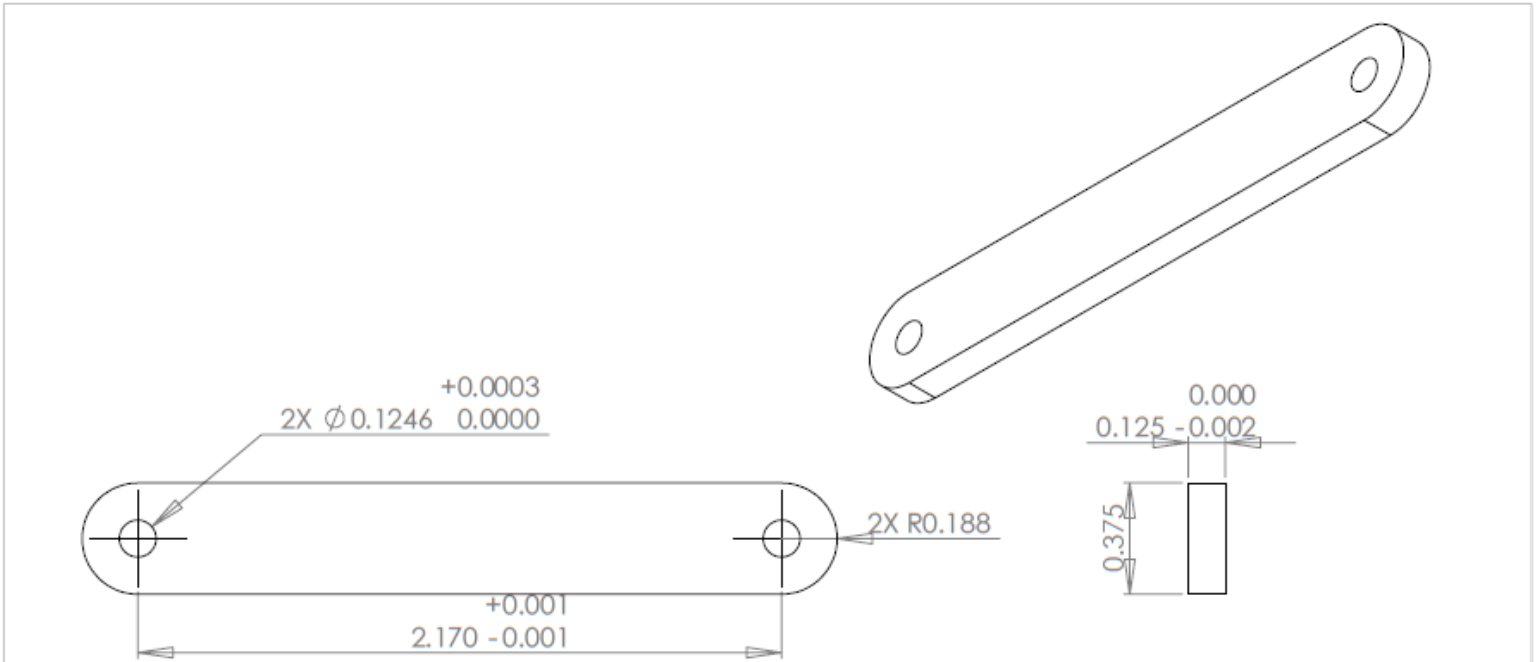

		UNLESS OTHERWISE SPECIFIED:		NAME	DATE
		DIMENSIONS ARE IN INCHES TOLERANCES: 3 Decimal Places ± .01	DRAWN		
			CHECKED		
			ENG APPR.		
			MFG APPR.		
		INTERPRET GEOMETRIC TOLERANCING PER:	Q.A.		
		MATERIAL Steel	COMMENTS:		
NEXT ASSY	USED ON	FINISH			
APPLICATION		DO NOT SCALE DRAWING			

PROPRIETARY AND CONFIDENTIAL

THE INFORMATION CONTAINED IN THIS DRAWING IS THE SOLE PROPERTY OF <INSERT COMPANY NAME HERE>. ANY REPRODUCTION IN PART OR AS A WHOLE WITHOUT THE WRITTEN PERMISSION OF <INSERT COMPANY NAME HERE> IS PROHIBITED.

TITLE:

SIZE	DWG. NO.	REV
A	Coupler	
SCALE: 2:1	WEIGHT:	SHEET 1 OF 1

5 4 3 2 1

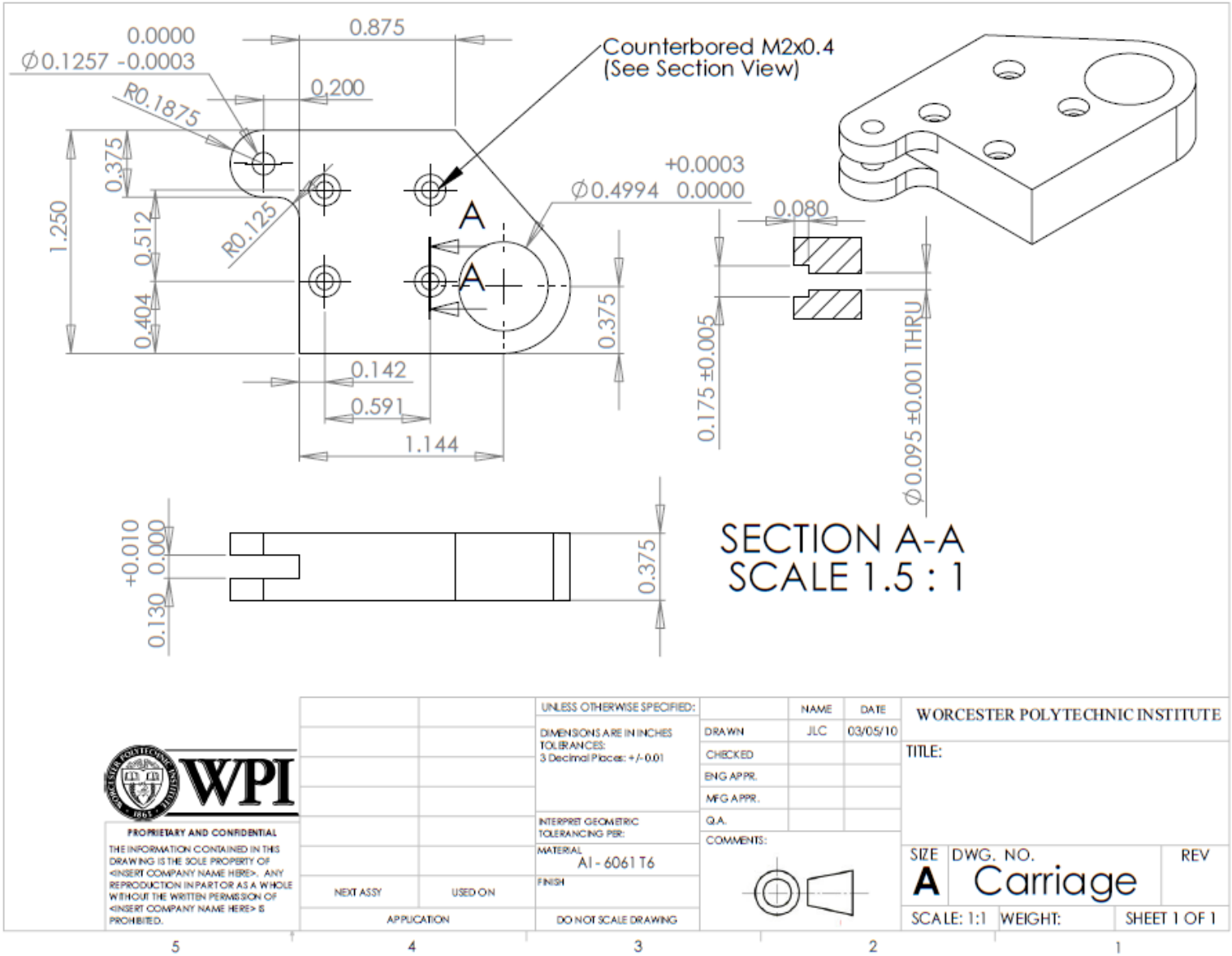
0.0000
Ø0.1257 -0.0003
0.875
Counterbored M2x0.4
(See Section View)
0.200
R0.1875
0.375
1.250
0.512
R0.125
0.404
+0.0003
Ø0.4994 0.0000
0.080
A
A
0.375
0.142
0.591
1.144
0.175 ±0.005
Ø0.095 ±0.001 THRU
+0.010
0.000
0.130
0.375
SECTION A-A
SCALE 1.5 : 1
UNLESS OTHERWISE SPECIFIED:
DIMENSIONS ARE IN INCHES
TOLERANCES:
3 Decimal Places: +/- 0.001
INTERPRET GEOMETRIC TOLERANCING PER:
MATERIAL
Al - 6061 T6
FINISH
DO NOT SCALE DRAWING
NEXT ASSY
USED ON
APPLICATION
NAME
DATE
DRAWN
JLC
03/05/10
CHECKED
ENG APPR.
MFG APPR.
Q.A.
COMMENTS:
WORCESTER POLYTECHNIC INSTITUTE
TITLE:
SIZE
A
DWG. NO.
Carriage
REV
SCALE: 1:1
WEIGHT:
SHEET 1 OF 1
PROPRIETARY AND CONFIDENTIAL
THE INFORMATION CONTAINED IN THIS DRAWING IS THE SOLE PROPERTY OF <INSERT COMPANY NAME HERE>. ANY REPRODUCTION IN PART OR AS A WHOLE WITHOUT THE WRITTEN PERMISSION OF <INSERT COMPANY NAME HERE> IS PROHIBITED.
5
4
3
2
1

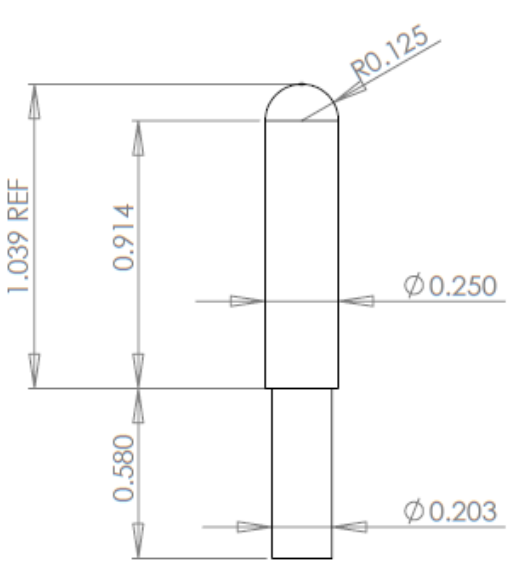

		UNLESS OTHERWISE SPECIFIED:		NAME	DATE
		DIMENSIONS ARE IN INCHES TOLERANCES: FRACTIONAL ± ANGULAR: MACH ± BEND ± TWO PLACE DECIMAL ± THREE PLACE DECIMAL ±	DRAWN		
			CHECKED		
			ENG APPR.		
			MFG APPR.		
		INTERPRET GEOMETRIC TOLERANCING PER:	Q.A.		
		MATERIAL AIS1 4140	COMMENTS:		
NEXT ASSY	USED ON	FINISH			
APPLICATION		DO NOT SCALE DRAWING			

PROPRIETARY AND CONFIDENTIAL
THE INFORMATION CONTAINED IN THIS DRAWING IS THE SOLE PROPERTY OF <INSERT COMPANY NAME HERE>. ANY REPRODUCTION IN PART OR AS A WHOLE WITHOUT THE WRITTEN PERMISSION OF <INSERT COMPANY NAME HERE> IS PROHIBITED.

TITLE:

SIZE A | DWG. NO. Follower | REV

SCALE: 2:1 | WEIGHT: | SHEET 1 OF 1

5 4 3 2 1

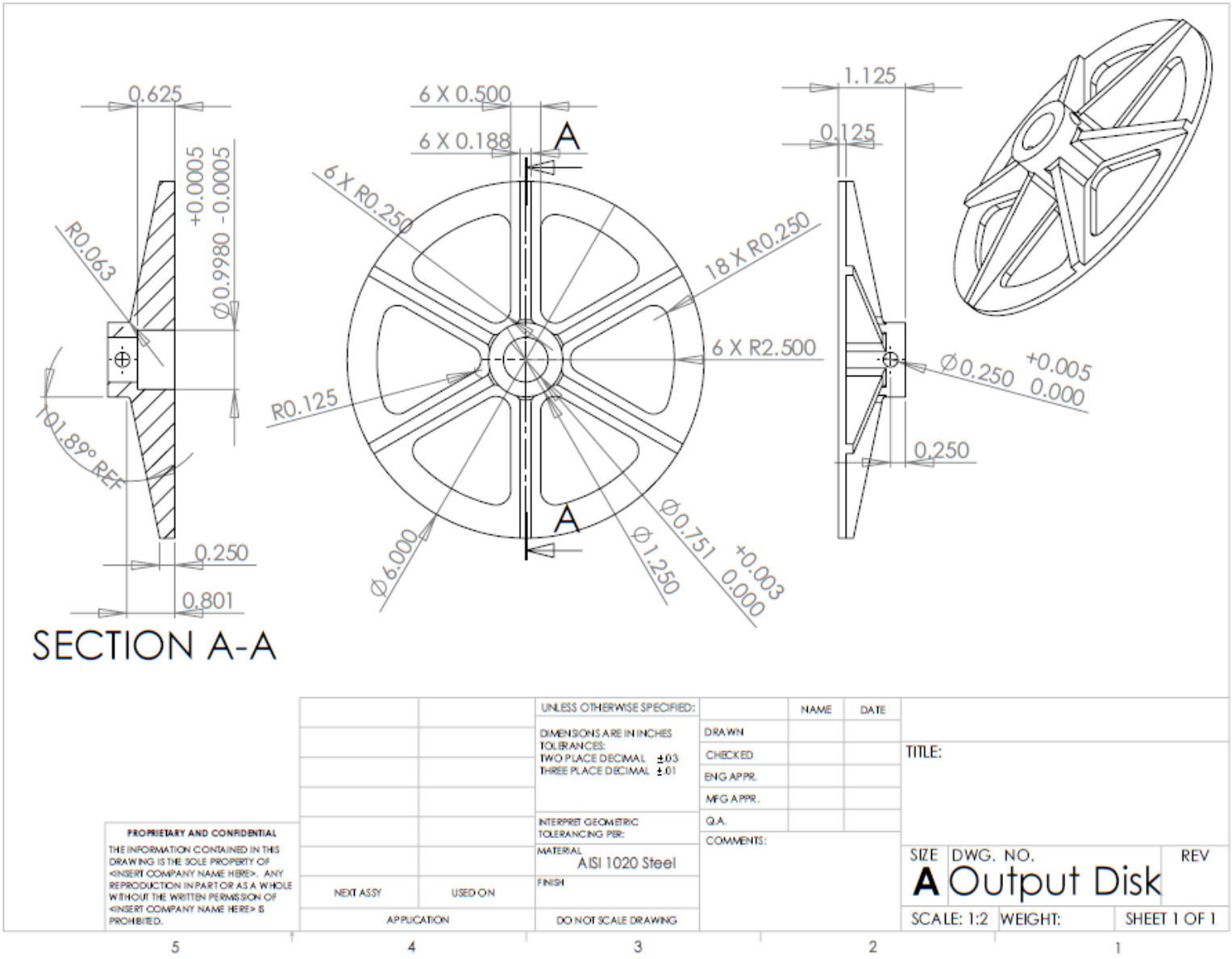
0.625
+0.0005
Ø0.9980 -0.0005
R0.063
101.89° REF
0.250
0.801
SECTION A-A
6 X 0.500
6 X 0.188
A
6 X R0.250
18 X R0.250
6 X R2.500
R0.125
Ø6.000
Ø1.250
Ø0.751 +0.003 0.000
1.125
0.125
Ø0.250 +0.005 0.000
0.250
UNLESS OTHERWISE SPECIFIED:
DIMENSIONS ARE IN INCHES
TOLERANCES:
TWO PLACE DECIMAL ±.03
THREE PLACE DECIMAL ±.01
INTERPRET GEOMETRIC TOLERANCING PER:
MATERIAL
AISI 1020 Steel
FINISH
DO NOT SCALE DRAWING
NAME
DATE
DRAWN
CHECKED
ENG APPR.
MFG APPR.
Q.A.
COMMENTS:
NEXT ASSY
USED ON
APPLICATION
PROPRIETARY AND CONFIDENTIAL
THE INFORMATION CONTAINED IN THIS DRAWING IS THE SOLE PROPERTY OF <INSERT COMPANY NAME HERE>. ANY REPRODUCTION IN PART OR AS A WHOLE WITHOUT THE WRITTEN PERMISSION OF <INSERT COMPANY NAME HERE> IS PROHIBITED.
TITLE:
SIZE
DWG. NO.
REV
A
Output Disk
SCALE: 1:2
WEIGHT:
SHEET 1 OF 1
5
4
3
2
1

Appendix B: Control Linkage Static Analysis

To determine the forces exerted on the control linkage and verify structural adequacy of the design, a static analysis was carried out. Due to the pressure angle of the cam, the compression of the disk springs due to cam displacement exerts force on the control linkage, as well as moments on the linear slides. Figure 22 shows the coordinate system used in the analysis, with the force from the cam applied at the follower tip.

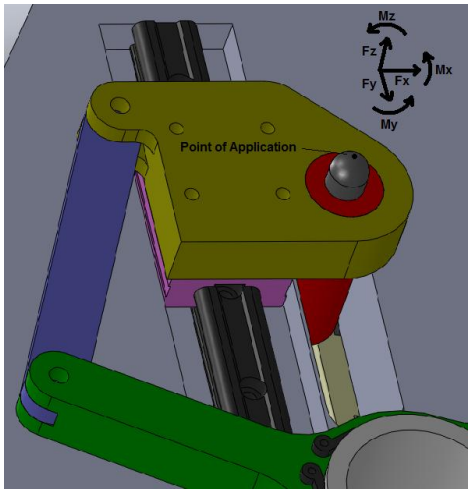

Figure B.1: Linkage static analysis coordinate system. Forces from the cam are considered to be applied at the tip of the follower.

Forces from the cam in the x, y, and z directions are:

F_z - force in direction of follower displacement. As the follower slides in a smooth brass bearing, forces applied to the linkage in this direction are considered negligible, and so:

$F_z = 0$

F_x = force from the rise and fall segments due to the pressure angle of the cam. Maximum pressure angle as detailed in Section 3.2.1 is 28.2˚. This occurs at $\frac{\beta}{\theta}$ = 0.5, where follower acceleration is 0 and the spring has been compressed 0.95mm after closing the air gap. Given the stacked disk spring stiffness of 288.5 $\frac{N}{mm}$ as detailed in Section 2.8, this gives a resulting spring force of 274N. The lateral component of this force due to the pressure angle of the cam is then:

$$F_x = 274N * \sin(28.2^\circ) = 129.5N$$

F_y - force from radial translation of the followers over the transition section from 0% duty cycle to the outer radii at full rise height as detailed in Section 3.2.2. The pressure angle over this profile is the same as in the rise and fall, and so the component of force is calculated the same as for F_x:

$$F_x = 274N * \sin(28.2^\circ) = 129.5N$$

To calculate moments applied to the linear guide, F_x nd F_y are multiplied by their effective moment arms from the tip of the follower to the center of the slide block. These moment arms as measured from the CAD geometry are:

L_x = 17.8mm

L_y = 6.5mm

L_z = 20.6mm

and the resultant moments are:

$$M_x = F_y * L_z = 2.67\ Nm$$

$M_y = F_x * L_z = 2.67\ Nm$

$M_z = F_y * L_x = 2.31\ Nm$

It should be noted that a moment about the z axis is also created by $F_x * L_y$, however it is of the opposite sign as $F_y * L_x$ and the forces F_x and F_y will never occur simultaneously, and so the greater of the two moments was used. The maximum allowable moment recommended by the linear slide manufacturer PBC Linear are M_x = 6.33 Nm, M_y = 9.94 Nm, and M_z = 6.33 Nm, and so the applied moments are within specification.

The linkage is only loaded by F_y, as F_x is reacted by the linear slide. The possible failure modes of the linkage are bending of the arms of the center link, or "tearout" failure of the pin joints. Stress in the pins, coupler links, and clevises of the carriages and center arm is estimated as [32]:

$$\sigma_{pin,coupler,clevis} = \frac{F_y}{A_{pin,coupler,clevis}} \qquad \text{Equation B.1}$$

where A_{pin}, $A_{coupler}$, and A_{clevis} are the area of material supporting load in the pin, coupler, and clevises of the carriage and center link. The pin is loaded in double shear, and so its area is:

$A_{pin} = 2\pi r_{pin}^2$

where r_{pin} is equal to the pin radius of 1.59mm (0.625") for all pins used in the linkage. The coupler link is loaded in tension, and its area around the pins is:

$A_{coupler} = h_{coupler} * (w_{coupler} - 2r_{pin})$

where $h_{coupler}$ and $w_{coupler}$ are the height of the coupler link at 3.18mm (.125") and width of the coupler link at 9.53mm (.375"), respectively. The clevises of the center arm and carriage are also loaded in tension, and their area around the pins is:

$A_{clevis} = (h_{clevis} - h_{coupler})* (w_{clevis} - 2r_{pin})$

where h_{clevis} and w_{clevis} are the height and width of the clevises, both equal to 9.53mm (.375”).

With these areas known, Equation B.1 may be solved for the stresses in each component, giving σ_{pin} = 8.15 MPa, $\sigma_{coupler}$ = 6.40 MPa, and σ_{clevis} = 3.20 Mpa. The chosen material for the center arm and carriages was 6061 T6 aluminum, giving a tensile yield strength of 276 MPa. To avoid aluminum-on-aluminum bearing surfaces which perform poorly [32], the material for the pin and coupler was chosen to be AISI 1020 steel, giving a tensile yield strength of 384 MPa. As such, the design of the pin joints is well within the material limits.

The stress in the arms of the center link due to bending is estimated via the classical Euler-Bernoulli beam bending stress equation to be:

$$\sigma_{arm} = \frac{F_y L_{arm} \frac{h_{arm}}{2}}{I_{arm}} \qquad \text{Equation B.2}$$

where L_{arm} is the length of the arm at 37.77mm, h_{arm} is the height of the arm at 9.53mm, and I_{arm} is the area moment of inertia of the arm at $6.87E^{-10}m^4$, height, and area moment of inertia of the arm. This gives a resulting stress of σ_{arm} = 33.9 MPa, well under the yield stress of aluminum.

Appendix C: Finite Element Procedure

Component loading simulations were performed in the CosmosWorks Finite Element feature of Solidworks. A mesh convergence study on the input and output disks showed a mesh size of 1.27mm (0.05") to offer sufficient resolution, and this mesh size was used for most components. A smaller mesh size was necessary for the followers, while a larger mesh was sufficient for the support posts and other enclosure components.

To determine the stiffness of each part, loads and boundary conditions representative of operational use were applied. Table B.1 lists the boundary conditions and loading conditions of each part that was simulated, as well as the displacement response and resultant stiffness.

Component	Fixed Location	Loaded Location	Load (N)	Deflection (mm)	Stiffness (N/mm)
Posts	top and bottom surfaces	flange bearing mounting holes	2045	1.17E-02	1.75E+05
Top Plate	right side post mounting holes	left side post mounting holes	2045	7.78E-03	2.63E+05
Base Plate	right side post mounting holes	left side post mounting holes	2045	4.67E-03	4.38E+05
Flywheel	inner diameter	3 point loads at rmax (81mm)	3 X 682	7.30E-04	2.80E+06
Follower	stepped surface	tip	682	1.62E-03	4.21E+05
Guide	bearing mating surface	3 point loads at rmax (81mm)	3 X 682	5.83E-02	3.51E+04
Input Disk	bearing mating surface	contact surface	2045	2.09E-02	9.80E+04
Output Disk	inner diameter	contact surface	2045	5.86E-02	3.49E+04
Input Shaft	axial position of flange bearing	axial position of flywheel	2045	1.14E-03	1.79E+06
Output Shaft	axial position of flange bearing	axial position of input disk	2045	5.71E-04	3.58E+06

Table C.1: FEA setup details

Appendix D: Data Processing Matlab Code

```
% ClutchPostProc.m script m-file
% AUTHORS:
% Jessy Cusack and James D. Van de Ven
% Worcester Polytechnic Institute
% Department of Mechanical Engineering
%
% CREATION DATE:
% 2/23/2011
%
% PURPOSE:
% Post process data acquired through Labview for the switch-mode clutch
% experiments
%
% UPDATES:
% Code based on BMPostProc_v8.m
%
% PHYSICAL DESCRIPTION:
% Ch1=Theta1(deg), Ch2=Theta2(deg)
%
% Clear command window, clear all variables from memory, close all
figures.
clc; clear all; close all;

%%%%%%%%%%%%%%%%%%% Reading Data File %%%%%%%%%%%%%%%%%%%%%

filename='_';
[filename, dirpath]=uigetfile('*.csv', 'Select Data File to Process');
channels = csvread([dirpath filename], 13, 1, [13 1 13 1]);
data=csvread([dirpath filename], 23, 1);

fprintf('Input Brake Torque (N*m) = ')
TauBrake = input(''); %N*m  Torque of the brake on output shaft
(dynamic friction)

%%%%%%%%%%%%%%%%%%% Defined Variables %%%%%%%%%%%%%%%%%%%%%

Inertia1 = .2013; %kg*m^2 Inertia of flywheel, input shaft, input disk,
and thrust bearing
Inertia2 = .0026; %kg*m^2  Inertia of the output shaft, output disc,
brake, and hub
% TauBrake = 10; %N*m  Torque of the brake on output shaft (dynamic
friction)

delta_t = .00002; %s  Timestep
samples = length(data);
endtime = delta_t*samples;

OmegaThres = 8; %rad/s  Threshold ang velocity for an engagement

CutFreq = 500; %Hz  Cutoff Frequency for Butterworth Low Pass Filter
CutFreq2 = 2000; %Hz  Cutoff Frequency for Butterworth Low Pass Filter
Fs = samples(1) / endtime(1); %S/s  Sample frequency for PTs (for
normalizing filter frequency)
```

```
%%%%%%%%%%%%%%%%%%% Beginning of Main Code %%%%%%%%%%%%%%%%%%%%%

Theta1 = data([1:samples],1) * pi/180; %radians  Position of Input
Shaft
Theta2 = data([1:samples],2) * pi/180; %radians  Position of Output
Shaft
time = (0:delta_t:delta_t*(samples-1))';

%Create Butterworth Filter
[z,p,k] = butter(2,CutFreq/Fs,'low'); %2nd order, normalized cutoff
freq, lowpass
[sos,g] = zp2sos(z,p,k);
h = dfilt.df2sos(sos,g);

[z2,p2,k2] = butter(2,CutFreq2/Fs,'low'); %2nd order, normalized cutoff
freq, lowpass
[sos2,g2] = zp2sos(z2,p2,k2);
h2 = dfilt.df2sos(sos2,g2);
% fvtool(h)

Theta1Filt = filter(h,Theta1);
Theta2Filt = filter(h,Theta2);

Omega1 = (Theta1(2:end)-Theta1(1:end-1))/delta_t; %rad/s  Angular Vel
of Input Shaft
Omega2 = (Theta2(2:end)-Theta2(1:end-1))/delta_t; %rad/s  Angular Vel
of Output Shaft

Omega1Filt = (Theta1Filt(2:end)-Theta1Filt(1:end-1))/delta_t; %rad/s
Angular Vel of Input Shaft
Omega2Filt = (Theta2Filt(2:end)-Theta2Filt(1:end-1))/delta_t; %rad/s
Angular Vel of Output Shaft

Alpha1 = (Omega1(2:end)-Omega1(1:end-1))/delta_t; %rad/s^2  Angular
Accel of Input Shaft
Alpha2 = (Omega2(2:end)-Omega2(1:end-1))/delta_t; %rad/s^2  Angular
Accel of Output Shaft

Alpha1Filt = (Omega1Filt(2:end)-Omega1Filt(1:end-1))/delta_t; %rad/s^2
Angular Accel of Input Shaft
Alpha2Filt = (Omega2Filt(2:end)-Omega2Filt(1:end-1))/delta_t; %rad/s^2
Angular Accel of Output Shaft

Alpha1Filt2 = filter(h2,Alpha1Filt);
Alpha2Filt2 = filter(h2,Alpha2Filt);

%Finding the engagement pulses.
%Reference:
http://www.mathworks.com/products/daq/demos.html?file=/products/demos/s
hipping/daq/demoai_counter.html
Omega2Offset = [Omega2Filt(2:end); NaN]; %Create Offset Data Set to
Find Edges
RiseEdge = find(Omega2Filt < OmegaThres & Omega2Offset > OmegaThres);
FallEdge = find(Omega2Filt > OmegaThres & Omega2Offset < OmegaThres);
Edges = min([length(RiseEdge) length(FallEdge)]);

%Preallocating Variables
```

```
StartRise = zeros(Edges, 1);  EndRise = zeros(Edges, 1);
StartFall = zeros(Edges, 1);  EndFall = zeros(Edges, 1);

for j = 1:Edges
   for k = RiseEdge(j):-1:1
       if Omega2Filt(k) > Omega2Offset(k)
           StartRise(j) = k;
           break;
       else
           StartRise(j) = 1; %Prevent assigning 0 in case where the
rise edge is before the sample
       end
   end
   for k = RiseEdge(j):samples
       if Omega2Filt(k) > Omega2Offset(k)
           EndRise(j) = k;
           break;
       end
   end
   for k = FallEdge(j):-1:1
       if Omega2Filt(k) < Omega2Offset(k)
           StartFall(j) = k;
           break;
       end
   end
   for k = FallEdge(j):samples
       if Omega2Filt(k) < Omega2Offset(k)
           EndFall(j) = k;
           break;
       else
           EndFall(j) = samples; %Prevent assigning 0 in case where the
fall edge is after the sample
       end
   end
end


tRise = (EndRise - StartRise) * delta_t;
tEngage = (StartFall - EndRise) * delta_t;
tFall = (EndFall - StartFall) * delta_t;
tPulse = tRise/2 + tEngage + tFall/2;

Theta1Rise = Theta1Filt(EndRise) - Theta1Filt(StartRise);
Theta1Fall = Theta1Filt(EndFall) - Theta1Filt(StartFall);

Theta2Rise = Theta2Filt(EndRise) - Theta2Filt(StartRise);
Theta2Fall = Theta2Filt(EndFall) - Theta2Filt(StartFall);

TauDyn = Inertia2 * Alpha2Filt; %N*m  Dynamic Torque due to output
shaft angular acceleration


%Preallocating Variables
Omega1Rise = zeros(Edges, 1);  Omega1Fall = zeros(Edges, 1);
Omega1Engage = zeros(Edges, 1);
slipRise = zeros(Edges, 1); slipFall = zeros(Edges, 1);
E_slipRise = zeros(Edges, 1);  E_slipFall = zeros(Edges, 1);
```

```
E_slipTotal = zeros(Edges, 1);  E_pulse = zeros(Edges, 1);
TauDynMeanRise = zeros(Edges, 1);  TauDynMeanFall = zeros(Edges, 1);
E_flyLoss = zeros(Edges-1, 1);
Rise = zeros(Edges, 1); Fall = zeros(Edges, 1); E_Trans = zeros(Edges,
1);

for j=1:Edges
    Omega1Rise(j) = mean(Omega1Filt(StartRise(j): EndRise(j)),1);
    Omega1Fall(j) = mean(Omega1Filt(StartFall(j): EndFall(j)));
       Omega1Engage(j) = mean(Omega1Filt(StartRise(j): EndFall(j)));
        if isnan(Omega1Engage(j)) %Flip order of points for evaluation
if creates an NaN
            Omega1Engage(j) = mean(Omega1Filt(StartFall(j):
EndRise(j)));
        end

        if j < Edges
            Period(j) = (StartRise(j+1) - StartRise (j)) .* delta_t;
        end

        if j == 1
            E_flyLoss(j) = 0.5*Inertia1*(mean(Omega1Filt(5:
StartRise(j)))^2 - mean(Omega1Filt(EndFall(j): StartRise(j+1)))^2);

        elseif j == Edges
            E_flyLoss(j) = 0.5*Inertia1*(mean(Omega1Filt(EndFall(j-1):
StartRise(j)))^2 - mean(Omega1Filt(EndFall(j): samples-1))^2);

        else
            E_flyLoss(j) = 0.5*Inertia1*(mean(Omega1Filt(EndFall(j-1):
StartRise(j)))^2 - mean(Omega1Filt(EndFall(j): StartRise(j+1)))^2);

        end

    Rise(j) = Theta2Filt(EndRise(j)) - Theta2Filt(StartRise(j));
    Fall(j) = Theta2Filt(StartFall(j)) - Theta2Filt(EndFall(j));

    E_Trans(j) = TauBrake * (Theta2Filt(EndFall(j)) -
Theta2Filt(StartRise(j))); %J Energy transmitted to output during pulse


    slipRise(j) = sum((Omega1Filt(StartRise(j):EndRise(j)) -
Omega2Filt(StartRise(j):EndRise(j))) .* delta_t, 1); %Deg  Angle of
slip during engagement
    slipFall(j) = sum((Omega1Filt(StartFall(j):EndFall(j)) -
Omega2Filt(StartFall(j):EndFall(j))) .* delta_t, 1); %Deg  Angle of
slip during disengagement

    E_slipRise(j) = sum((Omega1Filt(StartRise(j):EndRise(j)) -
Omega2Filt(StartRise(j):EndRise(j))) .*...
        (TauDyn(StartRise(j):EndRise(j))+TauBrake) .* delta_t, 1); %J
Energy dissipated through clutch slip during engagement
    E_slipFall(j) = sum((Omega1Filt(StartFall(j):EndFall(j)) -
Omega2Filt(StartFall(j):EndFall(j))) .*...
        TauBrake .* delta_t, 1); %J  Energy dissipated through clutch
slip during disengagement
```

```
    TauDynMeanRise(j) = mean(TauDyn(StartRise(j): EndRise(j))); %N*m
Average Dynamic Torque During Rise
    TauDynMeanFall(j) = mean(TauDyn(StartFall(j): EndFall(j))); %N*m
Average Dynamic Torque During Fall

    E_slipTotal(j) = E_slipRise(j) + E_slipFall(j); %J  Total energy
dissipated through clutch slip during pulse

end

Frequency = Omega1Engage*3/(2*pi);
DutyCycle = tPulse ./(Frequency .^ -1);
```